The University of Manitoba

POOL BOILING SIMULATION

by

SHERIF ATEF BARAKAT

A Thesis

Submitted to the Faculty of Graduate Studies

in Partial Fulfilment of the Requirements for the Degree

of Master of Science

Department of Mechanical Engineering

Winnipeg, Manitoba

February, 1973

ABSTRACT

Recently, the importance of boiling heat transfer has considerably increased the interest in performing studies which illuminate the heat transfer mechanisms in bubble-stirred boundary layers. In the present study, air bubbles were generated at an orifice on a flat plate in a pool of n-hexane. On the plate, in close proximity to the orifice, there were deposited a series of small film heaters, which also acted as resistance thermometers giving easily-distinguishable signals on an oscilloscope. High-speed cine photographs of the bubble growth and departure cycle were taken while simultaneously recording the oscilloscope trace over the bubble images on the film. This then allowed the relationship between the instantaneous values of the heat-transfer coefficient and the bubble cycle to be unambiguously determined. In conjunction with the above experiment, hydrogen-bubble flow-visualization studies, in the vicinity of an orifice at which air bubbles were generated in a pool of water, indicated the liquid flow patterns near the heater surface. The behaviour of the heat-transfer coefficient as a function of time in the air-hexane experiment was explained in terms of the bubble-

induced liquid motion near the heaters.

It was found that the method described is well-suited to the detailed study of the heat-transfer variations with time in barbotage and the data obtained showed that the maximum heat-transfer coefficients are generated at the moment of bubble detachment from its site.

ACKNOWLEDGEMENTS

The author gratefully acknowledges the help he has received from Dr. G.E. Sims over the course of this investigation without whose guidance and encouragement this work would not have been possible. The author also wishes to express his sincere thanks to the staff and colleagues in the Mechanical Engineering Department and to the Materials Research Group of the Electrical Engineering Department for their help and cooperation.

The author is also grateful to the University of Manitoba and the National Research Council of Canada for the financial support received during this study.

TABLE OF CONTENTS

LIST OF FIGURES

LIST OF TABLES

NOMENCLATURE

a	half the film heater width	cm
A	film heater surface area	cm^2
A_o	orifice area	cm^2
c	speed of sound	cm/s
C_p	heat capacity of plate	cal/gm °C
D_o	orifice diameter	cm
E	supply voltage	volts
h	heat-transfer coefficient	cal/cm^2 s °C
h_o	time mean heat-transfer coefficient	cal/cm^2 s °C
$\bar{h}$	apparent heat-transfer coefficient	cal/cm^2 s °C
$\bar{h}_o$	apparent time mean heat-transfer coefficient	cal/cm^2 s °C
$H(s)$	transfer function $\tilde{\theta}$ to $\tilde{h}$	cm^2 s$(°C)^2$/cal
$\tilde{h}$	heat-transfer coefficient fluctuation	cm^2 s$(°C)^2$/cal
K	thermal conductivity of plate material	cal/cm s °C
$M(\omega)$	frequency response function of $\tilde{\theta}$ with respect to $\tilde{h}$	cm s$(°C)^2$/cal
N_C	ante-chamber parameter defined in equation (A·1)	
N_R	orifice parameter defined in equation (A·2)	
P	signal period	s
q	heat flux	cal/cm^2 s

R	resistance of film heater	ohm
$\bar{R}$	decade box variable resistance	ohm
R_1	fixed resistance in series with heater	ohm
R_2	fixed parallel bridge arm resistance	ohm
R_o	reference resistance at 0°C	ohm
R'_o	reference resistance at bulk liquid temperature	ohm
s	Laplace transform variable	
t	temperature, average over heater surface	°C
T	time	s
T_d	bubble detachment time	s
V	voltage accross film heater	volts
V_c	ante-chamber volume	

Greek Symbols:

β	dimensionless parameter defined as $2ah/k$	
$\bar{\beta}$	dimensionless parameter defined as $2a\bar{h}/k$	
γ	temperature coefficient of resistance	
η	dimensionless parameter defined as $h_o/\sqrt{K\rho C_p}$	
θ	average value (over film area) of temperature above bulk liquid	°C
θ_o	time average of θ	°C
$\tilde{\theta}$	fluctuation of θ	°C
ρ	density of plate material	gm/cm^3

ρ_L	density of liquid (hexane)	gm/cm^3
ρ_g	density of gas (air)	gm/cm^3
ϕ	conversion factor	cm/volt
ω	angular frequency	rad/s

CHAPTER 1

INTRODUCTION

1.1 Background

Boiling heat transfer is of great importance to engineering since it gives rise to relatively high heat-transfer coefficients. Boiling therefore finds application in systems having high heat-flux densities such as nuclear reactors, evaporators, liquid-propellant rocket motors and chemical process equipment.

However, boiling is a complex phenomenon affected by many variables. The complexity arises partly because of the interdependence of bubble evolution and heat transfer rate. Several authors [1,2,13,14,15,23,29,30, 38,39] have therefore sought to improve the understanding of heat transfer across bubble-stirred boundary layers by simulating nucleate boiling using 'barbotage' which is the bubbling of gas through a drilled or porous surface into a liquid. Such systems are attractive for the study of bubble-stirred boundary layers because the bubble generation rate is independent of the rate of heat transfer and can be accurately controlled and measured. Further, in boiling,

there are heat transfer mechanisms involving both latent heat effects and heat transfer through the liquid, while in general, in barbotage, only heat transfer through the liquid is present. This is an advantageous simplification which will no doubt help to establish the relative contribution of these mechanisms in boiling.

There is at the present time, however, still some confusion as to the relative importance of the various heat-transfer mechanisms which occur in boiling. All mechanisms combine one or more of the following assumptions: (i) heat transmission is essentially due to convective phenomena, enhanced by the bubble formation, through agitation produced in the liquid [12,16,25,34,35]; (ii) the growing bubble displaces the boundary layer from the surface; when the bubble detaches a returning flow of relatively cold liquid takes place, subtracting heat from the heating wall; evaporization for bubble growth occurs at the liquid-vapor interface and the required heat comes from the cooling of the superheated liquid layer, being pushed away by the growing bubble [10,21,42]; (iii) the growing bubble leaves a liquid microlayer adhering to the wall; because of the rapid evaporization of such microlayers into the bubble, removal of large quantities of heat occurs directly from the heating surface while the bubble is growing [8,31,33,37].

A number of authors [1,13,14,15,29,30,38,39] have

studied heat transfer in barbotage, dealing with time-average heat-transfer coefficients. Bard and Leonard [3] were the first to obtain local instantaneous values of the heat-transfer coefficient as a function of time. On the basis of their evidence they indicated that heat transfer is most intensive during the time that the bubble detaches from the surface. Their conclusions were based on heat transfer measurements and other observations, but without simultaneous high-speed cine photographs of the bubble cycle.

1.2 Purpose and Scope

In the present work high-speed cine photographs of the bubble cycle were taken while simultaneously using oscillography to trace the heat transfer behaviour over the image of the bubbles. This gave a precise and unambiguous record of the relationship between h, the heat-transfer coefficient, and the various phases of the bubble cycle. In addition, as an aid in explaining the heat transfer behaviour, flow visualization studies were made using the hydrogen bubble technique.

In brief, air was introduced through an orifice in a plate submerged horizontally in a pool of hexane. On the plate, four thin film heaters were vapor-deposited at varying distances from the orifice. These films were used also as resistance thermometers to indicate the temperature

variation on the heat-transfer surface around the bubble. The signal produced by any of the film heaters could be displayed on an oscilloscope. High-speed motion pictures were taken showing a continuous record of the bubble cycle simultaneously with the signal displayed on the oscilloscope. The voltage fluctuations were measured and converted to heat-transfer fluctuations and then examined in relation to the bubble cycle.

1.3 Layout of the Thesis

Following a general review of the work in the fields of nucleate boiling and barbotage concerning the different mechanisms of heat transfer in Chapter 2, Chapter 3 includes a detailed description of the experimental apparatus and all measuring and photographic equipment used. Chapter 4 covers the experimental procedures together with the method of data reduction. Chapter 5 includes the experimental observations and results as well as discussion. The most important experimental results are shown in Figs. 5.1, 5.3 and 5.7 with the attendant discussion appearing in Section 5.2. Finally, conclusions are given in Chapter 6.

CHAPTER 2

REVIEW OF BOILING AND BARBOTAGE HEAT-TRANSFER MECHANISMS

2.1 Boiling Heat Transfer

Much of the research concerning nucleate boiling has been conducted during the past several years in order to determine the mechanisms, evidently due to bubble formation, that are responsible for producing the high heat fluxes associated with boiling.

It was often assumed in early work that the violent agitation caused by the bubbling process explains the high heat-transfer coefficients observed [12,25]. Thus, boiling was regarded as a form of forced convection heat transfer. Gunther and Kreith [16] and also Rohsenow and Clark [34,35] proposed that growing and collapsing bubbles create random microconvection currents of high velocity in the region of liquid adjacent to the heated wall and suggested that this microconvection is the dominant transport mechanism for the high heat fluxes observed with surface boiling. Forster and Zuber [12] favored the movement of the bubble boundary while bubbles are still attached to the heating surface to

be the main factor in promoting the heat transfer. On the other hand, Forster and Greif [11] suggested that a more efficient heat transfer mechanism occurs when the growing bubble displaces the superheated liquid layer entirely from the surface. Cooling then occurs during departure when cold liquid suddenly quenches the hot surface, increasing the heat flux locally.

In recent years other models have been proposed; each envisioned some specific flow pattern in the liquid and attempted to predict the heat-transfer coefficient. In a theoretical paper Hara [17] traced the trajectories of fluid particles on the edge of the thermal boundary layer. He predicted that each particle moves away from the bubble while the latter is growing, but reverses direction after bubble detachment. There is a net step towards the bubbling site during each cycle. Eventually the particle reaches the site and evaporates. Hara calculated the heat flux carried by this liquid motion to the nucleation site and equated it to the heat transferred from the heating surface to the liquid by conduction and to the latent heat carried away per unit time, thus obtaining a correlation for the heat-transfer coefficient. Ruckenstein [36] assumed that the liquid is displaced horizontally outwards from the bubble site at a velocity that equals the rate of growth of the bubble radius. He used the general correlation for the steady flow along

horizontal plates to predict the equation for the heat-transfer coefficient without any experimental verification. The present study, however, provides evidence that there is an outward flow during bubble growth but the inward flow at detachment is more intense and causes the higher peaks of the heat-transfer coefficient.

Tien [40] hypothesized that the updraft caused by the rising bubble produces a flow field in the liquid similar to a reversed stagnation flow. He employed equations for such flow to predict the heat-transfer coefficients on the surface. While Zuber [46] did not trace any specific pattern in the liquid he rather viewed the hydrodynamic aspect of the boiling process as a case of turbulent natural convection induced by the lower density of the vapor phase forming on the boiling surface. He postulated that the heat transfer mechanism is due to the bubble-induced flows in the boundary layer adjacent to the heating surface.

Some recent work has cast some doubt on the dominant role assigned to bubble-induced agitation as the main promoter of heat transfer. Moore and Mesler [31] have observed the temperature-time fluctuation of a boiling surface with a high-response thermocouple. They noted regularly an exceedingly rapid drop in temperature followed by a smaller rapid rise and a gradual reattainment of the initial temperature. They estimated that a value of heat-transfer coefficient up to 47,000 BTU/hr ft^2 °F (6.34

cal/cm^2 s °C) would be required in order that sufficient heat be withdrawn from the surface to cause the observed temperature drop. As these coefficients were well above what would be expected if convection were the important factor, they postulated the existence of a microlayer of liquid underneath the bubble and attributed the large rate of heat removal to the rapid evaporation of this microlayer.

Bankoff and Mason [5] injected steam bubbles into subcooled water and measured heat-transfer coefficients at the surface of single bubbles. To account for the observed transfer of latent heat, values of the heat-transfer coefficient over the surface of the bubbles has to be as high as 320,000 BTU/hr ft^2 °F (44.2 cal/cm^2 s °C). They, as well as Bankoff [4] concluded that, although the stirring action dominates at relatively low heat fluxes, the latent heat transport becomes the dominant mechanism near the upper limit (burnout) in nucleate boiling.

Rogers and Mesler [33], using a technique to photograph the growing bubble while measuring the surface temperature beneath it, showed that the surface cools during bubble growth and recovers during bubble departure; a sudden temperature drop corresponding to the initiation of a bubble growth occurs. Their study did no indicate the reason for the cooling to stop so suddenly when the

bubble departs as was observed.

Hendricks and Sharp [18] also suggested that an evaporating microlayer at the base of the bubble is responsible for most of the high heat flux in nucleate boiling. They observed that the drop of temperature is during the growth period and the temperature reaches a minimum as the bubble approaches its maximum diameter. They also observed a small but measurable rise in heat flux in the area near the bubble during bubble release. Thus, they mentioned that the evidence was not quite conclusive that the quenching mechanism due to bubble detachment is ineffective in all cases of boiling. This conclusion was made since the heat ribbons used in their experiments had a very small heat capacity. Hendricks and Sharp indicated that if boiling takes place on a more massive solid it is possible that the quenching mechanism may be significant.

Sharp [37] demonstrated the existence of an evaporating liquid film at the base of the bubbles during nucleate boiling. The microlayer thickness was computed by Hospeti and Mesler [19] who showed that the bubble behavior is consistent with the microlayer evaporation and the microlayer thickness agreed well with that reported by Moore and Mesler.

In pool boiling from a nickel wire, Rallis and Jawurek [32] obtained measurements from which it was indicated that at high heat fluxes latent heat transport

by vapor formation near the heating surface may represent the major portion of the total heat flux. They also concluded that latent heat transport and convection together account for the total flux in saturated nucleate boiling. In a very recent paper, Fontana [10] showed that an amount of heat equal to 60-70 per cent of the total heat necessary to produce the vapor contained in the bubble is transmitted from the hot surface to the bubble during its growth, the area of heat transmission being approximately the largest contact area of the bubble on the heater surface. He also showed that the remaining 30-40 per cent of the heat is transmitted during the waiting period from the hot wall to the liquid rushing into the bubble site after its detachment. Fontana observed two heat transfer increases; one at the beginning of bubble growth with a maximum heat-transfer coefficient of 30,500 - 41,000 BTU/hr ft^2°F (4.16 - 5.55 cal/cm^2 s °C), the second at bubble detachment with a peak of 2,050 - 3,050 BTU/hr ft^2°F (0.278 - 0.416 cal/cm^2 s °C) which is much higher than those obtained without ebullition. He thus agreed with the hypothesis that the bubble at detachment produces a return of relatively cold liquid subtracting more heat from the surface. It was also found by Fontana that the nucleation strengthens the thermal exchanges outside the bubbles area of contact producing approximately a doubling of the convection coefficients in comparison to the values obtained in the

absence of ebullition.

2.2 Barbotage (Simulated Boiling)

The state of confusion, in which our knowledge of the mechanism of boiling heat transfer still exists, was demonstrated above. The cause of this is to be found in the complexity of the process, in which several inter-dependent phenomena occur simultaneously. Thus, bubble growth depends, among other things, on agitation due to bubble growth and motion. In addition, the process depends on some stochastic factors such as nucleation, distribution of bubble sites and their condition at the start of boiling.

For this reason, one would like to separate heat transfer and bubble cycle, those being the phenomena where interaction is the most reciprocal. Therefore, as already mentioned, several authors [1,2,13,14,15,23, 29,30,36,39] have sought to improve the understanding of heat transfer across bubble-stirred boundary layers by simulating boiling using barbotage or electrolysis to produce bubbles on the heat transfer surface. As expected, the bubbling process promoted the transfer of heat to the liquid.

When considering barbotage as an analogue of boiling, various aspects may be examined, which may be

purely hydrodynamic or may include heat transfer. Zuber [45], Wallis [43,44] and Kudirka [23] have noted the similarities in appearance of the bubbling flow regimes in barbotage and in saturated nucleate boiling. The similarity of initiation, of growth rates and growth times have also been pointed out [44]. In boiling, a hydrodynamic crisis has been postulated to occur at the critical heat flux (burnout). In barbotage a similar one has been postulated and studied [1,39,44,45].

With regard to heat transfer, a first step towards understanding the connection between barbotage and boiling is to compare the heat-transfer coefficients in both phenomena. Mixon, Chon and Beatty [30] produced bubbles electrolytically and found that electrolytic bubbles, although much smaller than the usual boiling bubbles, are effective for the enhancement of heat transfer. Gose, Acrivos and Peterson [14], using both drilled and porous surfaces, found that the magnitude of the heat-transfer coefficient in barbotage increased greatly as the volume of the gas injected is increased and reaches values of the same order of magnitude as nucleate boiling heat transfer at comparable vapor rates. They, as well as Akturk [1] found that, for the porous plate, the increase in heat-transfer coefficient stops at a certain air rate after which it starts decreasing. The data of Gose *et al.* were correlated by Sims, Akturk and Lutterodt [39] and showed to

closely correspond with boiling data in the case of porous plates and within an order of magnitude for drilled plates. Sims and Duffield [38] defined a "heat-transfer-coefficient through-the-liquid" which accounts for the same heat transfer mechanisms in boiling and barbotage. This was used as the basis of comparison between heat transfer in boiling and barbotage. They concluded that, at the same dimensionless vapor/gas flow rates, the dimensionless heat-transfer coefficients-through-the-liquid are closely comparable in magnitude in boiling and barbotage.

Bard and Leonard [3] conducted experiments to determine the effect of air bubble trains injected into liquid (hexane) on the heat-transfer coefficient on the surface near the orifice as a function of both time and distance from the orifice. They proposed that the heat transfer is most intensive during the time of bubble detachment from the surface, i.e., the chief contribution of bubble-induced agitation to the promotion of heat transfer from the heating surface occurs around the time of bubble detachment. The phases of bubble growth and rise have at most a minor effect. Values of the heat-transfer coefficient up to 1,000 BTU/hr ft^2 °F (0.136 cal/cm^2 s °C) were observed in their studies of barbotage experiments while in actual pool boiling, values between 150 - 3,000 BTU/hr ft^2 °F (0.0204 and 0.416 cal/cm^2 s °C) were observed by Kurihara and Mayers [24] for hexane and other organic

liquids. Bard and Leonard also postulated that only at higher heat fluxes does it seem that agitation alone could not account for the observed heat-transfer rates. In those cases latent heat transfer must contribute significantly. However, even then, agitation plays an important role.

In a more recent experiment Frea and Hamelink [13] studied the heat transfer with gas injection through a porous wall into a pool of liquid, including vaporization effects. They have found that the heat transfer from the surface takes place through the action of the two mechanisms, bubble-induced convection and vaporization into the bubble. They indicated that gas injection can promote heat transfer from the surface to an extent such that, in some cases, the heating surface operates at low or negative temperature difference from the pool temperature. Under such conditions, the vaporization mechanism produces the major component of heat flux directed away from the heater.

CHAPTER 3

EXPERIMENTAL APPARATUS

This chapter presents a description of the experimental apparatus and the different instruments used for measurements as well as the photographic equipment.

3.1 The Plate

The main part of the apparatus was a circular plate on which the heaters were located. This plate could be fastened to the top of a cylindrical chamber. The assembly, with the plate horizontal, was immersed in a small tank filled with hexane which could then be considered as the bubbling chamber. The plate was made of acrylic ("Perspex") of ½ inch thickness as shown in Fig. 3.1a. Perspex was chosen since it combines the characteristics of (i) good machinability, (ii) low thermal conductivity, which decreases the amount of heat conducted into the plate, and (iii) good film adherance for deposition of heaters.

A 0.038 in. (0.95 mm) diameter orifice was drilled through the centre of the plate. The area around the orifice was reduced in thickness to 0.050 in. (1.27 mm) to

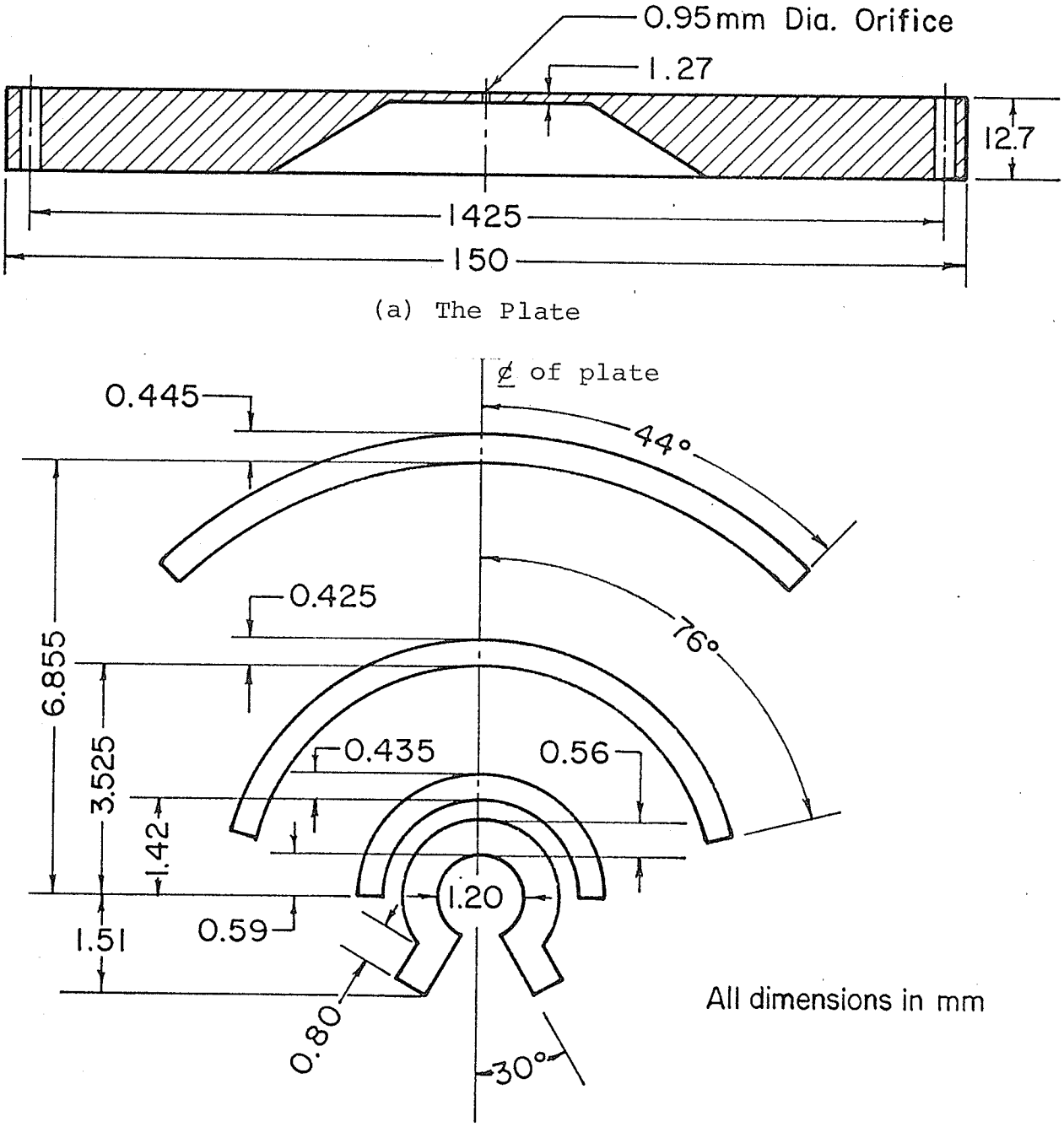

Fig. 3.1 The Heat Transfer Plate

reduce the pressure drop through the orifice. The final geometry with length to diameter ratio of 1.32 satisfies one of the criteria for constant pressure bubbling (see Appendix A for more details).

Four copper thin films, used as surface heaters and resistance thermometers, were vacuum-deposited at various distances from the plate centre, as shown in Fig. 3.1b. Each copper film was approximately 0.02 in. (0.5 mm) wide by 0.2 in. (5 mm) long having a resistance in the range 30 - 50 ohms, which corresponds to a thickness of approximately 56 - 34 Å. The film heaters and plate orifice dimensions were measured on a microscope provided with two micrometers at 90° to each other. The full dimensions are given in Fig. 3.1b and Table 4.1. The film heaters were made curved in shape so as to make all points of the film equidistant from the centre orifice, with the exception of the innermost one which has the shape shown in order to facilitate connections to the electrodes.

The films were deposited on the plate using the vacuum evaporation technique [28]. In order to achieve the design shown, a copper sheet mask was placed on the plate during deposition, baring only the spots where the heaters were to be located. This mask was made by a process of photographic etching.

Thin films were used by Foltz and Mesler [9] and by Bard and Leonard [3] in their experiments. The heaters were

found to give accurate surface temperatures beneath bubbles and were capable of indicating temperature changes as fast as 145 °F/ms.

To facilitate making electric contact, for each film heater, a pair of 0.018 in.(0.475 mm) diameter copper wires was inserted and glued into holes drilled where the ends of the film would ultimately be; the wires were trimmed and polished flush with the Perspex surface before the film was deposited. The wires from the heaters were then connected with another set of wires which left the plenum chamber through a "Conax" pressure seal gland.

Several depositions were tried using nickel and copper. Although nickel has a higher temperature-coefficient of resistance and higher resistivity, copper was found to be much easier to deposit because of its lower melting and boiling points. Also, by using copper, the generation of thermoelectric potentials at the contacts with the electrode due to any possible asymmetry in the orifice-film locations was avoided.

3.2 The Plenum Chamber

The plenum chamber was fastened to the bottom of the plate. It consisted of a 5.25 in.(133 mm) outside diameter Perspex cylinder of ¼ in.(63 mm) thickness and 6 in.(152 mm) length closed on the bottom end by a Perspex plate glued

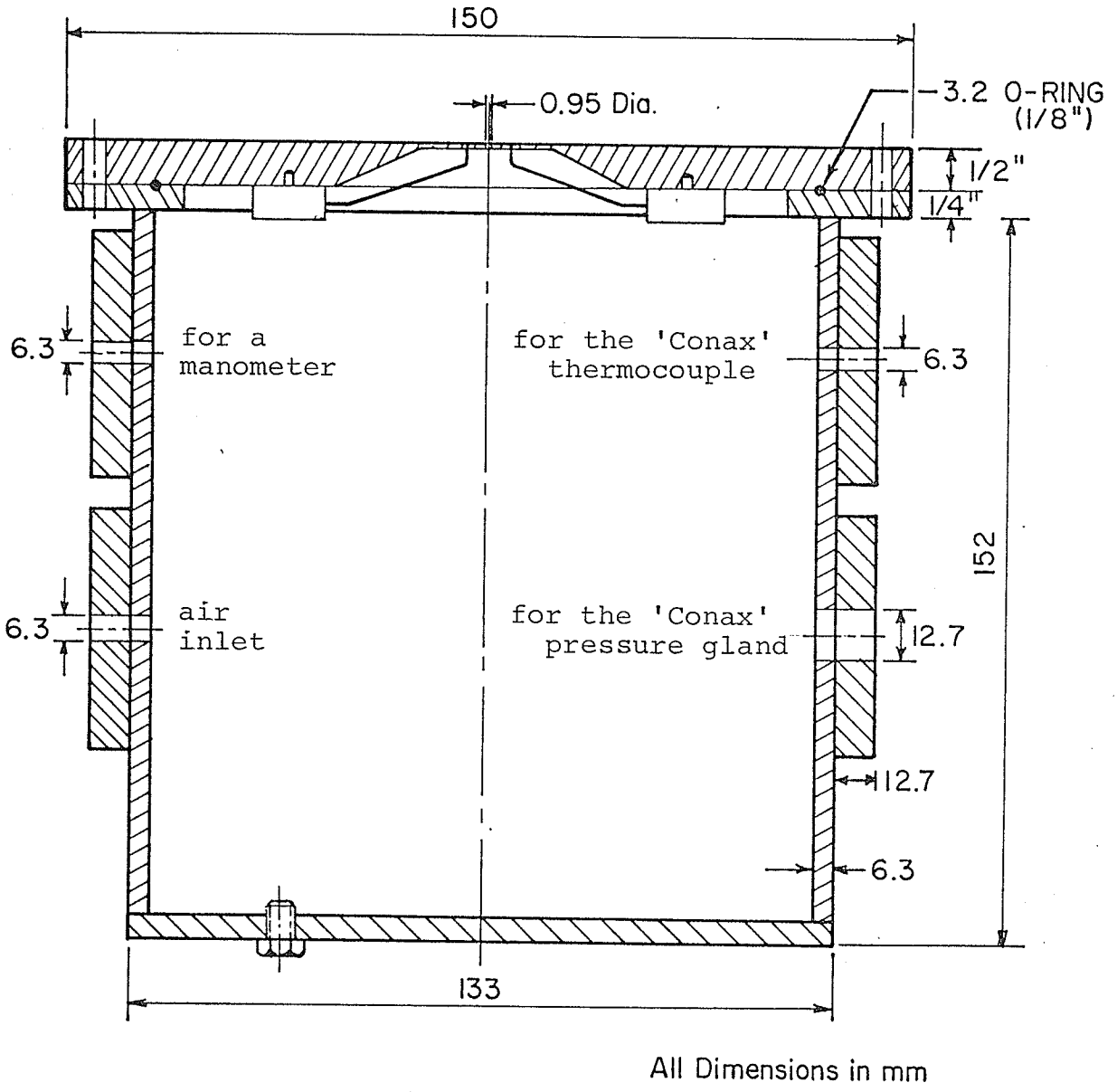

Fig. 3.2 The Plenum Chamber

to it. On the upper side a 5 15/16 in. (150 mm) diameter flange was also glued to allow the drilling of holes for fastening the plate, as shown in Fig. 3.2. The chamber had four side radial openings to take the "Conax" pressure gland, a connection for air inlet, a manometer connection and a "Conax" sealed iron-constantan thermocouple for measuring air temperature inside the chamber.

Here, again, to approximate the condition of "constant pressure" bubbling a further criteria (discussed in Appendix A) had to be met. That is, the supply ante-chamber volume had to be more than 10,000 times the bubble volume, or in other words, the value of the parameter N_c has to be much greater than unity. For the present case the estimated value of the ratio of the chamber to bubble volume was about 15,000 (based on a ¼ inch bubble diameter), while N_c value was about 200, which is far greater than unity.

3.3 The Bubbling Tank

The plate and plenum chamber assembly was suspended horizontally with three Perspex rods in the tank, which was a glass aquarium 7 x 12 x 12 in. filled with hexane and through which photographs were taken. Hexane was used because of its low electric conductivity (see Appendix D) and its physical properties which are reasonably similar to water.

3.4 Air Supply System

The schematic of the apparatus is shown in Fig. 3.3. Air was drawn from the building compressed air supply at 80 psi and reduced in pressure to 5 psi in passing through a pressure regulating valve, air then passed through a "SHORATE" Model 1355 flow meter with a maximum range of 7.8 SCFH (14.1 cc/s) and through a Fisher-Milligan gas washing bottle filled with hexane before finally going to the plenum chamber. The pressure inside the chamber was measured using a manometer filled with 0.827 sp. gravity oil.

3.5 Electric Instruments

The electric circuit, which was essentially a Wheatstone bridge and is shown in Fig. 3.4, was constructed for the purpose of measuring the film heater resistance and recording and displaying the resistance fluctuations for each of the four thin films. The power supply source was a 12 volt battery connected in parallel with a 2,500 ohm potentiometer which permits the change of voltage from zero to 12 volts. An electronic power supply was tried but it was found to give a high noise level of 60 c/s ripple. A Leeds and Northrup DC null indicator Model CAT 9834 was used in the bridge for null detection. It has a maximum sensitivity of 0.067 μv/mm (0.1 μv/scale division) and produces a noise level of only 0.1 micro-

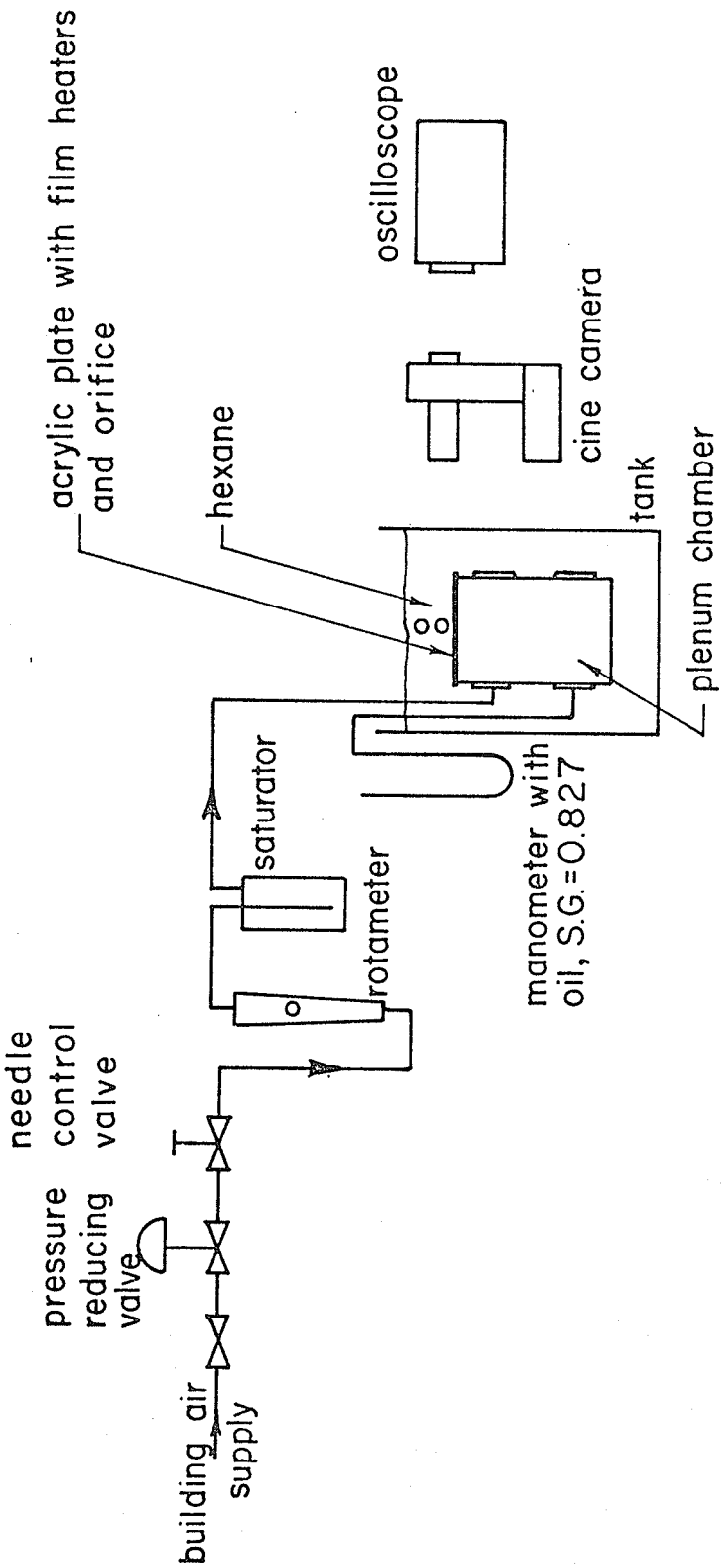

Fig. 3.3 Schematic of Apparatus

Fig. 3.3

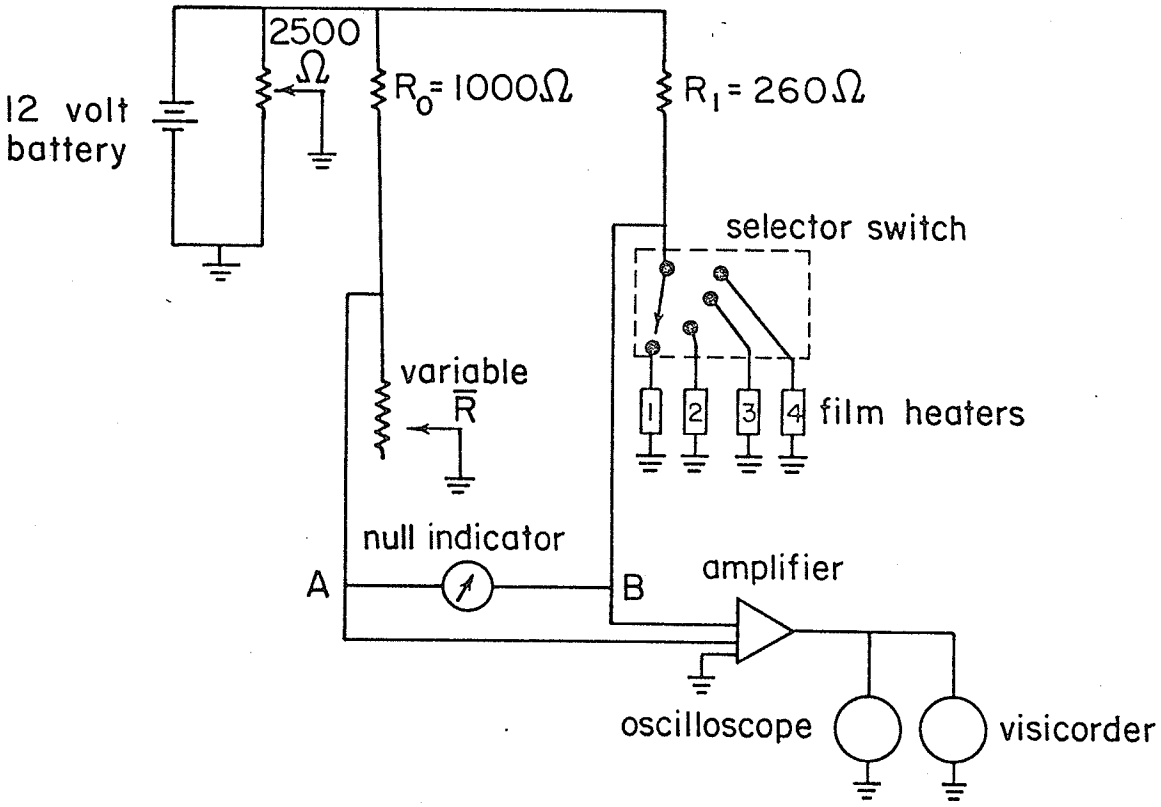

Fig. 3.4 Measuring Circuit

volt peak to peak.

For display purposes a Tektronix 453 oscilloscope was used. It has two channels and provides a vertical displacement up to 0.2 cm/mv each. This Tektronix oscilloscope was used since it has a high accelerating voltage (10 KV) and a P11 screen phosphor which is superior for photographic applications. A direct-recording optical galvanometer (Honeywell 1706 Visicorder) was used in parallel with the oscilloscope as an aid in setting the apparatus up and obtaining another form of record as a check. Before displaying the signal it had to be amplified to be detectable on the oscilloscope. This was done by a Hewlett and Packard 2470 A amplifier which can give gain up to 1,000 times.

The signal to be recorded was the variable component of the potential across the film, i.e., the voltage fluctuations only. Thus, the signal was measured between points A and B shown in Fig. 3.4. The decade box resistance $\bar{R}$ was adjusted until a zero DC reading was indicated by the oscilloscope and the null indicator.

All inputs and outputs were grounded to minimize any 60 cycle noise pick-up. Also, shielded cables were used for all connections.

3.6 Flow Visualization Equipment

In order to observe the liquid flow pattern around

growing and departing air bubbles, tiny hydrogen bubbles (0.05 - 0.2 mm in diameter) were generated in water on a plate similar to the one used in the heat transfer experiment and described in Section 3.1, except that there were no heaters. Instead, four copper wires of 0.008 in. (0.20 mm) diameter were inserted through the plate and glued in holes on a diameter on each side of the 0.038 in. orifice, as shown in Fig. 3.5. The wires on the upper side were trimmed and polished flush with the surface.

The plate formed the top side of the plenum chamber, the whole being immersed in distilled water. Sodium sulfate (approximately 4 grams per gallon of water) was added to the water making it more conductive. Upon application of a voltage the wires in the plate acted as cathodes, so generating a continuous stream of hydrogen bubbles from each wire, while a stainless steel plate 2 x 3 in. (51 x 76 mm) immersed in the electrolyte acted as the anode. The air circuitry was the same as described earlier, except for water being in the saturator.

During operation, air was bubbled through the orifice and the resulting motion of the hydrogen bubbles was photographed. The hydrogen bubbles were small enough that their motion due to buoyancy during the time of one air bubble cycle could be neglected. (The maximum hydrogen bubble rise during a time equal to one air bubble cycle was found to be about 0.5 mm compared to an air bubble detachment diameter

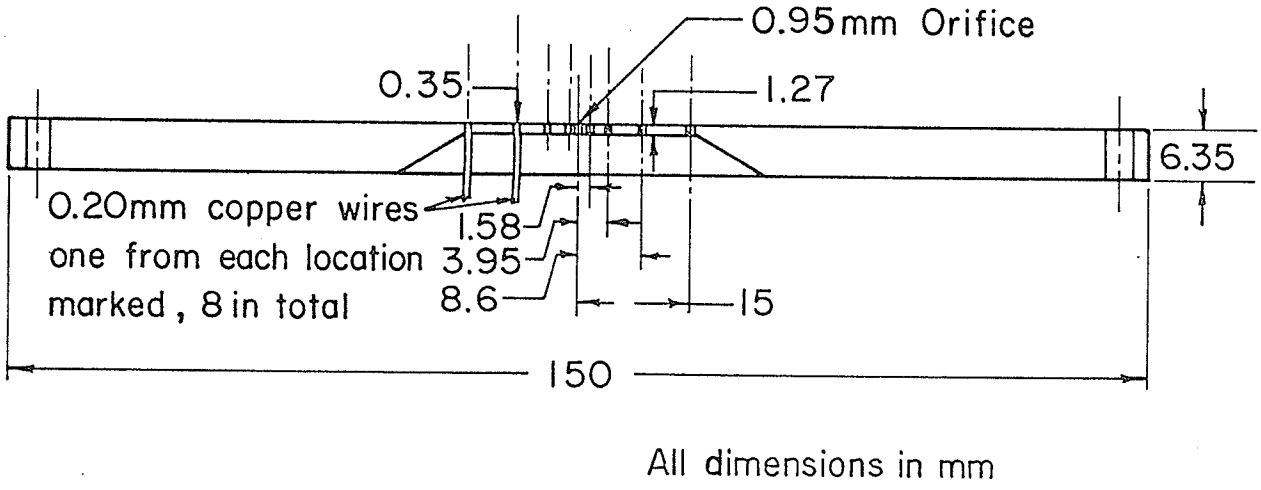

Fig. 3.5 Plate for Flow Visualization Experiment

of about 7 mm).

3.7 Photographic Equipment

A Hycam Model 41-0004 16 mm high-speed rotating-prism camera was used to photograph the bubble growth and departure cycle at the orifice. It has a speed range from 10 - 11,000 frames/s and a film capacity of up to 400 feet. The objective lens was a Cosmicar 4 in. FL f/2.5 used with a 30 mm 'c' mount extension tube. An auxilliary lens (Pentax 50 mm FL f/1.4) was mounted, using a special adaptor, on the viewing eyepiece to enable simultaneous recording of the bubble images and the oscilloscope trace. The photographic film used was 100 feet rolls of Kodak 4-X reversal.

The camera is equipped with an event synchronizer which can be set to any length of the film. The event switch is triggered to open or close the event circuit as the film reaches some predetermined position. It is also equipped with two timing lights for identification and frame rate determination. A Redlake Model RLTLG-4 Millimite timing light generatorwas connected to one of the lights and gives 10, 100 or 1,000 pulses per second output.

To mark the same instant on the film and the signal recorded on the visicorder, the Millimite generator was connected through the event synchronizer switch to the timing light and to a second channel on the recorder. When the event switch was triggered at a certain setting,

a circuit was closed which connected the generator output to the timing light and to the visicorder, so marking lines on the recorder sheet and marking the film at the same instant. It was noted that the mark on the film was lagging about 4 frames with respect to the image, due to the distance between the timing lights location and the image incidence place.

The light arrangement used is shown in Fig. 3.6a. For illumination purposes two Smith Victor 650 watt (at 115 volts) Quartz Bromine lights were used. For the heat-transfer experiment, the lights were mounted behind the tank with a diffusing screen between the tank and the lights. When photographing hydrogen bubbles, experiments showed that the clearest cine photographs of the hydrogen bubbles were obtained using a black background with the lights arranged as shown in Fig. 3.6b. To adjust and choose the correct combination of film speed (ASA), f/stop and camera speed, a Pentax Spotmeter III was used.

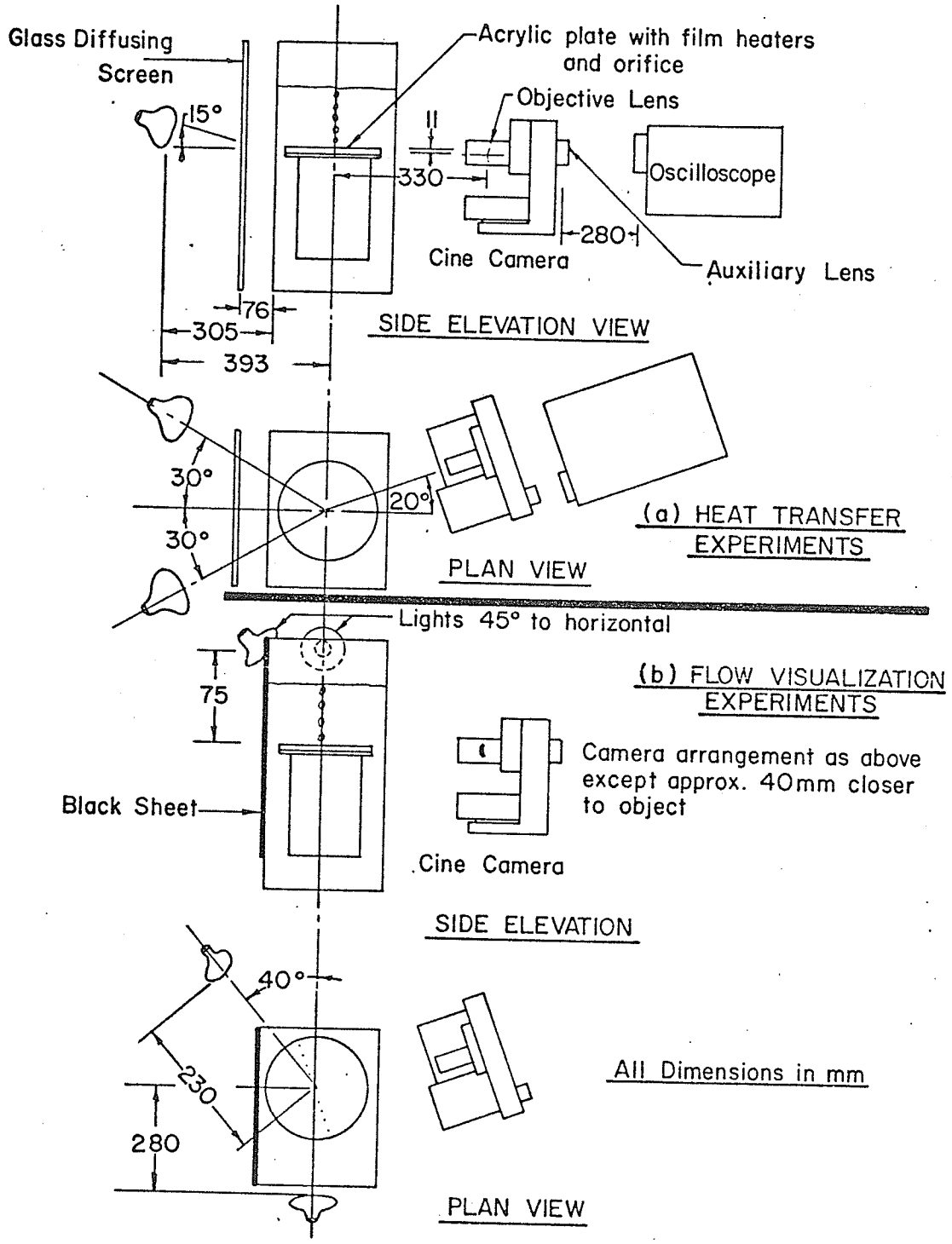

Fig. 3.6 Arrangement of Photographic Equipment

CHAPTER 4

PROCEDURE

4.1 Average Resistance Measurement

The following procedure was followed in measuring the resistance of the heaters with no bubbling as well as their average resistance with bubbling.

1. The bubbling tank was filled with hexane at room temperature. The plate was fastened to the Perspex chamber and placed in the hexane bath.

2. The air-supply valve was opened and the needle valve set to the desired flow rate, thus obtaining a certain bubble frequency which could be determined from the visicorder trace.

3. The heater, whose resistance was to be measured, was connected as the input in the measuring circuit through a selector switch. The supply voltage was adjusted to the desired value which was only a small value in this case (less than one volt).

4. The decade resistance $\bar{R}$ was adjusted until the null indicator was as close to zero reading as possible (the reading fluctuated around zero). From the Wheatstone

bridge balance (Fig. 4.1) it follows that

$$R = \frac{R_1}{R_2} \bar{R} \qquad (4.1)$$

where

R is the heater resistance, ohms

$\bar{R}$ is the decade box setting, ohms

R_1, R_2 are constant resistances, ohms

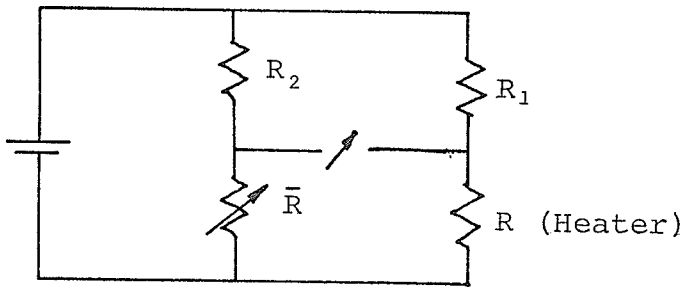

Fig. 4.1

4.2 Recording and Photographing Resistance Fluctuations

The procedure was as follows:

1. As for 1. in Section 4.1.

2. As for 2. in Section 4.1.

3. The selected heater was connected to the input terminal of the measuring circuit through the selector switch. The supply voltage was set to the operating value (usually ~11.0 volts).

4. The oscilloscope and the visicorder were switched on and the amplifier setting was changed until a good

observable signal was seen on the scope clearly enough to be recorded photographically. The paper speed on the visicorder was 800 mm/s (32 in/s) which is the fastest speed.

5. The camera was located between the bubbling tank and the oscilloscope. With the auxiliary lens set to infinity, the bubbles image was focussed with the objective lens. The objective was then set to infinity and the oscilloscope image was focussed with the auxiliary lens. The objective was set back to the first adjusted setting. The camera was then loaded and the event synchronizer adjusted to close the event switch at about 25 ft of the film. With the camera running at low speed (20 frame/s) the maximum, minimum and zero points of the oscilloscope were photographed. Switching the camera to high speed (usually 2,000 frame/s) the bubbles image and the oscilloscope trace were simultaneously photographed.

6. The visicorder was switched on a few seconds before the camera. After 25 ft of film, which was during the high speed run, the event synchronizer switch was automatically triggered, connecting the timing light generator to both the camera timing light (to mark the film) and to the visicorder (to mark the recorder sheet).

4.3 Temperature Coefficient of Resistance

To measure the temperature coefficient of resistance

for each heater, the bubbling tank was placed in a larger aquarium filled with water which could be heated to different temperatures using an electric heater. The procedure of Section 4.1 was repeated and the resistance of the film heater was measured at various temperatures between 62 and 120°F (measured by thermometer to ±0.2°F).

The resistance of each heater was assumed to be a linear function of temperature, i.e.,

$$R = R_o + \gamma t \qquad (4.2)$$

where

R = film heater resistance, ohms

R_o = reference resistance at zero °C, ohms

t = average temperature of film heater, °C

γ = temperature coefficient of resistance, ohm/°C.

The value of γ was then computed by the method of least squares and the values for each film heater are given in Table 4.1. It should be noted that γ depends on film heater thickness and resistance, as well as on the deposition process which affects uniformity and continuity of the film heater [28].

4.4 System Gain

Since the heater output signal passed through an amplifier before being displayed, it was necessary to check

Table 4.1

Heater Data

Heater Number	Distance From Plate Centre to Heater Centre mm	Width mm	Surface Area mm^2	Resistance ohms	γ From Eqn. 4.2 ohms/°C
1	0.88	0.56	0.01845	32.2	0.0516
2	1.635	0.435	0.0198	42.4	0.091
3	3.737	0.425	0.0164	47.5	0.049
4	7.077	0.445	0.0165	45.5	0.051

the gain of the whole system. A sinusoidal signal of known magnitude was introduced as an input to the system, instead of the original signal, displayed on the oscilloscope, and measured. The sinusoidal signal was generated by an IEC Function Generator Model F 51 and the magnitude of the gain for each film heater is given in Table 4.2.

4.5 Calculation of the Heat-Transfer Coefficient

The photographic films were projected (using an L-W Model 900 B Motion Analyzer) on a white paper giving an image of 6½ x 8 in (162 x 205 mm) and the signal was measured in each frame (0.5 ms interval at 2,000 pps film speed). The measured voltage signal was then transformed to heat-transfer coefficient using the method given by Bard [2] and described in Appendix B. The computation was done on an IBM 360 computer at the University of Manitoba Computer Centre with the detailed programme given in Appendix E.

4.6 Conditions During Tests

For the results analyzed, in order to have the same test conditions (air flow rate, liquid height and supply pressure) for all the heaters, four films were taken in quick succession, one for each heater. The conditions during tests were as follows:

Table 4.2

System Gain

Cine Film No.	Heater No.	Gain mv/mv	Scope Setting mv/div
25	1	10	5
26	2	10	5
27	3	30	10
28	4	30	10
29	1	10	5
30	2	30	10

Liquid	:	hexane
Gas	:	air
Temperature of the liquid pool	:	72°F (22°C)
Liquid height above heater plate	:	2.0 in (50 mm)
Air flow rate	:	0.94 cc/s*
Supply voltage	:	11.0 volts
Camera speed	:	20 frame/s for low speed runs
		2,000 frame/s for high speed runs
		1,000 frame/s for flow visualization experiment
Visicorder paper speed	:	800 cm/s (maximum available)

* Films for Heaters 1 and 2 at 2.2 cc/s were also taken.

CHAPTER 5

RESULTS AND DISCUSSION

5.1 Observations

During experiments it was found that at air flow rates below approximately 1.7 cc/s, the bubbles would come in a series of two to six bubbles, followed by a lull, then another series of bubbles, and so on; at air flow rates above 1.7 cc/s, regular bubbling occurred. This may be the effect of using a small plenum chamber and a small orifice which suggests that the criteria for 'constant pressure' bubbling needs more investigation.

A series of four films was selected. As mentioned in Section 4.6, films were taken in quick succession at the same conditions, one for each heater. On each film about six or seven bubble series were photographed. Since all the series were almost identical, one for each heater was analyzed. Also, two films were taken for Heaters 1 and 2 at a higher flow rate. Results of those two films will also be presented.

Fig. 5.1 gives a typical reproduction from one of the photographic films showing one bubble cycle with the

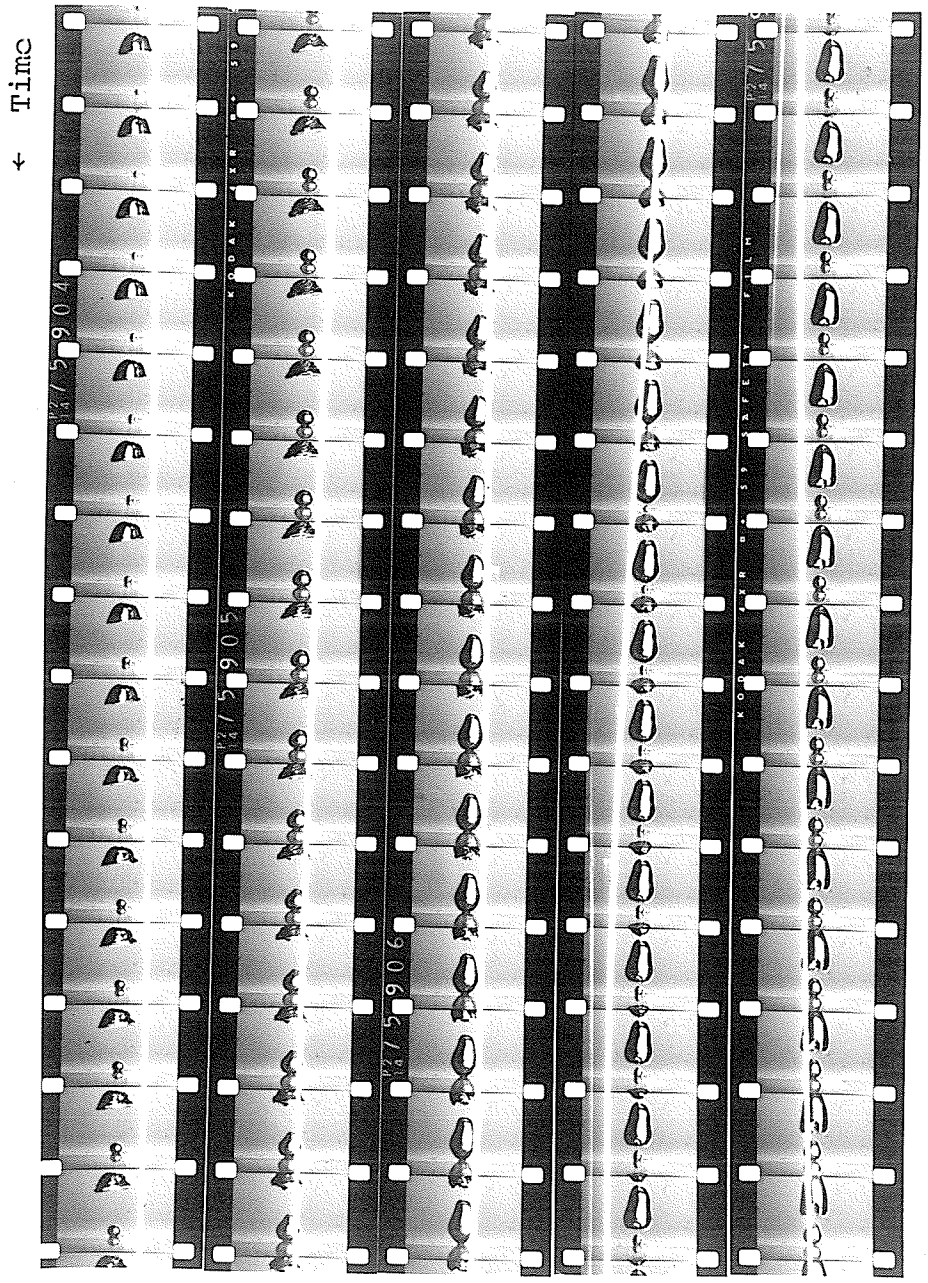

Fig. 5.1 Typical Photographic Film in Heat Transfer (Film No. 30, air flow rate 2.2 c.c/s, camera speed 2000 pps.)

oscilloscope signal clearly recorded on the film. As any such signal can be transformed into the heat-transfer coefficient, h, there can be no ambiguity as to the heat-transfer behavior at any instant in the bubble cycle.

A sample of the recorded signal on the visicorder for Heater 1 for a series of bubbles is shown in Fig. 5.2. Fig. 5.3 shows the result of analyzing a five-bubble series for each heater. The plot show instantaneous h versus time T normalized using T_d, the detachment time (time from initiation of a bubble to its detachment) for each individual bubble.† Figs. 5.4 and 5.5 show the variation of h versus T during two bubble cycles for Heaters 1 and 2, respectively at a higher flow rate. The results are also summarized in Table 5.1.

Examination of photographic films and recorded signals leads to the following observations:

1. In the first stages of growth of the first bubble in a series, the signal shows a sudden drop in temperature of the heater, i.e., an increase in the heat-transfer coefficient h, while the bubble interface near the plate surface is moving outward. As the interface is decelerating and going through a reversal in direction, h starts decreasing and goes through a minimum. The point of reversal of interface direction at a height of one orifice

---

† Tabulated data each ~0.0125 T/T_d are also available from the author.

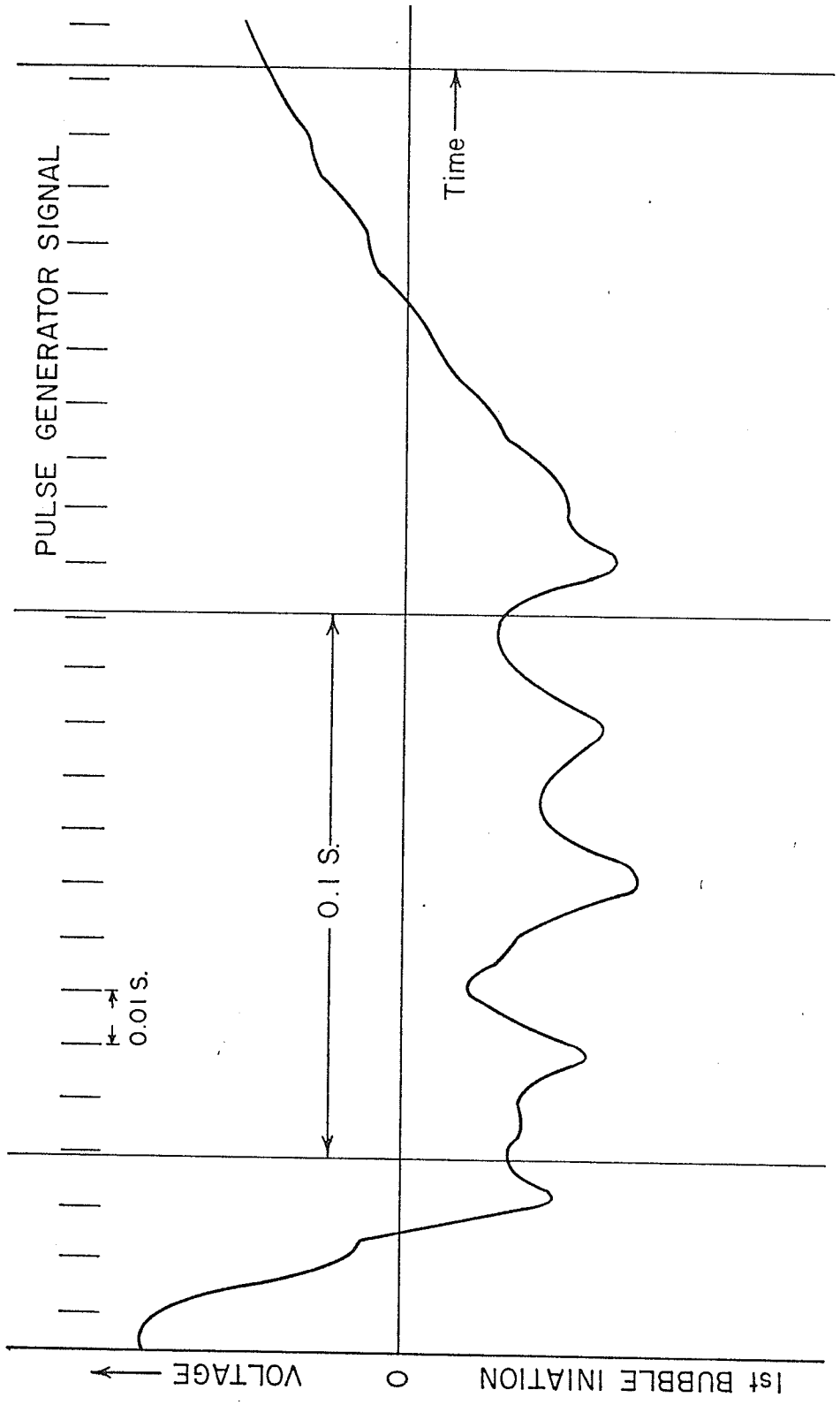

Fig. 5.2 Recorded Signal for Heater 1 - Bubbles 25-3-1 to 25-3-5 (Paper Speed 800 mm/s, Air Flow Rate = 0.94 cc/s)

Fig. 5.2

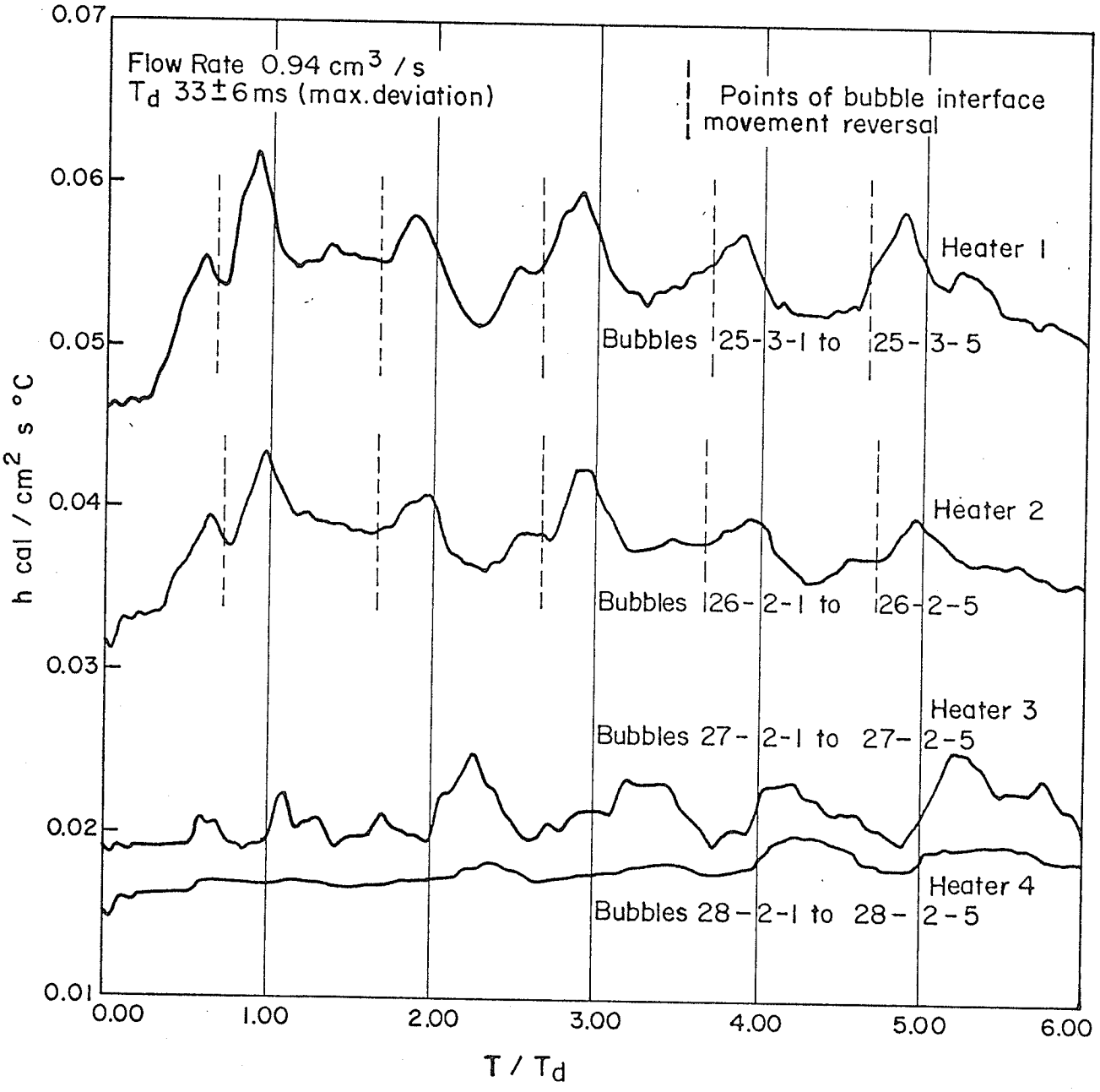

Fig. 5.3 Heat Transfer Results

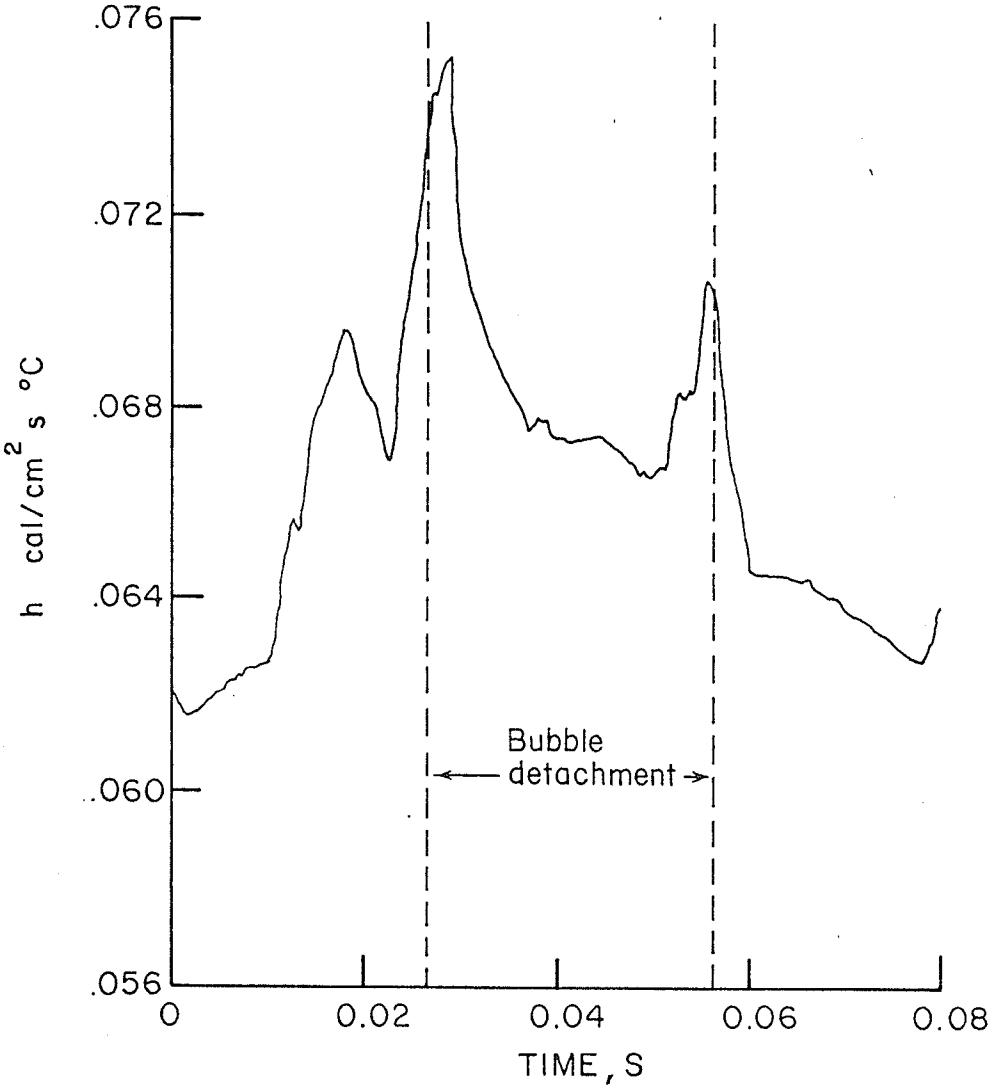

Fig. 5.4 Heat Transfer Fluctuation Over Heater 1 During Two Bubble Cycles (Film 29, Air Flow Rate 2.2 cc/s)

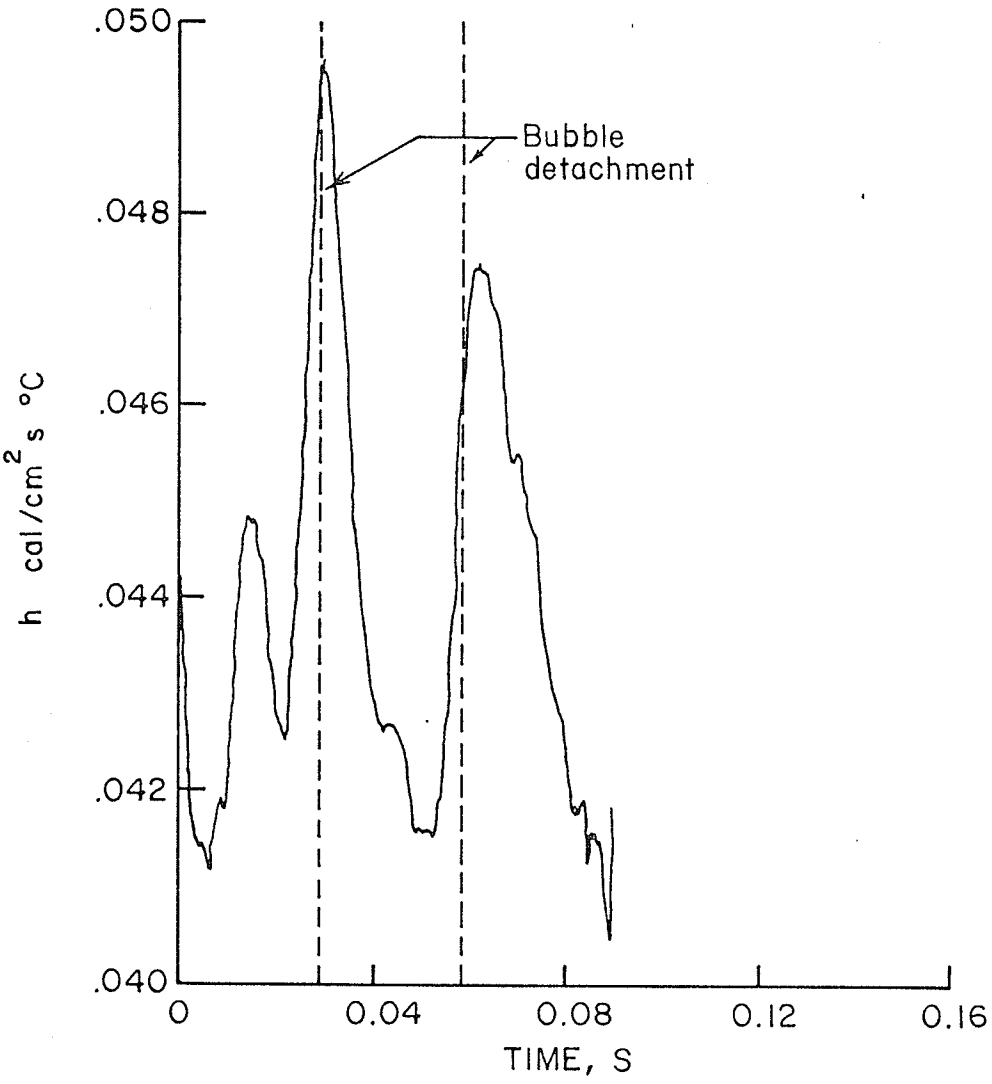

Fig. 5.5 Heat Transfer Fluctuation Over Heater 2 During Two Bubble Cycles (Heater 2, Film 30, Air Flow Rate 2.2 cc/s)

Table 5.1

Summary of Results

Heater No.	Bubble Series	Air Flow Rate cc/s	Av. T_d ± Extreme Deviation ms	Electric Current Through Heater mA	Av. Temp. Difference θ_o °C	Max. Temp. Drop (θ) Below Av. °C	h av. cal/cm²s°C	h min. cal/cm²s°C	h max. cal/cm²s°C	Figure
1	25-3	0.94	$34.5^{+3}_{-3.5}$	36	8.65	0.80	0.0515	0.04444	0.0622	5.3
2	26-2	0.94	35.7 ± 3.2	35	11.4	0.485	0.0365	0.0311	0.0436	5.3
3	27-2	0.94	$34.6^{+3.4}_{-1.6}$	21	9.05	0.314	0.0206	0.0186	0.0254	5.3
4	28-2	0.94	30 ± 5	33	24	0.423	0.0178	0.0156	0.0199	5.3
1	Film 29	2.2	29 ± 2	36	6.6	0.3504	0.067	0.0585	0.0753	5.4
2	Film 30	2.2	27 ± 1.8	35	10.6	0.1885	0.0435	0.0404	0.0496	5.5

radius from the plate is shown in Fig. 5.3 for each bubble on Heaters 1 and 2. As the bubble interface is moving inward a second rise in h, larger in magnitude than the first, was observed. The maximum h is reached as the bubble was about to detach from the surface followed by a decrease in h after the bubble leaves the surface.

2. The first heat-transfer increase is most apparent for the first bubble of each series while it is less clear or absent for the subsequent bubbles.

3. The heat-transfer rise at detachment was obtained for all the bubbles for all heaters with only a small time lag between the signal generated by each following heater, i.e., from 1 through 4. This is demonstrated in Fig. 5.3 where it can be seen that while the h peak is just before detachment for Heater 1, it is almost at detachment for Heater 2 and after detachment for Heaters 3 and 4.

4. The signal intensity decreases with distance from the bubble site, that is, the peak values as well as the average values of the heat-transfer coefficient. This is also shown in Fig. 5.3 where the peak and average values of h can be compared.

5. The highest value of the heat-transfer coefficient during experiments was 555 BTU/hr ft^2 °F (0.0753 $cal/cm^2 s°C$) obtained for Heater 1 with an average value of 493 BTU/hr ft^2 °F (0.067 cal/cm^2 s °C). The value of the heat-transfer coefficient with no bubbling was approxi-

mately 114.5 BTU/hr ft^2 °F (0.0156 cal/cm^2 s °C) for all the heaters at the same current conditions as during bubbling.

5.2 Flow Pattern

To explain the heat transfer variations in terms of the liquid motion on the surface, it was desirable to examine the flow pattern near the surface surrounding a bubble. High-speed cine films were taken of hydrogen bubbles around the air bubble generated at the orifice in water. The air flow rate was set at the same value (0.94 cc/s) as for the heat-transfer experiments analyzed in detail. However, it should be noted that the bubble break-off diameter in water was about 1.5 times that in hexane according to measurements taken from photographs; this ratio agreed with that predicted using the correlations of Zuber [45] and Fritz [41].

Fig. 5.6 reproduces four frames from one bubble cycle in water in the flow visualization experiments. Since individual hydrogen bubbles could be identified and followed during the life cycle of any main bubble, Fig. 5.7 could be constructed; this figure allows the relationship among the liquid flow motions, bubble cycle and heat transfer to be examined in detail. It will be seen that the shape of the h versus T/T_d curves can be explained by reference to the liquid flow movement near the heater surface.

In Fig. 5.7, the first bubble in a series of five in

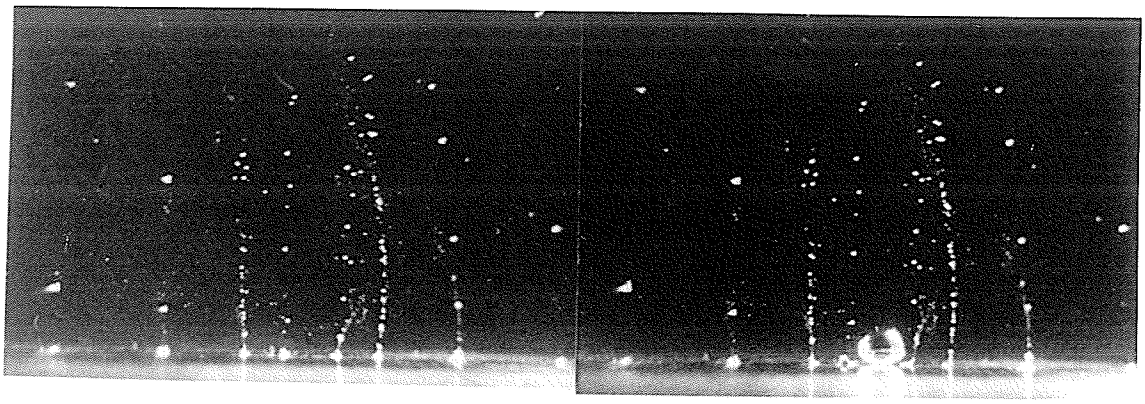

(a) (b)

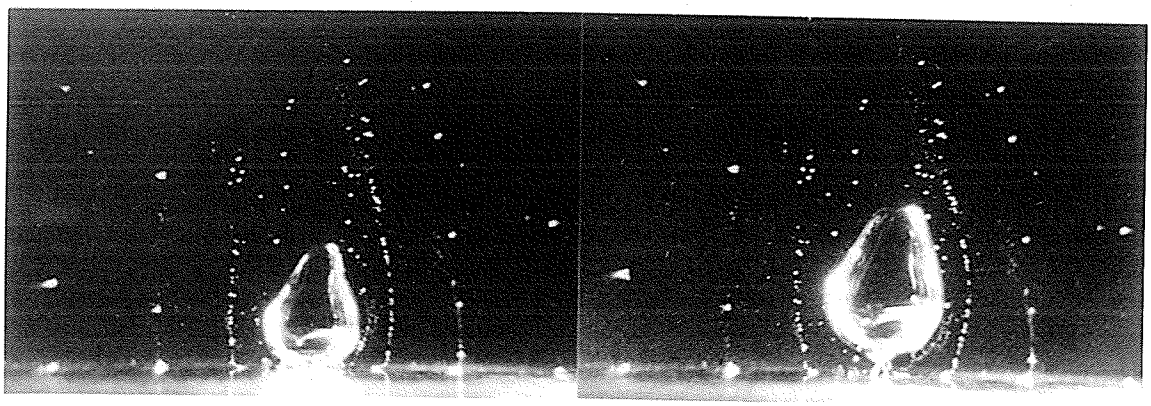

(c) (d)

Fig. 5.6 Flow Visualization Photographs

(Bubble No. 18-1-1; air flow rate 0.94 c.c/s; camera speed 1000 pps; T/T_d for (a) 0.0, (b) 0.32, (c) 0.61, (d) 1.0)

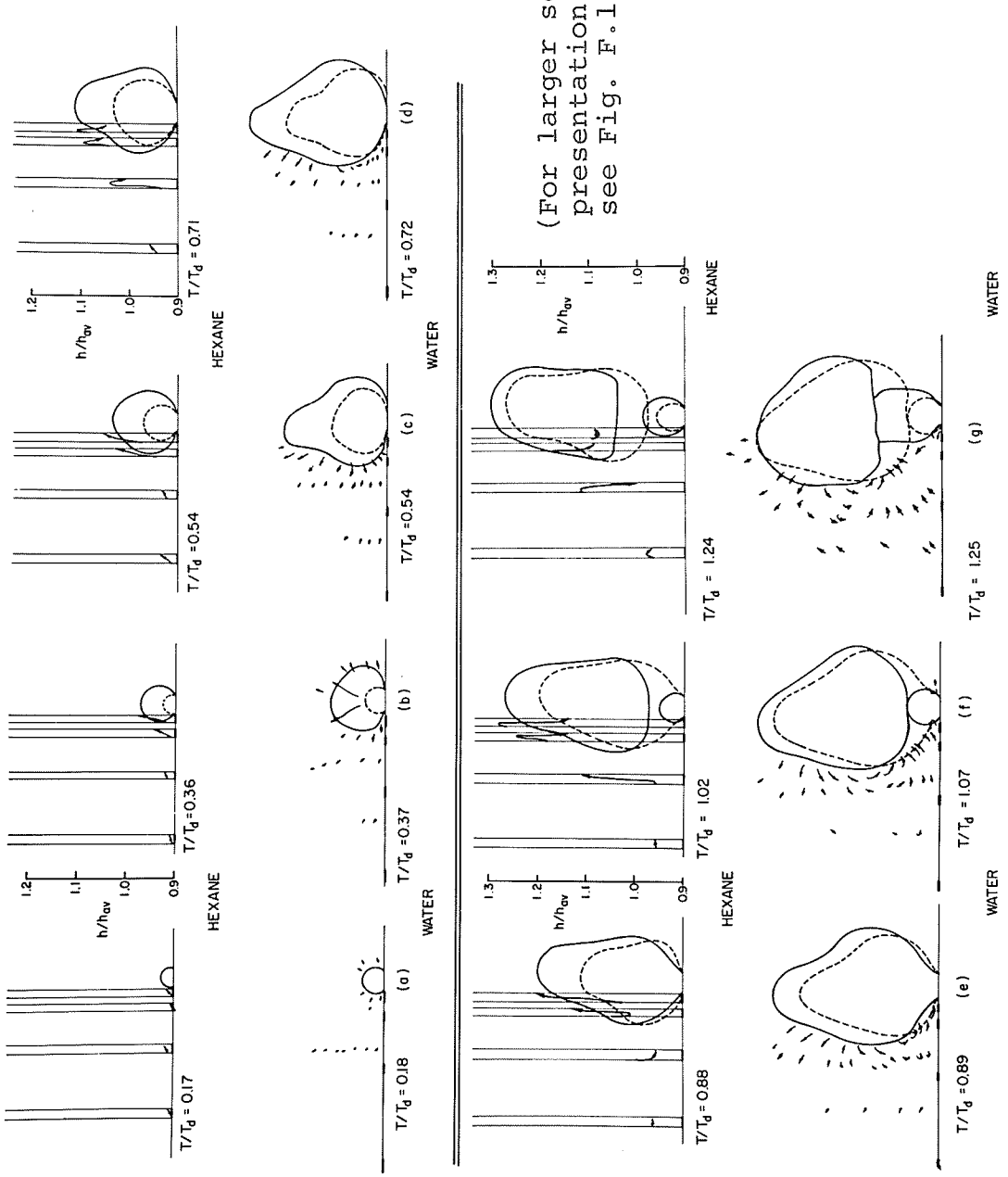

Fig. 5.7 Combined heat transfer and flow visualization results (Hexane bubble 25-3-1, water bubble 18-1-1)

hexane has been traced at various T/T_d from projected photographic films; the bubble used is the first one for Heater 1 in Fig. 5.3. The intervals of time between any two successive sketches (a, b, c, etc.) are approximately equal, the dashed line in the sketch showing the bubble profile at the time of the previous sketch. The heat-transfer coefficient is also shown for the four heaters; the scale is h/h_{av} where h_{av} is the time average of h including the time between series of bubbles. The change in h/h_{av} for any heater is given above the heater representing the change in h during the time interval between the previous sketch and the one under consideration.

The water bubble* shown in Fig. 5.7 is the first of a series of five and is reproduced in the same manner as the hexane bubble. The detachment time T_d for the hexane bubble is 34.5 ms while that for the water bubble is 28 ms. The arrows around the air bubble in water show the movement of individual hydrogen bubbles in the time interval between the previous sketch and the sketch under consideration; similarly for changes in h/h_{av} shown with the hexane bubble. For the water bubble, fictitious heaters are shown in each sketch at the same ratio of distances to detachment diameter D_d as for the hexane bubbles. The same figures as well as similar figures drawn for the last bubble of the series are shown

---

*'Water bubble' here is understood to mean an air bubble in water, 'hexane bubble' would mean an air bubble in hexane.

in much larger scale in Appendix F.

In detail, then, in Fig. 5.7, (a), (b) and (c) show that, between initiation and $T/T_d \simeq 0.6$, the flow near the surface is radially outward and the heat-transfer coefficients increase, with the two heaters nearest the bubble where the liquid velocities are the highest, showing the most marked increases. Between (c) and (d) the flow near the heat transfer surface begins to decelerate, causing a maximum in, and then a decreasing h for Heaters 1, 2 and 3. At (e) the bubble interface near the heat-transfer surface is moving inward and the flow has gone through a reversal in direction which causes first a minimum in h and then a rapidly increasing h for Heaters 1 and 2 as the flow accelerates inward. Between (e) and (f) the bubble detaches and at Heaters 1 and 2 the flow is slowed down by the newly-appearing bubble whose interface is moving outward, thus causing a decrease in h. At (g), h reaches a minimum, at least for Heater 1. Note that the maximum in h occurs approximately at detachment. Heater 3 follows the same behavior as Heaters 1 and 2 except that there is a time lag; indeed there appears to be a definite time lag from Heater 1 to Heater 2 to Heater 3. Heater 4, in general, appears to follow the same behavior as the other heaters, but with a time lag. However, as can be seen in Fig. 5.3, the changes in h for Heater 4 are small and it is difficult to justify examining the variations in detail.

As the cycle continues, there are two effects opposing each other; one is the inward and upward flow generated by the detached and rising bubble, the other is the radially outward flow generated by the growing bubble at the orifice. As the bubble at the orifice begins its detachment phase (defined here as beginning when the bubble interface near the heat-transfer surface starts to move inward, and ending at detachment) the inward flow dominates to give another maximum in h approximately at detachment. The peak in h at detachment is apparent for all bubbles for all heaters. As for the effect of the bubble growth phase, it is expected to be more significant at low bubbling frequencies, where there is enough time for the inward flow to die out before the formation of a new bubble starts a new cycle.

After the last bubble of the series, the flow resembles a reversed stagnation flow. This flow decays with h dropping roughly 15 per cent below its time-average value before the next bubble series begins, for the conditions shown in Fig. 5.3, at roughly 150 ms later.

The above-mentioned reversed stagnation flow agrees with Tien's model [40]. However, the model neglects any outward cyclic motion (as observed in the present study); as this outward movement of liquid also generates high heat-transfer coefficient, Tien's model should be considered as a qualitative one.

Some of the results of Bard and Leonard are shown in

comparison with the present results in Figs. 5.8, 5.9 and 5.10. In Fig. 5.8 the shape of h versus T curves is examined. The signal produced by Heater 1 in the present study is compared with that produced by their Heater 1 operating under the most similar conditions (as regards bubbling frequency, orifice diameter and heater distance from orifice); the conditions are listed on the figure. Figures 5.9 and 5.10 present values of h_{peak} (the 'peak' or maximum heat-transfer coefficient obtained for each heater) and h_{av} at different distances from the orifice edge, respectively. The agreement with the Bard and Leonard results is good, showing essentially the same shape of h against T with closely-corresponding values of h_{av} and h_{peak}.

Bard and Leonard reasoned that the detachment phase governed the agitation heat transfer. The present study does provide evidence that h_{peak} is generated at detachment. However, although it was observed in most of Bard's graphs [2] of h versus T that there are two heat transfer peaks for each bubble, he referred to the first peak (the smaller one) as a "violent fluctuation". This first peak certainly appears to be the same as observed in the present experiment, i.e., to be caused by the outflow during bubble growth.

5.3 Relation to Boiling

The present experimental results indicate that the

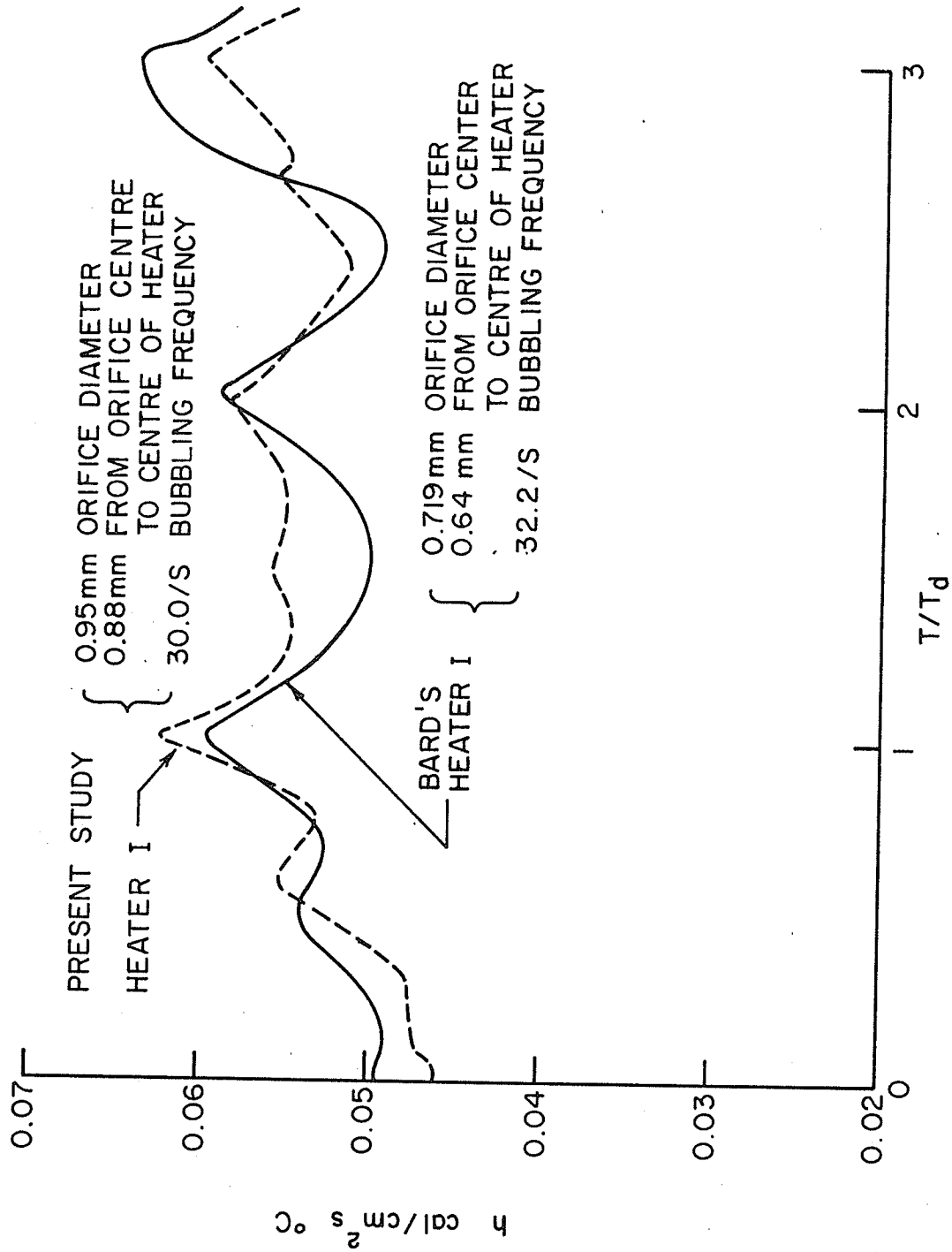

Fig. 5.8 Comparison Between the Signal Shapes in the Present Experiment and in the Bard and Leonard Experiment

Fig. 5.8

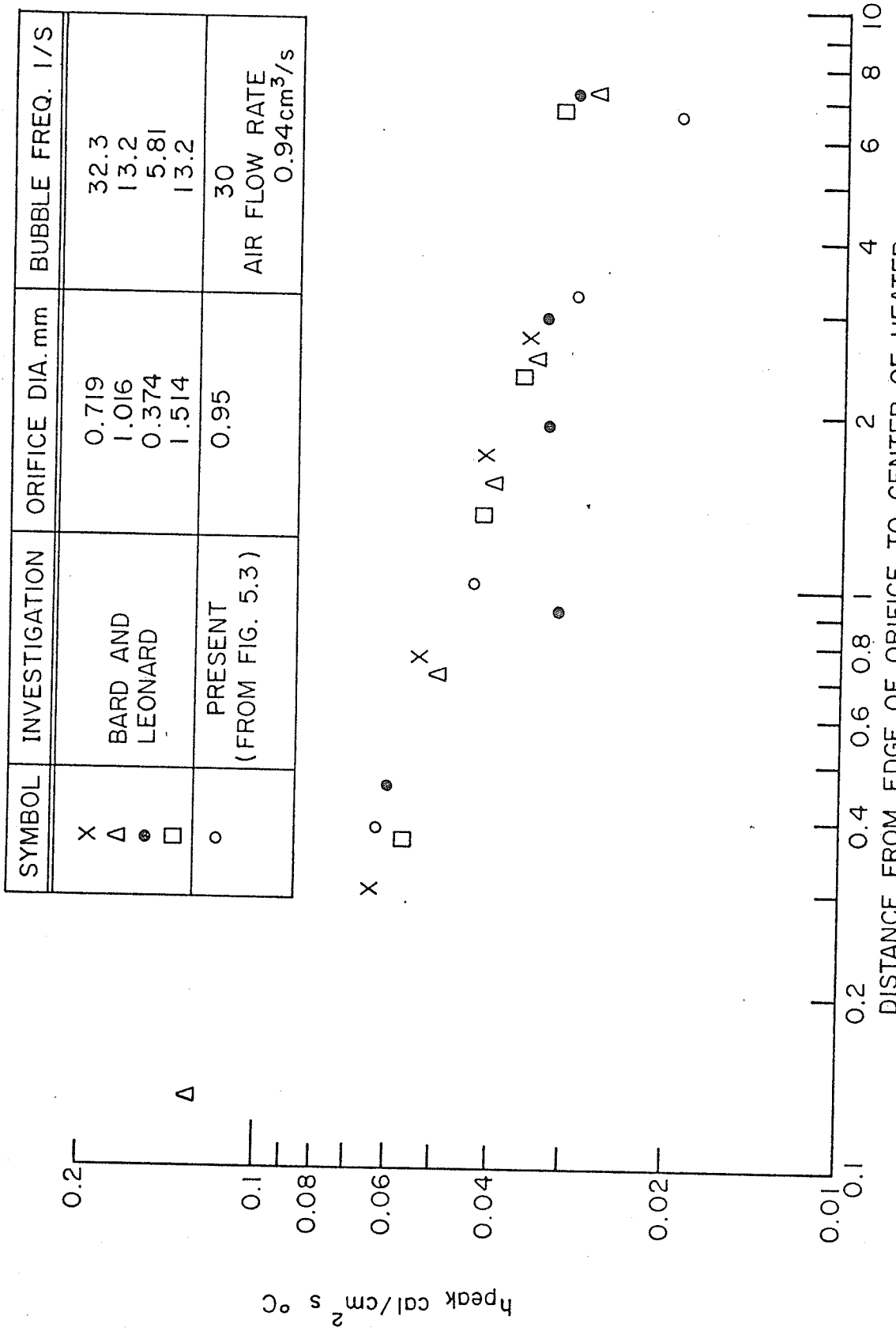

Fig. 5.9 Comparison of Present Heat Transfer Peaks with the Bard and Leonard Results

Fig. 5.9

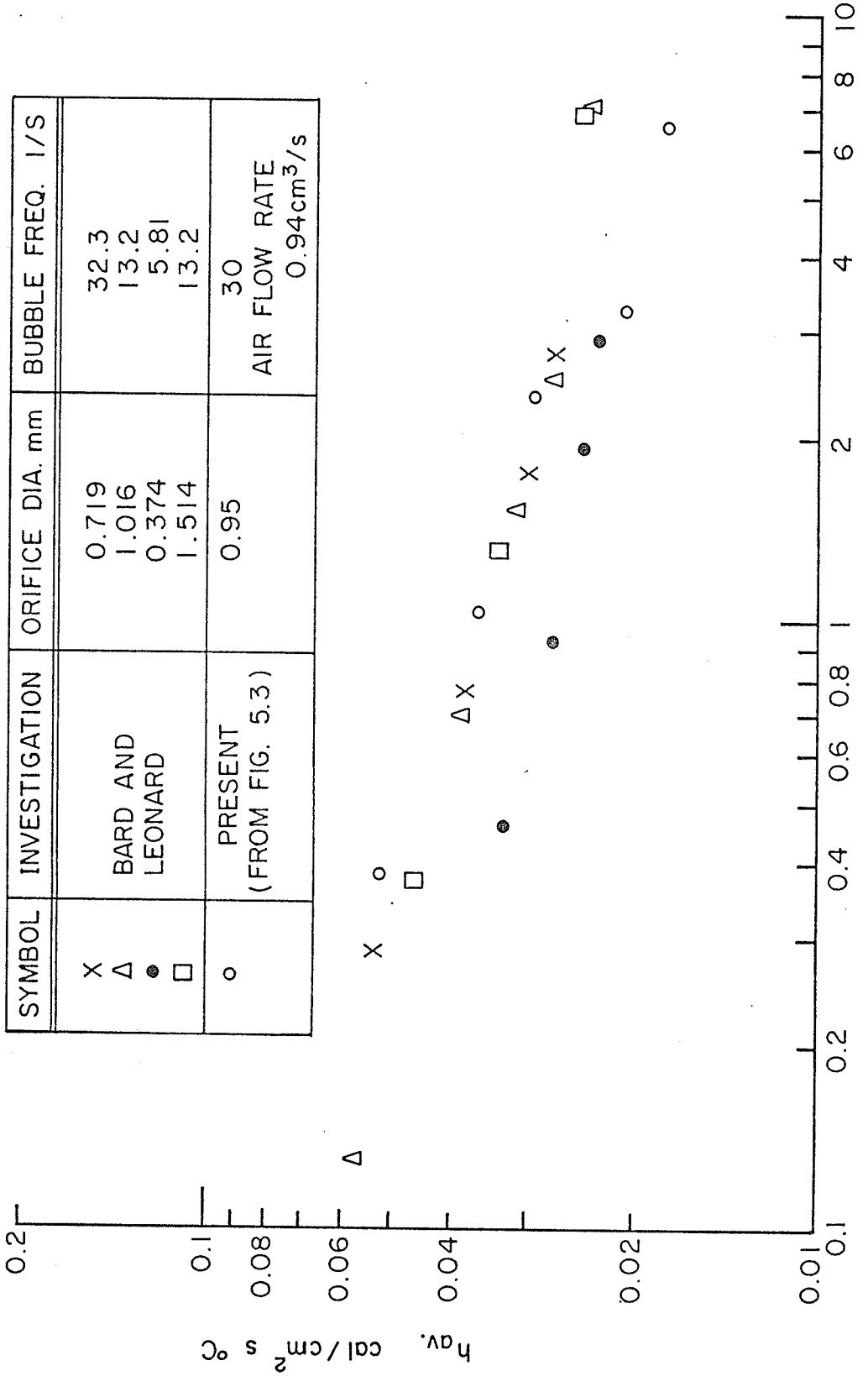

Fig. 5.10 Comparison of the Average Heat-transfer Coefficient Values with the Bard and Leonard Values

Fig. 5.10

bubble-induced agitation plays a significant role in promoting the heat transfer in barbotage at the stage of bubble detachment, although to a lesser extent during bubble growth. Maximum values of the heat-transfer coefficient of approximately 555 BTU/hr ft^2 °F (0.0735 cal/cm^2 s °C) were obtained at bubble detachment. This value is about five times that obtained with no bubbling. Heat-transfer coefficient close to this maximum value might be expected over the surface in the presence of many closely packed bubbling sites. In pool boiling of hexane at atmospheric pressure, the observed values for the heat-transfer coefficient range between 150 and 3,000 BTU/hr ft^2°F (0.0204 - 0.416 cal/cm^2 s °C) depending on the surface conditions and the amount of superheat [24]. This shows that the peak values of h in barbotage are within the range of h obtained for boiling, which suggests that agitation effects make a significant contribution in boiling for increasing h above free convective values. However, in order to assess the relative contribution of latent heat effects and agitation in boiling, more data, currently unavailable for hexane boiling at the same conditions as in barbotage, is still needed.

As was mentioned in Chapter 2, Fontana [10], in a nucleate boiling experiment with water, observed two heat transfer rises per bubble cycle. He defined h*, an equivalent heat-transfer coefficient, as $h^* = Q_b/\pi r_a^2$ where

Q_b is the heat transferred from an area equal to the maximum area of contact of the bubble with the surface, and r_a is the radius of this maximum area of contact. Fig. 5.11 shows the variation of h*, as calculated from Fontana's data, plotted against T/T_d where T_d is the time between bubble birth and detachment. On the same graph (to a different scale) the heat-transfer coefficient h for Heater 1 of the present experiment is plotted.

As expected, h* shows a very large peak generated due to microlayer evaporation under the bubble at the early stages of bubble growth in nucleate boiling as compared to a small peak of h due to liquid motion away from the bubble in barbotage. Shortly before bubble detachment, the area of contact of the bubble in Fontana's experiments is observed to be very small and much less than "πr_a^2"; thus, h* would approximate the heat-transfer coefficient from the annular area around the bubble base and h* would be expected to have the same behavior as h of the first heater in the present experiment. Fig. 5.11 shows that h* and h both have a maximum approximately at bubble detachment.

It is evident that the high heat-transfer coefficient values obtained during bubble growth in boiling due to microlayer evaporation is also aided by agitation induced by the bubble, although it should be noted that agitation affects a larger surface area over a longer time period than does microlayer evaporation. At the time of bubble detachment

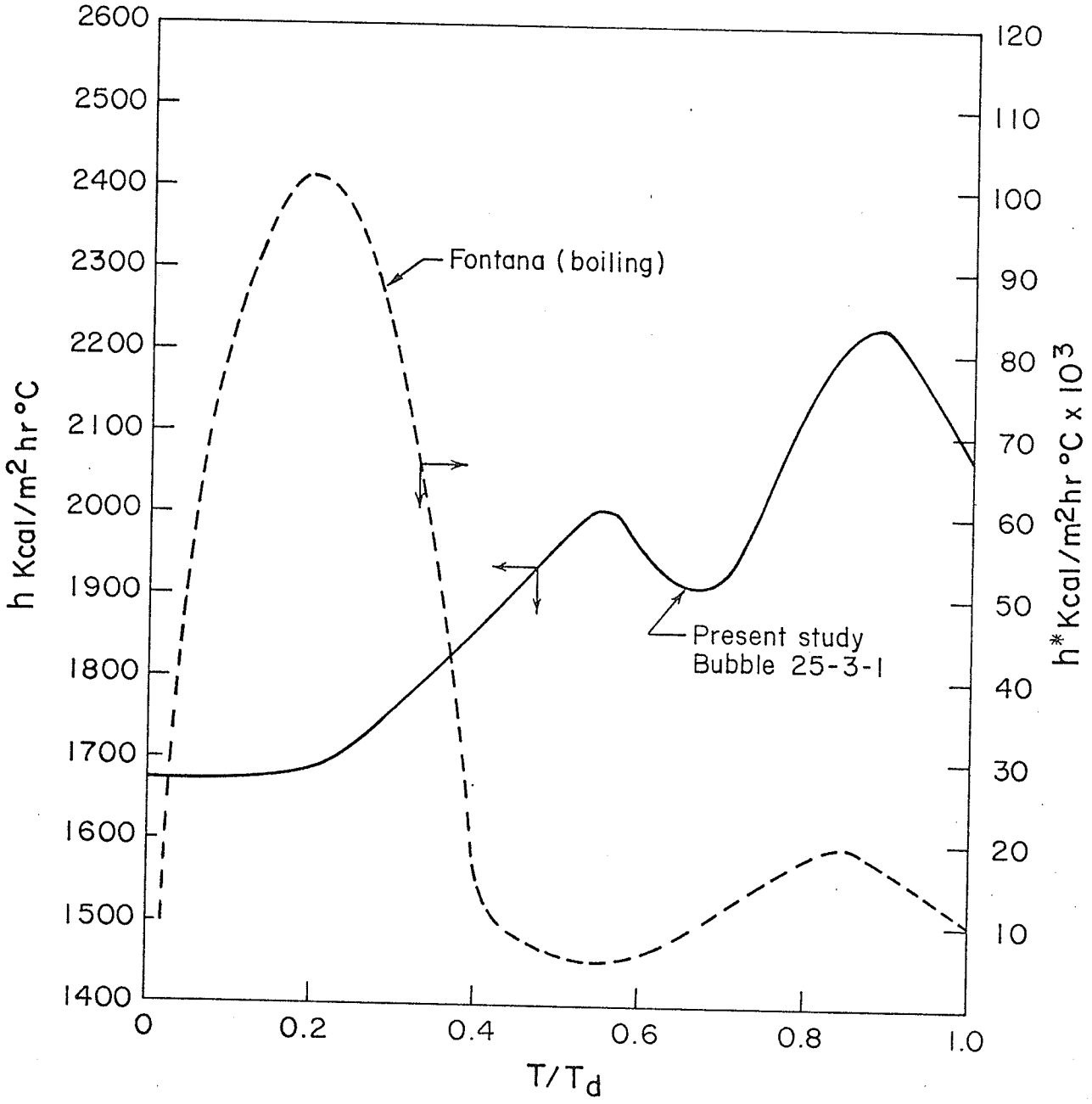

Fig. 5.11 Comparison of the Present Barbotage Results with Fontana's Results of Nucleate Boiling in Water

the high heat transfer observed is only a result of the bubble induced agitation on the surface.

5.4 Suggestions for Future Research

1. For a more precise description of the heat-transfer behaviour over the different heaters, attempts should be made to photograph the different signals generated by all the heaters on the same film together with the bubble image.

2. Flow visualization studies with the same liquid (hexane in the present case) and performed simultaneously with the heat-transfer experiments would be advantageous.

3. Carrying out similar experiments with an actual boiling site substituted for the orifice using the same liquid at the same temperature should allow the relative contribution of agitation and latent heat effects to be established. It would be instructive as well to use simultaneous flow visualization in such an experiment.

CHAPTER 6

CONCLUSIONS

1. The method of combined high-speed cine photography, oscillography and the described flow visualization techniques provides a method well-suited to the detailed study of heat transfer and flow patterns in barbotage. In particular, it is possible to explain the shape of the instantaneous heat-transfer coefficient versus time curves in terms of bubble-induced liquid motion near the heaters.

2. The present results give strong evidence that the agitation created by the bubble during its life cycle has a great effect in promoting the heat transfer on the surface during bubble growth and detachment phases.

3. In barbotage, the maximum heat-transfer coefficient is generated at detachment.

REFERENCES

1. Akturk, N.U., Heat transfer from a heated porous surface to a pool of liquid with gas injection at the interface. Proceedings of the Symposium on Two Phase Flow, Vol. II, Exeter, D501 (1965).

2. Bard, Y., Heat transfer in simulated boiling. Ph.D. Dissertation, Columbia University (1964).

3. Bard, Y. and E.F. Leonard, Heat transfer in simulated boiling. Int. J. Heat Mass Transfer 10, 1727 (1967).

4. Bankoff, S.G., A note on latent heat transport in nucleate boiling. A.I.Ch.E. Jl 8, 630 (1962).

5. Bankoff, S.G. and J.P. Mason, Heat transfer from the surface of a steam bubble in turbulent subcooled liquid stream. A.I.Ch.E. Jl 8, 30 (1962)

6. Carmichael, C., Mechanical Engineering Handbook, 12th Edition, 1-04 (1952).

7. Churchill, R.V., Fourier Series and Boundary Value Problems, 2nd Edition, 89 (1963).

8. DiMenza, R.G., Flow regimes in a two phase boiling analogy. S.M. Thesis, Dept. Nuclear Engineering, Massachusetts Institute of Technology (1958).

9. Foltz, G.E. and R.B. Mesler, The measurement of surface temperatures with platinum films during nucleate boiling of water. A.I.Ch.E. Jl 16, 44 (1970).

10. Fontana, D.H., Simultaneous measurement of bubble growth rates and thermal flux from the heating wall to the boiling fluid near the nucleation site. Int. J. Heat Mass Transfer 15, 707 (1972).

11. Forster, H.K. and R. Greif, Heat transfer to a boiling liquid - Mechanisms and correlations. Trans. ASME, J. Heat Transfer, Series C, 81, 43 (1959).

12. Forster, H.K. and N. Zuber, Dynamics of vapor bubbles and boiling heat transfer. A.I.Ch.E. Jl 1, 531 (1955).

13. Frea, W.J. and J.H. Hamelink, Heat transfer from the wall of a porous solid involving gas injection and vaporization. Trans. ASME, J. Heat Transfer, Series C, 92, 153 (1970).

14. Gose, E.E. and A. Acrivos and E.E. Petersen, Heat transfer to liquids with gas evolution at the interface, presented at the Mexico City meeting of the A.I.Ch.E. (1960).

15. Greif, R., Heat transfer with gas injection at the surface. Int. J. Heat Mass Transfer 8, 1253 (1965).

16. Gunther, F.C. and F. Kreith, Photographic study of bubble formation in heat transfer to subcooled water. Prog. Rep. No. 4-120, Jet Prop. Lab., Calif. Inst. Tech. (1950).

17. Hara, T., The mechanism of nucleate boiling heat transfer. Int. J. Heat Mass Transfer 6, 959 (1963).

18. Hendricks, R.C. and R.R. Sharp, Initiation of cooling due to bubble growth on a heating surface. NASA TND-2290 (1964).

19. Hospeti, N.B. and R.B. Mesler, Deposits formed beneath bubbles during nucleate boiling of radioactive calcium sulfate solution. A.I.Ch.E. Jl 11, 663 (1965).

20. Hsu, S.T. and F.W. Schmidt, Measured variations in local surface temperatures in pool boiling of water. Trans. ASME, J. Heat Transfer, Series C, 83, 254 (1961).

21. Hsu, Y.Y. and R.W. Graham, An analytical and experimental study of the thermal boundary layer and ebullition cycle in nucleate boiling. NASA TND-594 (1961).

22. Handbook of Chemistry and Physics, Chemical Rubber Publishing Company, 44th Edition, 1032 (1962).

23. Kudirka, A.A., Two-phase heat transfer with gas injection through a porous boundary surface. U.S. Atomic Energy Commission Report ANL-6062 (1964).

24. Kurihara, H.M. and J.E. Mayers, The effect of superheat and surface roughness on boiling coefficients. A.I.Ch.E. Jl 16, 83 (1960).

25. Kutateladze, S., Fundamentals of heat transfer (1963).

26. L'Ecuyer, H.R. and S.N. Murthy, Energy transfer from a liquid to gas bubbles forming at a submerged orifice. NASA TND-2547 (1965).

27. Lubin, G., Handbook of Fiberglass and Advanced Plastic Composites (1969).

28. Maissel and Glang, Handbook of Thin Film Technology, 13-10 (1970).

29. Martin, B.W. and G.E. Sims, Forced convection heat transfer to water with airinjection in a rectangular duct. Int. J. Heat Mass Transfer 14, 1115 (1971).

30. Mixon, F.D., W.Y. Chon and K.G. Beatty, The effect of electrolytic gas evolution on heat transfer. Chem. Eng. Prog. Symp. Series 56, 75 (1960).

31. Moore, F.D. and R.B. Mesler, The measurement of rapid temperature fluctuation during nucleate boiling of water. A.I.Ch.E. Jl 7, 620 (1961).

32. Rallis, C.J. and H.H. Jawurek, Latent heat transport in saturated nucleate boiling. Int. J. Heat Mass Transfer 7, 1051 (1964).

33. Rogers, T.F. and R.B. Mesler, An experimental study of surface cooling by bubbles during nucleate boiling of water. A.I.Ch.E. Jl 10, 656 (1964).

34. Rohsenow, W.M., A method of correlating latent heat transfer data for surface boiling of liquids. Trans. ASME 74, 969 (1952).

35. Rohsenow, W.M. and J.A. Clark, A study of the mechanism of boiling heat transfer. Trans. ASME 73, 609 (1951).

36. Ruckenstein, E., A physical model for nucleate boiling heat transfer. Int. J. Heat Mass Transfer 7, 191 (1964).

37. Sharp, R.R., The nature of liquid film evaporation during nucleate boiling. NASA TND-1997 (1964).

38. Sims, G.E. and P. Duffield, Comparison of heat transfer coefficients in pool barbotage and saturated pool boiling, Transactions of the CSME, Paper 70-CSME-12, published in the Engineering Journal, May 1971.

39. Sims, G.E., U. Akturk and K.O. Evans-Lutterodt, Simulation of pool boiling heat transfer by gas injection at the interface. Int. J. Heat Mass Transfer 6, 531-575 (1963).

40. Tien, C.L., A hydrodynamic model for nucleate pool boiling. Int. J. Heat Mass Transfer 5, 533 (1965).

41. Tong, L.S., Boiling Heat Transfer and Two-phase Flow, 18 (1965).

42. Van Stralen, S.J.D. and W.M. Sluyter, Local temperature fluctuations in saturated pool boiling of pure liquids and binary mixtures. Int. J. Heat Mass Transfer 12, 187 (1969).

43. Wallis, G.B., A gas-liquid analogue of nucleate boiling. Nuclear Power 5, 99 (1960).

44. Wallis, G.B., The analogy between the bubbling of air into water and nucleate boiling at saturation temperature. U.K. Atomic Energy Authority Report AEEW-R 28 (1960).

45. Zuber, N., Hydrodynamic aspects of boiling heat transfer (Thesis) U.S. Atomic Energy Commission Report AECU-4439 (1959).

46. Zuber, N., The region of isolated bubbles and the similarity with natural convection. Int. J. Heat Mass Transfer 6, 53 (1963).

APPENDICES

APPENDIX A

TYPES OF GAS FLOW IN BARBOTAGE

As regards gas flow into a bubble during formation, there are two limiting cases [26]:

(a) Constant gas flow rate; which pertains to bubble formation in which the rate of gas flow into the bubble is essentially constant. Such has been found [A.1] to be the case, for example, for bubble formation at the tip of a long capillary tube. The flow rate of gas is governed by the pressure drop in the capillary, and perhaps some controlling device upstream of the capillary. Nevertheless, the pressure fluctuations at the top of the capillary which result from bubble formation are not transmitted upstream. Thus, the flow is essentially independent of the bubble formation process.

(b) Constant pressure; which pertains to bubble formation at an orifice which is supplied with gas from an ante-chamber (defined as the volume of the gas supply system from the orifice to the point where a large pressure drop occurs in the system) at constant pressure. This case is approximated in practice when an orifice is supplied

with gas by a very large ante-chamber. The rate of gas flow into a bubble for such a system has been found to vary throughout the formation period [A.1].

An actual bubble formation system will operate under conditions in between the aforementioned limiting case of flow and, therefore, will exhibit, to some extent, a coupling of the bubble formation mechanism with the gas supply system as well as a possible dependence of the process of bubble formation upon (i) the volume of the ante-chamber, and (ii) the L/D ratio of the orifice channel. Hughes *et al.* [A.2] have derived two dimensionless groups to characterize the influence of the gas supply system upon bubble formation by considering the acoustical capacitance of the ante-chamber and the resistance to flow of the orifice channel. These are:

$$N_C = \frac{g(\rho_L - \rho_g)V_c}{A_o \rho_g c^2} \qquad (A.1)$$

and

$$N_R = L/D_o \qquad (A.2)$$

where

g = acceleration of gravity

ρ_L = density of the liquid

ρ_g = density of the gas

V_c = ante-chamber volume

A_o = orifice area

c = acoustic speed in the gas

L = length of the orifice channel

D_o = orifice diameter

Values of the ante-chamber volume which make $N_C \ll 1$ approximate the condition of 'constant flow rate', whereas those which make $N_C \gg 1$ approximate the condition of a constant-pressure one. Further, it has been observed [A.3] that an ante-chamber volume 10,000 times that of the bubble volume is required to approximate the condition of constant-pressure bubbling. The influence of the orifice channel, on the other hand, has been observed [A.2] to be significant only when $N_R > 100$ or $N_R < 1$. Though not thoroughly tested, the parameters N_C and N_R have provided one means of characterizing the types of gas injection systems for the two limiting cases of flow.

In the present experiment, in order to operate under constant-pressure conditions, the volume of the ante-chamber was designed to give a value of 200 for the parameter N_C. The value of the parameter N_R was 1.32.

APPENDIX A REFERENCES

A1. Davidson, J.F. and B.O.G. Schuler, Bubble formation at an orifice in a viscous liquid. Trans. Inst. Chem. Engr. 38, 144 (1960).

A2. Hughes, R.R., A.E. Handlos, H.D. Evans and R.L. Maycock, The formation of bubbles at simple orifices. Chem. Eng. Prog. 51, No. 12, 556 (1955).

A3. Turner, G.M., Formation of bubbles at simple orifices, presented at the San Francisco A.I.Ch.E. meeting, September 14, 1953, as reported by H.R. L'Ecuyer and S.N. Murthy, Ref. 26 of this thesis.

APPENDIX B

CALCULATION OF THE HEAT-TRANSFER COEFFICIENT

This appendix gives the method for converting the voltage signal produced by the heaters into heat-transfer coefficient. The method follows exactly that given by Bard [2] except for the point discussed in Sections B.2 and B.3.

B.1 Surface Temperature Computation

As mentioned before, the signal was measured for each frame from the photographic film projected on a paper screen. The scale between this measured signal and the actual signal was determined as follows: before photographing the bubbles, the camera was set to photograph the scope screen only, through the auxiliary lens. Using the level control of the oscilloscope, the trace was moved to the extreme upper position of the screen which is equivalent to a known voltage depending on the oscilloscope setting. The camera was then run at low speed (20 pps) photographing this upper limit. The procedure was repeated photographing the lower limit and the central point of the screen. As the film was projected the three lines were

marked and the scale of projection of the signal was determined accordingly in volts/cm of projection.

The surface temperature of the heater can be calculated at each time interval in the following way. Let the voltage across the heater be given by v. Referring to Fig. 4.1 we get

$$v = \frac{RE}{R+R_1} \quad ,$$

or

$$v = E\left(1 - \frac{R_1}{R+R_1}\right) \quad . \tag{B.1}$$

Differentiation yields the voltage fluctuation dv that results from a small resistance fluctuation dR;

$$dv = \frac{ER_1}{(R+R_1)^2} dR \quad , \tag{B.2}$$

or

$$dR = \frac{(R+R_1)^2}{ER_1} dv \quad .$$

Since $R = R_o' + \gamma\theta$, then

$$\frac{d\theta}{dR} = \frac{1}{\gamma} \quad ,$$

i.e.,

$$d\theta = \frac{d\theta}{dR} dR = \frac{(R+R_1)^2}{ER_1\gamma} dv \quad ,$$

or

$$\tilde{\theta} = d\theta = \frac{(R+R_1)^2 D}{ER_1\gamma\phi} \quad . \tag{B.3}$$

where

D is the recorded signal

ϕ is the proportionality between the recorded data and the actual signal

R is the average resistance of the film

θ is the average temperature of heater with respect to bulk liquid temperature.

B.2 Conversion of Temperature Fluctuations to Heat-transfer Coefficient Fluctuations

To establish the relation between the temperature θ and the heat-transfer coefficient h. Bard [2] assumed that a film of infinitesimal thickness, infinite length and width 2a is placed on the upper surface of an infinitely wide and thick plate and immersed in fluid (Fig. B.1).

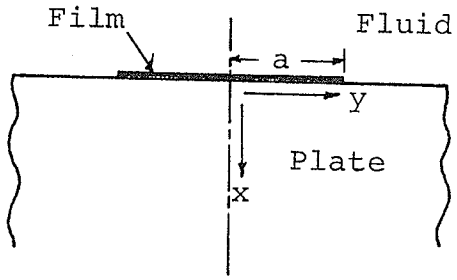

Fig. B.1

It is assumed that Fourier's law governs the conduction of heat through the solid, that the bulk temperature of the fluid is constant at t=0, and that the heat transfer

from the solid to the liquid is proportional to the difference between the solid surface and bulk fluid temperatures. Thus, in the plate:

$$\frac{\partial t}{\partial T} = \alpha\left(\frac{\partial^2 t}{\partial x^2} + \frac{\partial^2 t}{\partial y^2}\right) \qquad (B.4)$$

where $\alpha = \frac{k}{\rho C_p}$ is the thermal diffusivity of the plate material. On the film ($x=0$, $-a \leq y \leq a$), the heat generated per unit area $F(y)$ is carried away by conduction into the plate and by convection into the fluid, thus

$$F(y) = ht - k\frac{\partial t}{\partial x} \quad \text{at } x=0 \quad . \qquad (B.5)$$

Clearly

$$F(y) = \begin{cases} q & |y| \leq a \\ 0 & |y| > a \end{cases} \qquad (B.6)$$

On the lower face of the plate which is considered at $x=\infty$, the condition is

$$t = 0 \qquad (B.7)$$

Also, it follows from symmetry that

$$t(T,x,y) = t(T,x,-y) \quad \text{and} \quad \frac{\partial t}{\partial y} = 0 \text{ at } y=0 \qquad (B.8)$$

(a) Steady state behavior

At steady state $\frac{\partial t}{\partial T} = 0$, i.e., $t(T,x,y) = t_o(x,y)$ and Equation (B.4) reduces to

$$\frac{\partial t_o^2}{\partial x^2} + \frac{\partial t_o^2}{\partial y^2} = 0 \qquad (B.9)$$

Separation of variables leads to the solution

$$t_{o,\lambda} = (Ae^{-\lambda x} + Be^{\lambda x})(C \sin \lambda y + D \cos \lambda y) \qquad (B.10)$$

where λ is a constant.

By Equations (B.7) and (B.8), C=0 and B=0, thus,

$$t_{o,\lambda} = \int_0^\infty A(\lambda)\ e^{-\lambda x} \cos \lambda y\ d\lambda\ . \qquad (B.11)$$

Differentiation yields

$$\frac{\partial t_o}{\partial x} = -\int_0^\infty \lambda A(\lambda)\ e^{-\lambda x} \cos \lambda y\ dy\ . \qquad (B.12)$$

Substituting from Equations (B.11) and (B.12) in (B.5), we obtain

$$\int_0^\infty (h+k\lambda)\ A(\lambda) \cos \lambda y\ d\lambda = F(y)\ . \qquad (B.13)$$

Thus $F(\lambda)$ is the cosine Fourier transform of $(h+k\lambda)\ A(\lambda)$. By the well known inversion formula we get

$$(h+k\lambda)\ A(\lambda) = \frac{2}{\pi} \int_0^\infty F(y) \cos \lambda y\ dy$$

$$= \frac{2}{\pi} \int_0^a q \cos \lambda y \, dy$$

$$= \frac{2}{\pi} \frac{q}{\lambda} \sin a\lambda \quad . \tag{B.14}$$

Therefore,

$$t_o(x,y) = \frac{2q}{\pi} \int_0^\infty \frac{\sin a\lambda \cos \lambda y \, e^{-\lambda x}}{\lambda(h+k\lambda)} \, d\lambda \tag{B.15}$$

The quantity actually measured by the thin film heater is not $t_o(0,y)$, but its average over the whole width of the film, designated by θ_o; that is

$$\theta_o = \frac{1}{a} \int_0^a t_o(0,y) \, dy$$

$$= \frac{2q}{\pi a} \int_0^\infty \frac{\sin \lambda a}{\lambda(h+k\lambda)} \int_0^a \cos \lambda y \, dy \, d\lambda \quad ,$$

or

$$\theta_o = \frac{4qa}{\pi k} \int_0^\infty \frac{1-\cos \psi}{\psi^2(\psi+\beta)} \, d\psi \tag{B.16}$$

Where $\psi = 2a\lambda$, $\beta = \frac{2ah}{k}$ and is dimensionless. Note that k is the thermal conductivity of the solid plate; thus β is not the Nusselt number.

Equation (B.16) is suitable for the computation of θ_o if β, and hence h, are known. In fact, θ_o is measured, and h is sought. Let $\bar{h} = q/\theta_o$ be the 'apparent' heat-transfer coefficient (neglecting heat loss due to conduction through the plate) and $\bar{\beta} = \frac{2a\bar{h}}{k}$, then rearrangement of Equation (B.16) would yield

$$\frac{1}{\bar{\beta}} = \frac{2}{\pi} \int_0^{\infty} \frac{1-\cos\psi}{\psi^2(\psi+\beta)}\, d\psi \qquad (B.17)$$

Values of $\bar{\beta}$ can be evaluated and plotted as a function of β by numerical integration. This plot (Fig. B.2) may be entered at an observed value of $\bar{\beta}$ to obtain the true value of β, and hence h. The results are also plotted in Fig. B.2 in the form $\beta/\bar{\beta} = h/\bar{h}$ versus $\bar{\beta}$ which is a more convenient form. Values are also given in Table B.1. Incidentally, $\beta/\bar{\beta}$ is the fraction of the total heat that is transmitted to the liquid directly from the film's surface. Note that as $\beta \to \infty$, $\beta/\bar{\beta} \to 1$, as one would expect.

(b) Dynamic response

Let $f^*(s)$ denote the Laplace transform of $f(T)$. Transforming Equations (B.4), (B.7) and (B.8) yields, respectively

$$st^* - t_{(T=0)} = \left(\frac{\partial^2 t^*}{\partial x^2} + \frac{\partial^2 t^*}{\partial y^2}\right) \qquad x>0\ , \qquad (B.18)$$

$$t^* = 0 \qquad x=\infty\ , \qquad (B.19)$$

and

$$\frac{\partial t^*}{\partial y} = 0 \qquad y=0\ . \qquad (B.20)$$

Assuming that both t and h are subject to relatively small variations from their steady state values, they can be represented as,

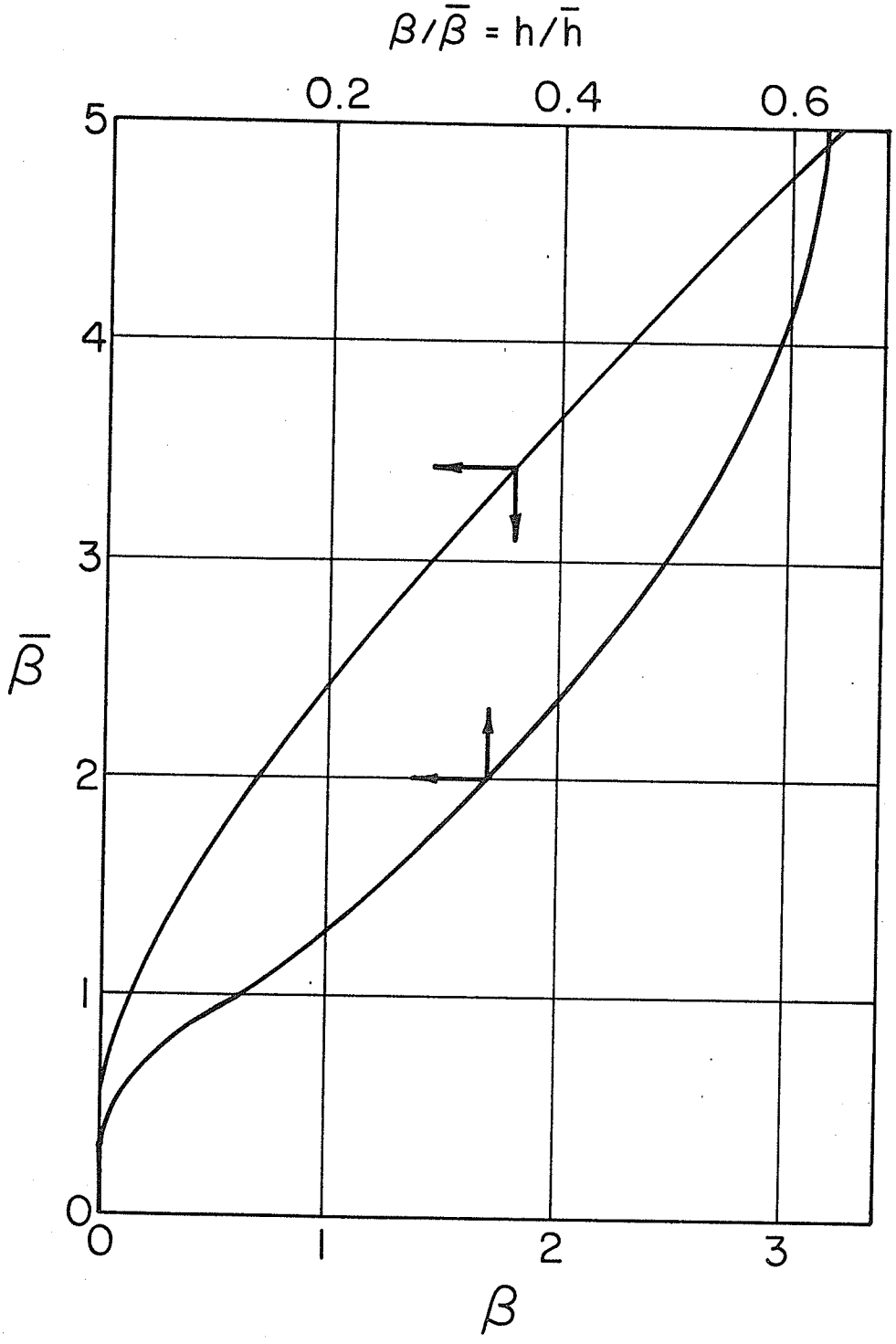

Fig. B.2 Apparent Vs True Heat-Transfer Coefficient

Table B.1

Values of β and $\beta/\bar{\beta}$ Against $\bar{\beta}$

β	$\bar{\beta}$	$\beta/\bar{\beta}$	β	$\bar{\beta}$	$\beta/\bar{\beta}$	β	$\bar{\beta}$	$\beta/\bar{\beta}$
.001	.3876	.002580	.3	1.389	.2161	1.8	3.404	.5289
.002	.4356	.004591	.35	1.476	.2371	1.9	3.522	.5395
.004	.4858	.008234	.4	1.559	.2565	2	3.639	.5496
.005	.5041	.009919	.45	1.640	.2744	2.1	3.756	.5591
.008	.5455	.01467	.5	1.718	.2911	2.2	3.871	.5683
.01	.5676	.01762	.55	1.793	.3067	2.3	3.987	.5769
.015	.6123	.02450	.6	1.867	.3213	2.4	4.102	.5851
.02	.6434	.03085	.65	1.940	.3351	2.5	4.216	.5930
.025	.6793	.03680	.7	2.011	.3481	2.6	4.330	.6005
.03	.7068	.04244	.75	2.081	.3605	2.7	4.443	.6077
.035	.7318	.04783	.8	2.149	.3722	2.8	4.556	.6146
.04	.7548	.05300	.85	2.217	.3834	2.9	4.668	.6212
.045	.7763	.05796	.9	2.284	.3940	3	4.780	.6276
.05	.7966	.06277	.95	2.350	.4042	5	6.974	.7169
.06	.8341	.07193	1	2.416	.4139	10	12.26	.8158
.07	.8686	.08059	1.1	2.545	.4322	30	32.78	.9153
.08	.9006	.08883	1.2	2.672	.4491	100	103.4	.9667
.09	.9308	.09669	1.3	2.798	.4647	300	304.1	.9866
.1	.9594	.1042	1.4	2.921	.4793	1000	1005	.9951
.15	1.087	.1380	1.5	3.044	.4929	3000	3006	.9980
.2	1.196	.1672	1.6	3.165	.5056	10000	10009	.9991
.25	1.296	.2161	1.7	3.285	.5176	30000	30018	.9994
						100000	100047	.9995
						∞	∞	1.0000

$$t(T,x,y) = t_o(x,y) + \tilde{t}(T,x,y)$$

and

$$h(T) = h_o + \tilde{h}(T)$$

where $t_o(x,y)$ is given by Equation (B.15). Thus,

$$t^* = \frac{t_o}{s} + \tilde{t}^*$$

$$h^* = \frac{h_o}{s} + \tilde{h}^* \ .$$

Therefore,

$$s\tilde{t}^* = \alpha\left(\frac{\partial^2 \tilde{t}^*}{\partial x^2} + \frac{\partial^2 \tilde{t}^*}{\partial y^2}\right) \qquad x>0 \ , \tag{B.21}$$

$$\frac{\partial \tilde{t}^*}{\partial y} = 0 \qquad \text{at } y=0 \ , \tag{B.22}$$

$$\tilde{t}^* = 0 \qquad \text{at } x=\infty \ , \tag{B.23}$$

and condition (B.5) becomes

$$F(y) = [h_o + \tilde{h}(T)][t_o + \tilde{t}(T)] - k\left(\frac{\partial t_o}{\partial x} + \frac{\partial \tilde{t}}{\partial x}\right)$$

$$= h_o t_o + \tilde{h} t_o + h_o \tilde{t} - k\frac{\partial t_o}{\partial x} - k\frac{\partial \tilde{t}}{\partial x} \qquad \text{at } x=0$$

where the second order term ht has been neglected. But

$$F(y) = h_o t_o - k\frac{\partial t_o}{\partial x} \qquad \text{at } x=0$$

and therefore

$$\tilde{h}t_o + h_o\tilde{t} - k\frac{\partial\tilde{t}}{\partial x} = 0 \quad \text{at } x=0 \ ,$$

or after transformation

$$t_o\tilde{h}^* + h_o\tilde{t}^* - k\frac{\partial\tilde{t}^*}{\partial x} = 0 \quad \text{at } x=0 \ , \qquad \text{(B.24)}$$

As before, Equation (B.21) may be solved by means of separation of variables; this time yielding (with conditions (B.22) and (B.23))

$$\tilde{t}^* = \int_0^\infty A(\lambda)\ e^{-\sqrt{\lambda^2 + \frac{s}{\alpha}}\,x} \cos \lambda y \, d\lambda \qquad \text{(B.25)}$$

whence

$$\frac{\partial\tilde{t}^*}{\partial x} = -\int_0^\infty \sqrt{\lambda^2 + \frac{s}{\lambda}}\ A(\lambda)\ e^{-\sqrt{\lambda^2 + \frac{s}{\alpha}}\,x} \cos \lambda y \, \partial\lambda \qquad \text{(B.26)}$$

Substituting (B.15), (B.25) and (B.26) into (B.24) yields,

$$\int_0^\infty [\frac{2q \sin a\lambda}{\pi\lambda(h_o+k\lambda)}\ \tilde{h}^*(s) + h_oA(\lambda) + k\sqrt{\lambda^2 + \frac{s}{\alpha}}\ A(\lambda)]\cos \lambda y \, d\lambda = 0$$

... (B.27)

Therefore

$$A(\lambda) = -\frac{2q \sin a\lambda}{\pi\lambda(h_o + k\lambda)(h_o + k\sqrt{\lambda^2 + \frac{s}{\alpha}})}\ \tilde{h}^*(s) \ ,$$

and

$$\tilde{t}^*(s,x,y) = -\frac{2q\tilde{h}^*(s)}{\pi}\int_0^\infty \frac{\sin a\lambda \cos \lambda y\ e^{-\sqrt{\lambda^2 + \frac{s}{\lambda}}\,x}}{\lambda(h_o + k\lambda)(h_o + k\sqrt{\lambda^2 + \frac{s}{\alpha}})}\, d\lambda \qquad \text{(B.28)}$$

with the average over the width of the film being

$$\tilde{\theta}^*(s) = \frac{1}{a}\int_0^a t^*(s,0,y)\,dy$$

$$= -\frac{q\tilde{h}^*(s)}{\pi a}\int_0^\infty \frac{1-\cos 2a\lambda}{\lambda^2(h_o + k\lambda)(h_o + k\sqrt{\lambda^2 + \frac{s}{\alpha}})}\,d\lambda \qquad (B.29)$$

Values of $\tilde{h}(T)$ and $\tilde{\theta}(T)$ may be regarded as an input and output to the thin film 'system', respectively. The transfer function of this system is, by definition

$$H(s) = \frac{\tilde{\theta}^*(s)}{\tilde{h}^*(s)} = \frac{-q}{\pi a}\int_0^\infty \frac{1-\cos 2a\lambda}{\lambda^2(h_o + k\lambda)(h_o + k(\lambda^2 + \frac{s}{\alpha}))}\,d\lambda\ ,$$

or

$$H(s) = -\frac{2q\beta^2}{\pi h_o^2}\int_0^\infty \frac{1-\cos\psi}{\psi^2(\beta+\psi)(\beta + \sqrt{\psi^2 + \beta^2\frac{s}{\eta^2}})}\,d\psi \qquad (B.30)$$

where $\beta = \dfrac{2ah_o}{k}$,

and $\eta = \dfrac{h_o}{\sqrt{k\rho c_p}}$.

The negative sign of H(s) is expected; when h increases, t decreases.

The frequency response of $\tilde{\theta}(T)$ to $\tilde{h}(T)$ may be obtained by substituting $i\omega$ for s in (B.30). The result is

$$M(\omega) = H(i\omega) = -\frac{2q\beta^2}{\pi h_o^2}\int_0^\infty \frac{1-\cos\psi}{\psi^2(\beta+\psi)(\beta + \sqrt{\psi^2 + i\beta^2\frac{\omega}{\eta^2}})}\,d\psi \qquad (B.31)$$

Typical frequency response curves are plotted in Fig. B.3 where the integration in Equation B.31 is evaluated

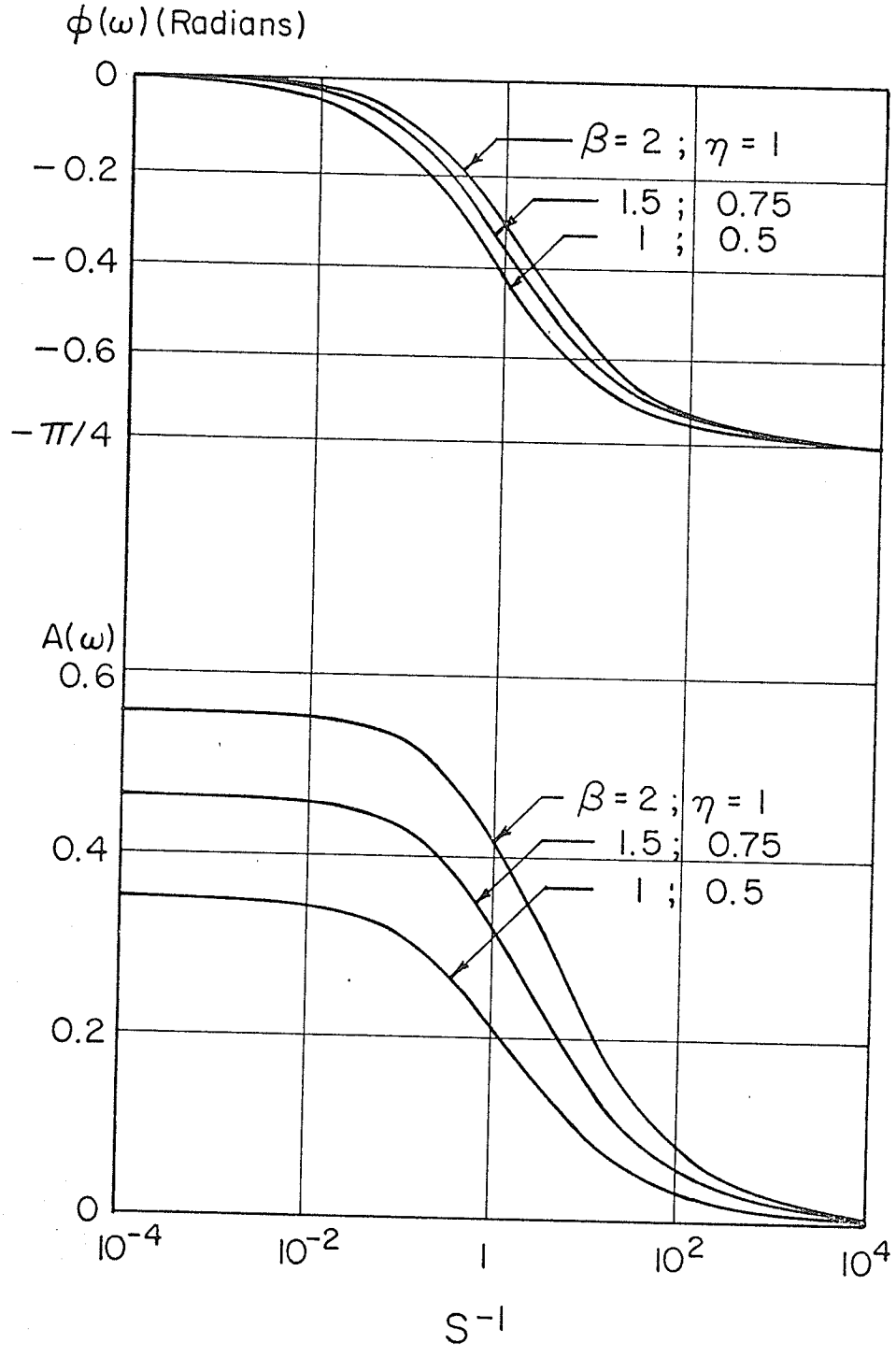

Fig. B.3 Frequency Response Function

numerically using the Gauss method.†

The function $\tilde{\theta}(T)$, as given by Equation (B.3) and hence $\tilde{h}(T)$ are very nearly periodic functions, as the signal repeats itself with each bubble or each series of bubbles. Thus $\tilde{\theta}$ and $\tilde{h}$ can be represented in a Fourier polynomial and H(s) is thus best expressed in its frequency response form. Bard [3] has set a technique to eliminate jump discontinuities which appear in derivatives of $\tilde{\theta}(T)$. He claims that a series of such a function with jump discontinuities converges slowly and the partial sum misrepresents the function at the points of discontinuities. The procedures suggested by him were found here to be lengthy and impractical since it was calculated that such a function converges quite rapidly and gives an error of only 2 to 3 per cent at the point of discontinuities, at least for the case of a triangular wave which has such jump discontinuities. Thus $\tilde{\theta}(T)$ can be represented directly as

$$\tilde{\theta}(T) = \sum_{k=0}^{n} a_k (\sin \frac{2\pi k}{p} T + b_k) \qquad (B.32)$$

where p is the period of the signal for the bubble or a series of bubbles. Now $\tilde{h}(T)$ can be calculated as

$$\tilde{h}(T) = \sum_{k=0}^{n} \frac{a_k}{\phi k} \sin(\frac{2\pi k}{p} T + b_k - \psi_k) \qquad (B.33)$$

where

---

† Handbook of Mathematical Functions, Edited by Milton Abramowitz and Irene A. Segun. P. 887.

$$\Phi_k e^{i\psi_k} = M\left(\frac{2\pi k}{p}\right)$$

which is the frequency response at each particular frequency. The constants a_k and b_k are determined by the formula

$$d_k = \frac{2}{N} \sum_{j=0}^{N-1} \tilde{\theta}_j \sin \frac{2jk\pi}{N}$$

$$e_k = \frac{2}{N} \sum_{j=0}^{N-1} \tilde{\theta}_j \cos \frac{2jk\pi}{N}$$

and

$$a_k = (e_k^2 + d_k^2)^{\frac{1}{2}}$$

$$b_k = \arctan\left(\frac{e_k}{d_k}\right)$$

where N = number of time intervals in a period. Following the magnitude of $\tilde{h}(T)$ at any time can be calculated as the sum of the series in Equation (B.35). Before doing any calculations the data measured from the films were smoothed to eliminate spikes and other gross random fluctuations. The procedure applied successively at all points of the period chosen for analyses was as follows. Let V_{n-2}, V_{n-1}, V_n and V_{n+1} be four successive voltage readings. The quantities

$$x = \tfrac{1}{2}(V_{n-1} + V_{n+1})$$

and

$$y = 2\,V_{n-1} - V_{n-2}$$

were calculated and V_n was adjusted as follows:

If $\min(x,y) \leq V_n \leq \max(x,y)$, V_n is unchanged.

If $V_n < \min(x,y)$, V_n is set equal to $\min(x,y)$.

If $V_n > \max(x,y)$, V_n is set equal to $\max(x,y)$.

The procedure is illustrated in the figure below.

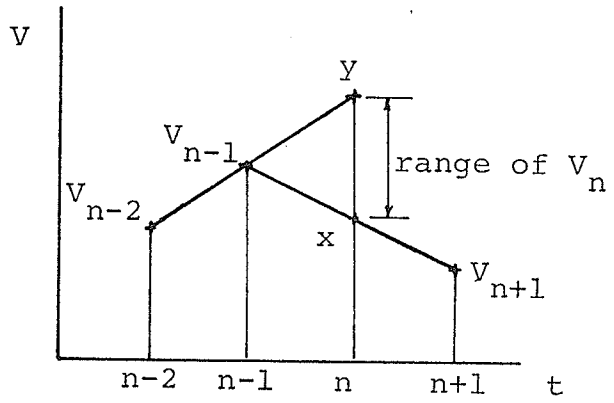

B.3 Computation of the Mean Values of Surface Temperature and Heat-transfer Coefficient

Since it is necessary to know the total value of the heat-transfer coefficient h we need to calculate the average heat-transfer coefficient (time mean) h_o. Also, h_o is needed for computation of Equations (B.30) and (B.31). The relation between the mean surface temperature and the mean h_o is given by Equations (B.16) and (B.17).

Thus, to calculate $\bar{h}_o$, combining the relations

$$R = R'_o + \gamma\theta_o$$

$$q = \frac{0.239\ V^2}{RA} \quad \text{cal/s}$$

where A is the surface area of the film heater, and

$$\theta_o = \frac{q}{\bar{h}_o}$$

we get

$$R = R'_o + \frac{0.239\ \gamma}{A\ \bar{h}_o} \frac{V^2}{R} \cdot \qquad (B.34)$$

The quantities γ and A are constants; thus, Bard claimed that with $\bar{h}_o$ independent of the heat flux, a plot of R versus $\frac{V^2}{R}$ is a straight line. Values of R and $\frac{V^2}{R}$ are calculated and the value of $\bar{h}_o$ is computed using the least square approximation.

The assumption made by Bard that $\bar{h}_o$ is independent of the heat flux could be correct in the case of bubbling especially for the heaters near the orifice (1 and 2) where the flow is highly agitated, but this assumption is less likely to be correct for the far heaters and is not correct for the no bubbling case where the heat transfers by free convection and $\bar{h}_o$ depends on the heat flux, i.e., on $\frac{V^2}{R}$. Therefore, the calculation of $\bar{h}_o$ is performed using the following method: the resistance of each heater was measured at the lowest and the highest voltages (0.1 and 11.0 volts, respectively), the latter actually having been used for recording the fluctuation during the bubbling experiments. At the lowest voltage the heat generated is so small that the film temperature is considered approximately equal to the bulk hexane temperature. The higher

resistance reading corresponds to the average temperature of the film heater either during bubbling or with no bubbling at 11.0 volts. Using the relation

$$R = R_o' + \gamma\theta_o \ ,$$

the average temperature of the film heater θ_o can be calculated and hence $\bar{h}_o$ from the relation $\bar{h}_o = \frac{q}{\theta_o}$ with values of h_o then being obtained from Fig. B.2. Values of $\bar{h}_o$ and h_o are given in Table B.2.

Table B-2

Values of Mean Heat-transfer Coefficient h_o

Heater No.	Air Flow Rate cc/s	$\bar{h}_o$ Cal/cm²s°C	h_o Cal/cm²s°C
1	0.94	0.069	0.0515
2	0.94	0.0554	0.0365
3	0.94	0.038	0.0206
4	0.94	0.0335	0.0178
1	2.2	0.090	0.067
2	2.2	0.063	0.0435
All Four Heaters	0 (no bubbling)	0.030-0.033	0.0158*

* The average value for the four heaters is given; the maximum deviation from the average for any individual heater is ± 2%.

APPENDIX C

ERROR ANALYSIS

C.1 Signal to Noise Ratio

The signal-to-noise ratio is measured for each heater from the recorded signal on the visicorder sheet. It is defined as the ratio between signal amplitude, peak to peak, and noise amplitude, peak to peak. The ratio was found to be

Heater No.	Signal-to-noise Ratio
1	40
2	35
3	12
4	22

The low ratio for Heater 3 may be due to poor connection between the heater and its two electrodes. Thus, the maximum error introduced due to noise is less than 10 per cent.

C.2 Computational Errors

The method in Appendix B introduces some approxi-

mations. These are discussed below.

1. The assumption of an infinitely thick plate was discussed by Bard who performed calculations for the case of a finite plate and found that the results did not differ by more than 3 per cent in the range of interest, though the method is more complicated. Therefore, little error will result if the infinite thickness results are used.

2. The geometry of the film heaters is not exactly that assumed in the derivation. They are not infinitely long. Since, however, their length is approximately ten times their width, heat loss from the ends may be neglected. Also, some error may be introduced in the calculations for the innermost heaters due to (a) the heaters curvature, and (b) the proximity to the orifice, which contravenes the assumption of an infinite plate.

3. Considering the error introduced due to neglecting $\tilde{h}\tilde{t}$ in deriving Equation (B.24), it was found in experiments that $\tilde{t}$ turned to be small relative to t_o (Table 5.1), and $\tilde{h}$ was of the order of 30 per cent of h_o. Retaining the term $\tilde{h}\tilde{t}$ would replace $\tilde{h}t_o$ with $\tilde{h}(t_o+\tilde{t})$ in Equation (B.24). Since this is the only term involving $\tilde{h}$, the expected relative error in $\tilde{h}$ is approximately $\frac{\tilde{t}}{t_o}$ which was found to vary between 0.2 and 9.3 per cent.

C.3 Measurement Errors

1. Resistance measurements: the measuring circuit

allowed the resistance measurement within 0.01 ohm. Since the range of resistance change during operation was about 1.5 ohms, the error introduced in $\bar{h}_o$ and γ measurement was only about 0.7 per cent.

2. Signal measurement from photographic film: the oscilloscope trace was about 1 cm wide on the projection screen. The mid point of the line was approximately traced for each frame within about two millimeters. With the projected signal having a magnitude of about 15 to 20 cm, the error introduced in the value of the measured signal amounts only to 1. - 1.4 per cent which is negligible.

APPENDIX D

PROPERTY VALUES

Listed below are the properties of hexane and the other materials used in the present experiment, which is actually used in the calculations. The properties of water are also listed in comparison with those of hexane.

D.1 Properties of n-hexane and Water [22]:

Property	hexane	water	
Temperature °C	20	20	100
Density gm/cc	0.66	1	0.96
Thermal Conductivity cal/cm s °K	3.13×10^{-4}	14.3×10^{-4}	16.5×10^{-4}
Specific Heat cal/gm °C	0.6	1.0	1.0
Viscosity Cp	0.326	1.0	0.31
Surface Tension dynes/cm	18.43	72.75	58.8
Boiling Point (atm. press.) °C	69	100	100
Prandtl Number	6.24	7.0	1.9
Electric Conductivity mho/cm	10^{-14}-10^{-18}	10^{-7}-10^{-8}	(Distilled)

D.2 Properties of Perspex [27]

Density	gm/cm^3	1.19
Thermal Conductivity	cal/cm s °C	4.5×10^{-4}
Specific Heat	cal/gm °C	0.35
Electric Resistivity	ohm-cm	10^{15}

D.3 Properties of Copper [6]

Density	gm/cm^3	8.94
Thermal Conductivity	cal/cm s °C	0.920
Electric Resistivity	ohm-cm	1.68×10^{-6}
Specific Heat	cal/gm °C	0.092
Temperature Coefficient of Resistance	/°C	0.0039
Boiling Point	°C	2582 *

---

* Boiling point of nickel is 3380°C.

APPENDIX E

COMPUTER PROGRAMMES

This appendix gives a sample of the computer programmes used for calculation of values of β against $\bar{\beta}$ from Equation (B.17) and for the conversion of the voltage signals into heat-transfer coefficient following procedures given in Appendix B.

E.1 Calculation of β versus $\bar{\beta}$

The various symbols used in the following programme have meanings described as follows:

FCN = integrand in Equation (B.17)

AB = lower limit of integration

AC = upper limit of integration

B = β values

BA = $\bar{\beta}$ values

R = ratio of $\beta/\bar{\beta}$

```
0001            DIMENSION Z(40),ZZ(40)
0002            COMMON B
0003            REAL INTEG
0004            EXTERNAL FCN
0005            AB=0.0
0006            AC=50
0007            DO 1 I=1,10
0008            B=0.01*I
0009            A=INTEG(AB,AC,FCN)
0010            BA=3.14/(2*A)
0011            R=B/BA
0012            WRITE(6,2) B,BA,R
0013          2 FORMAT (5X,3F15.5)
0014          1 CONTINUE
0015            STOP
0016            END
```

```
      C     SUBROUTINE FCN
0001        FUNCTION FCN(P)
0002        DIMENSION Z(40),ZZ(40)
0003        COMMON B
0004        D1=1-COS(P)
0005        D2=(P**2)*(B+P)
0006        FCN=D1/D2
0007        RETURN
0008        END
```

```
FORTRAN IV G LEVEL  20.1          MAIN          DATE = 72217        15/28/52          PI75 0001
      C     SUBROUTINE FOR NUMERICAL INTEGRATION BY GAUSS AND 96 INTERVALS          DECK
0001          CCMPLEX FUNCTION INTEG(A,B,FCNC)                                      4&&&-
0002          CCMPLEX SUM,Z,ZZ ,FCNC                                                DECK
0003          DIMENSION X(48),W(48)
0004          DATA X/.1627674484960296E-1,.4881298513604973E-1,.8129749546442555DECK
             1E-1,                                                                  DECK
             20.1136958501106659,0.1459737146548969,0.1780968823676186,             DECK
             30.2100313104605672,0.2417431561638400,0.2731988125910491 ,            DECK
             40.3043649443544963,0.3352085228926254,0.3656968614723136  ,           DECK
             5.3957976498289086,.4254789884073005,.4547094221677430,                DECK
             6.4834579739205963,.5116941771546676,.5393881083243574,                DECK
             7.5665104185613971,.5930323647775720,.6189258401254685,                DECK
             8.6441634037849671,.6687183100439161,.6925645366421715,                DECK
             9.7156768123489676,.7380306437444001,.7596023411766474,                DECK
             1.7803690438674332,.8003087441391408,.8194003107379316,                DECK
             2.8376235112281871,.8549590334346014,.8713885059092965,                DECK
             3.8868945174024204,.9014606353158523,.9150714231208980,                DECK
             4.9277124567223086,.9393703397527552,.9500327177844376,                DECK
             5.9596882914487425,.9683268284632642,.9759391745851364,                DECK
             6.9825172635630146,.9880541263296237,.9925439003237626,                DECK
             7.9959818429872092,.9983643758631816,.9996895038832307/                DECK
0005          DATA W/.3255061449236316E-1,.3251611871386883E-1,.3244716371406426DECK
             1E-1,                                                                  DECK
             2.3234382256857592E-1,.32206204 9403025E-1,.3203445623199266E-1,       DECK
             3.3182875889441100E-1,.3158933077072716E-1,.3131642559686135E-1,       DECK
             4.3101033258631383E-1,.3067137612366914E-1,.3029991542082759E-1,       DECK
             5.2989634413632838E-1,.2946108995816 79E-1,.2899461415055523E-1,       DECK
             6.2849741106508538E-1,.2797000761684833E-1,.2741296272602924E-1,       DECK
             7.2682686672559176E-1,.2621234073567241E-1,.2557003600534936E-1,       DECK
             8.2490063322248361E-1,.2420484179236469E-1,.2348339908592621E-1,       DECK
             9.2273706965832937E-1,.2196664443874434E-1,.2117293989219129E-1,       DECK
             1.2035679715433332E-1,.1951908114014502E-1,.1866067962741146E-1,       DECK
             2.1778250231604526E-1,.1688547986424517E-1,.1597056290256229E-1,       DECK
             3.1503872102699493E-1,.1409094177231486E-1,.1312822956696157E-1,       DECK
             4.1215160467108831E-1,.1116210209983849E-1,.1016077053500841E-1,       DECK
             5.9148671230783386E-2,.8126876925698759E-2,.7096470791153865E-2,       DECK
             6.6058545504235961E-2,.5014202742927517E-2,.3964554338444686E-2,       DECK
             7.2910731817934946E-2,.1853960788946921E-2,.7967920655520124E-3/       DECK
0006          M=2                                                                   DECK
0007          CM=M                                                                  DECK
0008          SUM=0.0                                                               DECK
0009          D=(B-A)/CM                                                            DECK
0010          DO 100 L=1,M                                                          DECK
0011          CI=L                                                                  DECK
0012          AA=A+(CI-1.)*D                                                        DECK
0013          AB=AA+D                                                               DECK
0014          C=(AB-AA)/2.DO                                                        DECK
0015          CC=(AB+AA)/2.DO                                                       DECK
0016          DO 100 N=1,48                                                         DECK
0017          Y=C*X(N)+CC                                                           DECK
0018          YY=-C*X(N)+CC                                                         DECK
0019          Z=FCNC(Y)                                                             DECK
0020          ZZ=FCNC(YY)                                                           DECK
0021          SUM=SUM+C*W(N)*(Z+ZZ)                                                 DECK
0022          K=L                                                                   DECK
0023      100 CONTINUE                                                              DECK
0024          INTEG=SUM                                                             DECK
0025        6 RETURN                                                                DECK
```

E.2 Conversion of Voltage Signal to Heat-transfer Coefficient

The symbols used in this programme are all listed in the first page of the programme.

```
FORTRAN IV G LEVEL  20.1          MAIN          DATE = 72363          15/13/36

                C                    SAMPLE OF COMPUTER PROGRAM
                C
                C
                C
                C     CONVERT OF VOLT.FLUCTUATIONS TO HEAT TRANSFER
                C     P=PERIOD  SECONDS
                C     N=NO OF INTERVALS IN A PERIOD
                C     L=NO OF TERMS IN FOURIER ANALYSIS
                C     PH=CONVERSION FACTOR FROM CM TO VOLT
                C     RR=FILM AV. RESISTANCE OHMS
                C     R1=RESISTANCE IN SERIES WITH RR OHMS
                C     GAMA=TEMP. COEFF OF FILM RESISTANCE OHMS/DEG.C
                C     AA=FILM SURFACE AREA SQ.CM
                C     AVARAGE HEAT-TRANSFER COEFFICIENT CAL/SQ.CM S DEG.C
                C     EE=SUPPLY VOLTAGE VOLTS
                C     VV=VOLTAGE ON FILM  VOLTS
                C     Q=HEAT O/P FROM FILM  CAL/SQ.CM S
                C     V(I)=VOLTAGE FLUCTUATIONS  VOLTS
                C     T(I)=TEMP.   FLUCTUATIONS  DEG.C
                C     H=HEAT TRANSFER COEFF.  CAL/SQ.CM S DEG C
                C     U=TIME SECONDS
                C     DELU=TIME INCRIMENT  SECONDS
0001                  DIMENSION V(800),T(800),D(90),A(90),B(90),C(90),F(90),ANG(90)
0002                  DIMENSION R(90),E(90),X(90),Y(90),H(800),HTC(800), U(800)
0003                  COMPLEX FR(50),INTEG,Z(40),ZZ(40),FCN
0004                  COMMON W,HO,WA
0005                  EXTERNAL FCN
0006                  DELU=0.0005
0007                  L=90
0008                  P=DELU*N
0009                  VV=RR*EE/(RR+R1)
0010                  Q=0.239*(VV**2)/(RR*AA)
0011                  READ(5,40) (V(I),I=1,N)
0012               40 FORMAT (10F7.3)
0013                  WRITE(6,50)
0014               50 FORMAT (5X,'VOLTAGE FLUCTUATIONS')
0015                  WRITE(6,44)(V(I),I=1,N)
0016               44 FORMAT( 5X,10F10.4)
                C     SMOOTHING DATA
0017                  IF(DELU.GT.0.001) GO TO 60
0018                  WRITE(6,51)
0019               51 FORMAT(/5X,'SMOOTH DATA')
0020                  DO 1 M=1,N
0021                  IF(M.GT.1) GO TO 8
0022                  XX=(V(N)+V(2))/2
0023                  YY=2*V(N)-V(N-1)
0024                  GO TO 7
0025               8  IF(M.EQ.2) GO TO 6
0026                  GO TO 9
0027               6  XX=(V(1)+V(3))/2
0028                  YY=2*V(1)-V(N)
0029                  GO TO 7
0030               9  XX=(V(M-1)+V(M+1))/2
0031                  YY=2*V(M-1)-V(M-2)
0032               7  IF(XX.GT.YY) GO TO 2
0033                  VMAX=YY
0034                  VMIN=XX
0035                  GO TO 3
```

```
0036              2 VMAX=XX
0037                VMIN=YY
0038              3 IF(V(M).LT.VMIN) GO TO 4
0039                IF(V(M).GT.VMAX) GO TO 5
0040                GO TO 1
0041              4 V(M)=VMIN
0042                GO TO 1
0043              5 V(M)=VMAX
0044              1 CONTINUE
0045                WRITE(6,45)(V(M),M=1,N)
0046             45 FORMAT(5X,10F10.4)
                C   CONVERT TO TEMP FLUCTUATIONS T
0047             60 WRITE(6,52)
0048             52 FORMAT(/5X,'TEMP.FLUCTUATIONS*PH')
0049                DO 10 M=1,N
0050                T(M)=((RR+R1)**2)* V(M)/(EE*R1*GAMA*PH)
0051             10 CONTINUE
0052                WRITE(6,46) (T(M),M=1,N)
0053             46 FORMAT(5X,10F10.4)
                C   FOURIER COEFF FOR TEMP FLUCTIATIONS
0054                WRITE(6,53)
0055             53 FORMAT(/5X,'FOURIER COEFF FOR TEMP FLUCT.')
0056                DO 21 K=1,L
0057                C(K)=0.0
0058                E(K)=0.0
0059                DO 22 J=1,N
0060                D(K)=D(K)+2*T(J)*SIN(2*3.14*(J-1)*(K-1)/N)/N
0061                E(K)=E(K)+2*T(J)*COS(2*3.14*(J-1)*(K-1)/N)/N
0062             22 CONTINUE
0063             21 CONTINUE
0064                WRITE(6,54)
0065             54 FORMAT(/5X,'T=A*SIN(W*U+B)')
0066                DO 23K=1,L
0067                A(K)=(D(K)**2+E(K)**2)**0.5
0068                B(K)=ATAN2(E(K),D(K))
0069                WRITE(6,43) A(K),B(K)
0070             48 FORMAT(5X,2F10.4)
0071             23 CONTINUE
                C   COMPUTE FREQUENCY RESPONSE
0072                AB=0.0
0073                AC=50
0074                WRITE(6,55)
0075             55 FORMAT (/5X,'FREQ.RESPONSE M=R*EXP(J*ANG)')
0076                DO30 K=1,L
0077                W=2*3.14*(K-1)/P
0078                FR(K)=INTEG(AB,AC,FCN)
0079                X(K)=REAL(FR(K))
0080                Y(K)=AIMAG(FR(K))
0081                R(K)=(X(K)**2+Y(K)**2)**0.5
0082                ANG(K)=ATAN2(Y(K),X(K))
0083                WRITE(6,42) W,R(K),ANG(K)
0084             42 FORMAT (5X,3F10.4)
0085             30 CONTINUE
                C   FOURIER COEFF FOR H
0086                WRITE(6,56)
0087             56 FORMAT (/5X,'FOURIER COEFF FOR H.T.COEFF  H=C*SIN(W*U+F)')
0088                DO 35 K=1,L
0089                C(K)=A(K)/(B(K)*( 2*Q/(3.14*(HO**2))))
```

```
0090                F(K)=B(K)-ANG(K)
0091                WRITE(6,49) C(K),F(K)
0092             49 FORMAT(5X,2F10.4)
0093             36 CONTINUE
                 C     COMPUTE VALUES FOR H
0094                WRITE(6,34)
0095             34 FORMAT(/5X,'HEAT TRANSFER FLUCTUATION')
0096                DO 63 I=1,N
0097                H(I)=0.0
0098                U(I)=0.0005*I-0.0005
0099             33 DO 31 K=1,L
0100                W=2*3.14*(K-1)/P
0101                DH=C(K)*SIN( W*U(I)+F(K))
0102                H(I)=H(I)+DH
0103             31 CONTINUE
0104                HTC(I)=H(I)+HO
0105                WRITE (6,32) U(I),H(I),HTC(I)
0106             32 FORMAT (5X,3F10.5)
0107                IF(U(I).GE.P) GO TO 64
0108             63 CONTINUE
0109             64 WRITE(7,67) (U(I),I=1,N)
0110             67 FORMAT (8F10.5)
0111                WRITE(7,65) (HTC(I),I=1,N)
0112             65 FORMAT (8F10.5)
0113                STOP
0114                END
```

```
      C     SUBROUTINE FCN
0001        COMPLEX FUNCTION FCN(T)
0002        COMPLEX Z(40),ZZ(40),D,S,D1,D2
0003        COMMON W,HO,WA
0004        S=(0.0,1.0)
0005        DEN=1.19
0006        CON=0.00045
0007        CP=0.35
0008        B=2*WA*HO/CON
0009        E=HO/((CON*DEN*CP)**0.5)
0010        A=1-COS(T)
0011        D1=T**2+(S*(B**2)*W/(E**2))
0012        D2=CSQRT(D1)
0013        D=(T**2)*(B+T)*(B+D2)
0014        FCN=-(B**2)*A/D
0015        RETURN
0016        END
```

12

```
                C     SUBROUTINE FOR NUMERICAL INTEGRATION BY GAUSS AND 96 INTERVALS      DECK
0001                  COMPLEX FUNCTION INTEG(A,B,FCNC)                                   4&&&-
0002                  COMPLEX SUM,Z,ZZ ,FCNC                                             DECK
0003                  DIMENSION X(48),W(48)
0004                  DATA X/.1627674849602962E-1,.4881298513504973E-1,.8129749546442555DECK
                     1E-1,                                                               DECK
                     2.1135658501105659,0.1459737146543969,0.1780966823676186,          DECK
                     3.2100313104606672,0.2417431561638400,0.2731988125910491 ,         DECK
                     4.3041664434544963,0.3352085228925254,0.3656968614723136  ,        DECK
                     5.3957376498233086,.4254733884073005,.4547094221677430,            DECK
                     6.4834579739205963,.5115941771545675,.5393881083243574,            DECK
                     7.5660104185613971,.5930323647775720,.6183253401254685,            DECK
                     8.6441383+0378+9671,.6687183100439161,.6925645366421715,           DECK
                     9.7156768123+86676,.7380306437444001,.7596023411766474,            DECK
                     1.7804690433674332,.8003087441391408,.8194003107379316,            DECK
                     2.8376235112281871,.8549590334346014,.8713885059092965,            DECK
                     3.8868945174024204,.9014606353158523,.9150714231208980,            DECK
                     4.9277124567223086,.9393703397527552,.9500327177844376,            DECK
                     5.9596832914487425,.9683268284632642,.9759391745851364,            DECK
                     6.9825172635630146,.9880541263296237,.9925439003237626,            DECK
                     7.9959818429872092,.9983643758631816,.9996895038832307/            DECK
0005                  DATA W/.3255061449236316E-1,.3251611871386883E-1,.3244716371406426DECK
                     1E-1,                                                               DECK
                     2.3234332256857592E-1,.32206204 9403025E-1,.3203445623199266E-1,    DECK
                     3.3182375839441100E-1,.3158933077072716E-1,.3131642559686135E-1,    DECK
                     4.3101033258631383E-1,.3067137612366914E-1,.3029991542082759E-1,    DECK
                     5.2989634413632838E-1,.2946108995816796E-1,.2899461415055523E-1,    DECK
                     6.2849741106508538E-1,.2797000751684833E-1,.2741296272602924E-1,    DECK
                     7.2682686672559176E-1,.2621234073567241E-1,.2557003600534936E-1,    DECK
                     8.2490063322+8361E-1,.2420484179236469E-1,.2348339908592621E-1,    DECK
                     9.2273706955832937E-1,.2196664443874434E-1,.2117293892191296E-1,    DECK
                     1.2035579715433332E-1,.1951908114014502E-1,.1866067952741146E-1,    DECK
                     2.1778250231604526E-1,.1688547986424517E-1,.1597056290256229E-1,    DECK
                     3.1503872102699493E-1,.1409094177231486E-1,.1312322956696157E-1,    DECK
                     4.1215160467108831E-1,.1116210209933849E-1,.1016077053500841E-1,    DECK
                     5.9143671230783386E-2,.8126876925993759E-2,.7096470791153865E-2,    DECK
                     6.6058545502359616E-2,.5014202742927517E-2,.3964554338446866E-2,    DECK
                     7.2910731817934946E-2,.1853960788946921E-2,.7967920655520124E-3/    DECK
0006                  M=2                                                                DECK
0007                  CM=M                                                               DECK
0008                  SUM=0.0                                                            DECK
0009                  D=(B-A)/CM                                                         DECK
0010                  DO 100 L=1,M                                                       DECK
0011                  CI=L                                                               DECK
0012                  AA=A+(CI-1.)*D                                                     DECK
0013                  AB=AA+D                                                            DECK
0014                  C=(AB-AA)/2.DO                                                     DECK
0015                  CC=(AB+AA)/2.DO                                                    DECK
0016                  DO 100 N=1,48                                                      DECK
0017                  Y=C*X(N)+CC                                                        DECK
0018                  YY=-C*X(N)+CC                                                      DECK
0019                  Z=FCNC(Y)                                                          DECK
0020                  ZZ=FCNC(YY)                                                        DECK
0021                  SUM=SUM+C*W(N)*(Z+ZZ)                                              DECK
0022                  K=L                                                                DECK
0023              100 CONTINUE                                                           DECK
0024                  INTEG=SUM                                                          DECK
0025                6 RETURN                                                             DECK
```

APPENDIX F

COMBINED HEAT TRANSFER AND FLOW VISUALIZATION RESULTS

This appendix presents the various sketches comprising Fig. 5.7 (first bubble of a series) in much larger scale in order that the hydrogen bubbles movement (as indicated in the water bubble sketches by the arrows) may be clearly seen; this material is shown as Figs. F.1(a) to F.1(g). Also presented here as Figs. F.2(a) to F.2(f) is similar material for Bubble 25-3-5 in hexane and Bubble 18-1-5 in water, each is the last bubble of a five bubble series.

The detailed behavior of the flow and h was discussed in Section 5.2 for the first bubble of a series (Fig. F.1). For the last bubble of the series (Fig. F.2) the heat transfer behavior during the bubble cycle is similar to that during the first bubble except for the following:

(i) The heat-transfer coefficient h does not undergo a marked increase as did h for the first bubble of a series in the same phase of growth (while the bubble interface is moving outward) as shown in Figs. F.2(a) to F.2(c). This is observed to be the case for all intermediate bubbles as well.

(ii) As the bubble departs from the surface the flow can be seen to resemble a reversed stagnation flow as described in Chapter 5. This is clear in Figs. F.2(f), F.2(g) and F.2(h). The flow starts decaying after F.2(f) causing a decrease in h.

(iii) The sudden rise in h for the first heater, shown in F.2(g), is due to the small bubble being drawn below the surface of the plate and the liquid rushing in to replace it.

(iv) The signal level is higher for Heaters 3 and 4 than for the same heaters with the first bubble of the series; this is no doubt because the flow in the vicinity of these heaters becomes significantly agitated after the third bubble of the series.

Other than the above four points the heat-transfer coefficient variations are almost the same, having a maximum h at approximately detachment for Heaters 1 and 2 and lagging after detachment for Heaters 3 and 4.

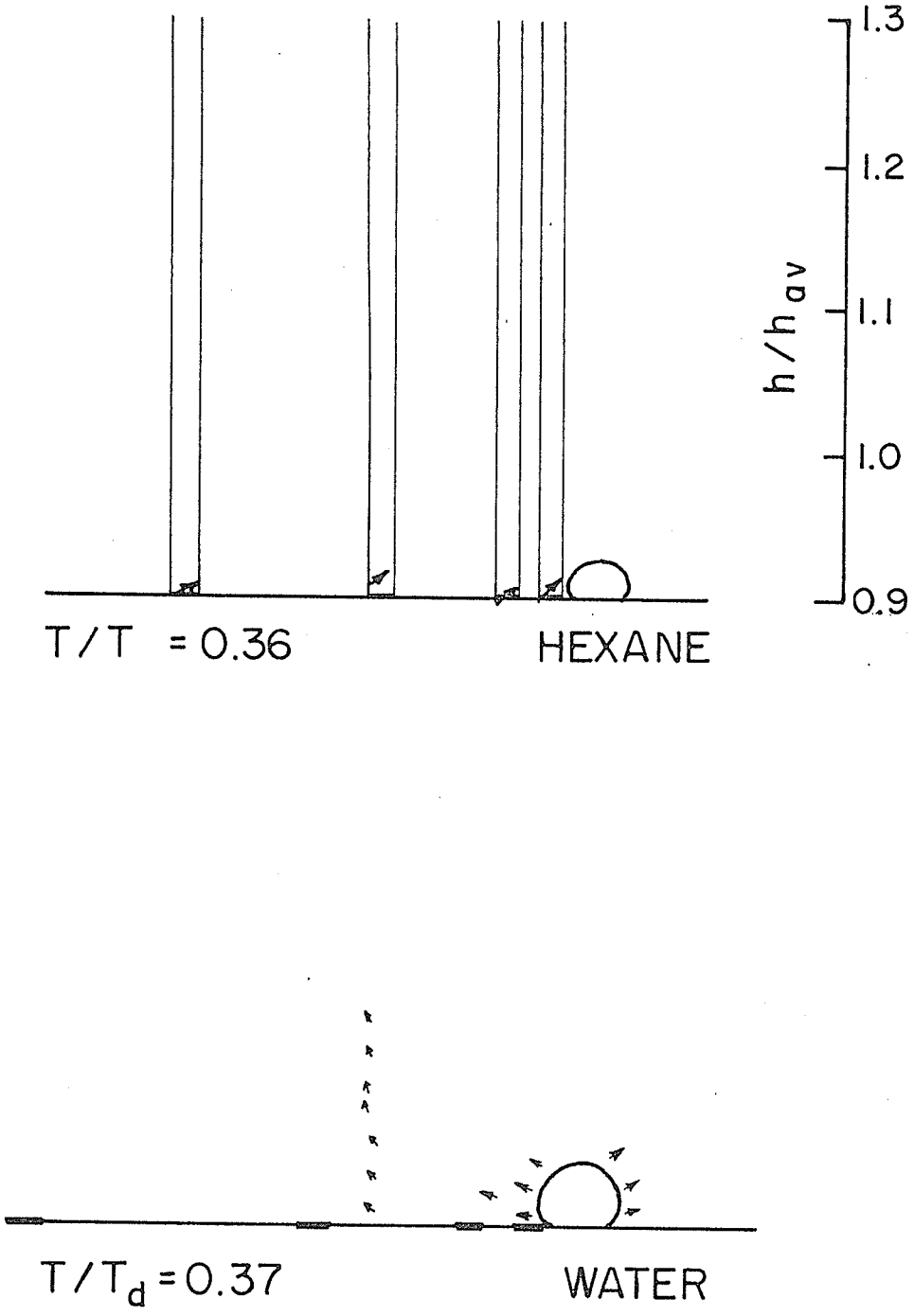

Fig. F.1 Combined Heat Transfer and Flow Visualization Results for a First Bubble of a Series (Bubble 25-3-1 in Hexane and Bubble 18-1-1 in Water)

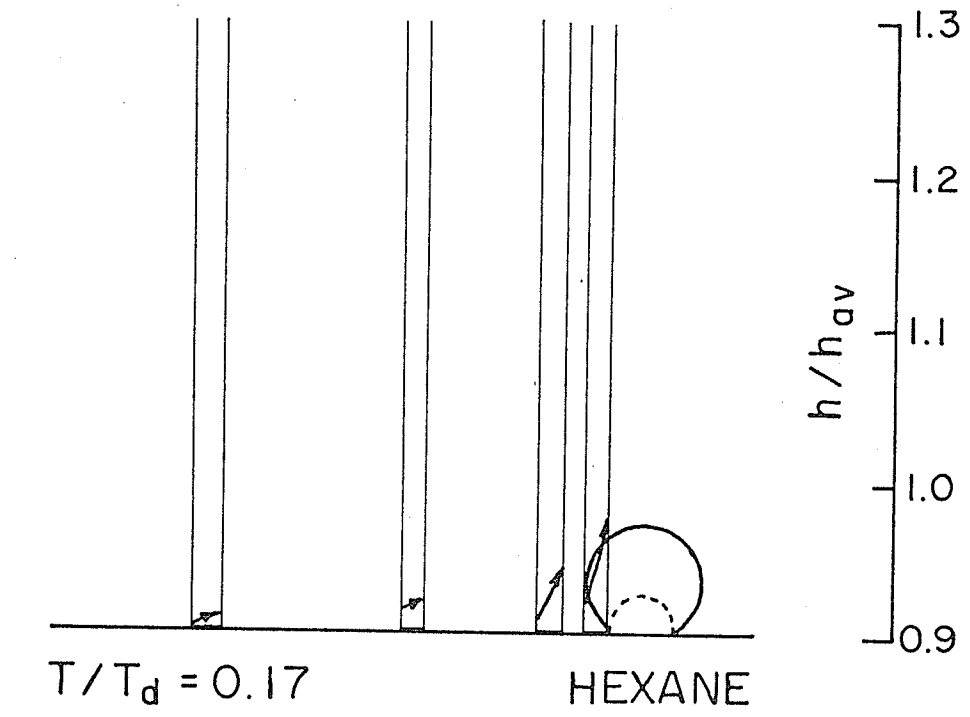

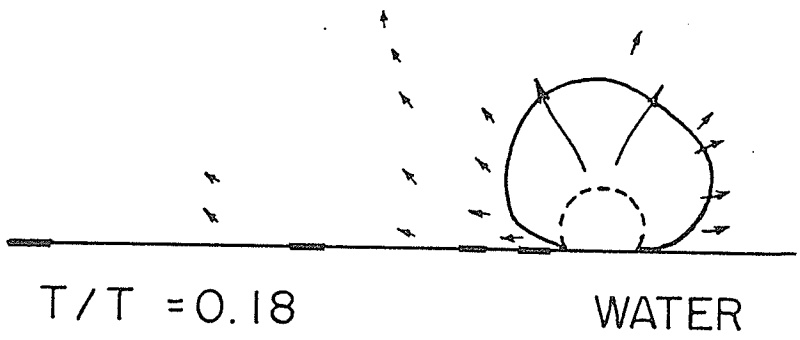

(b)

Fig. F.1

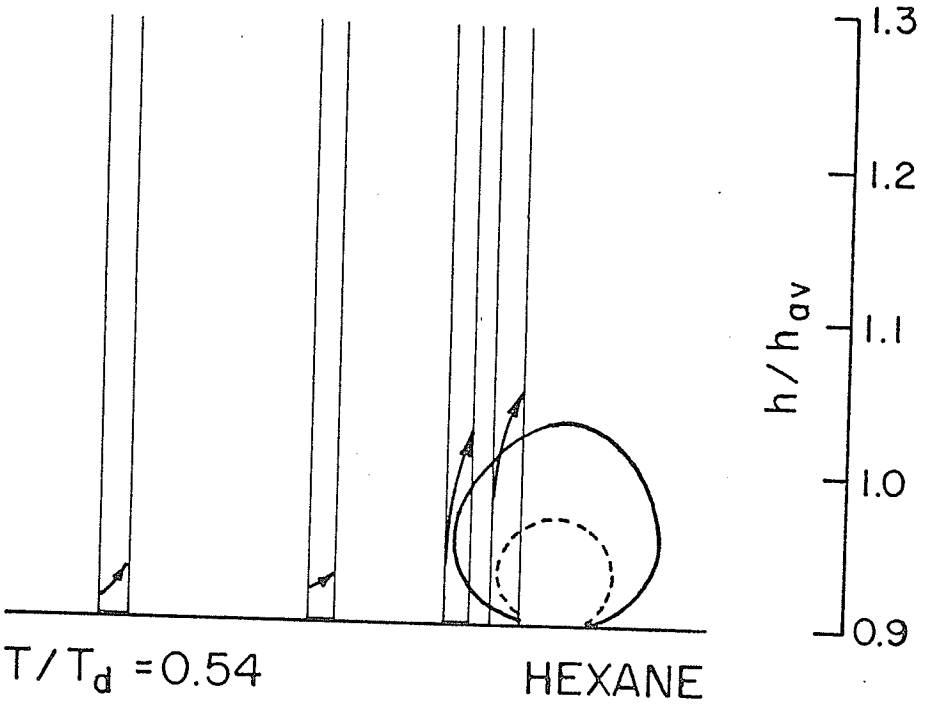

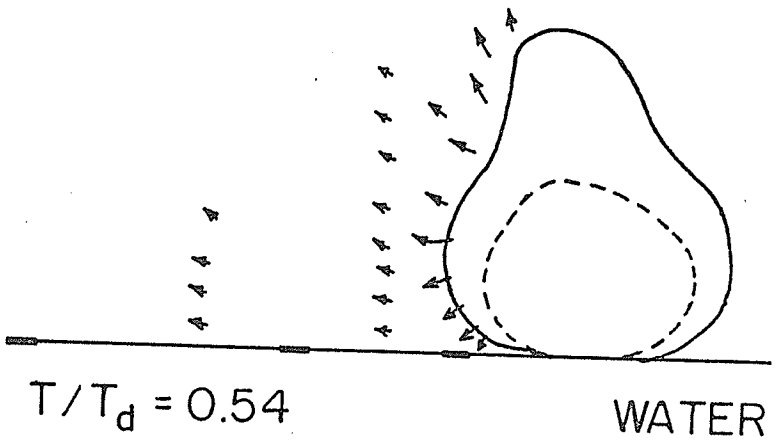

(c)

Fig. F.1

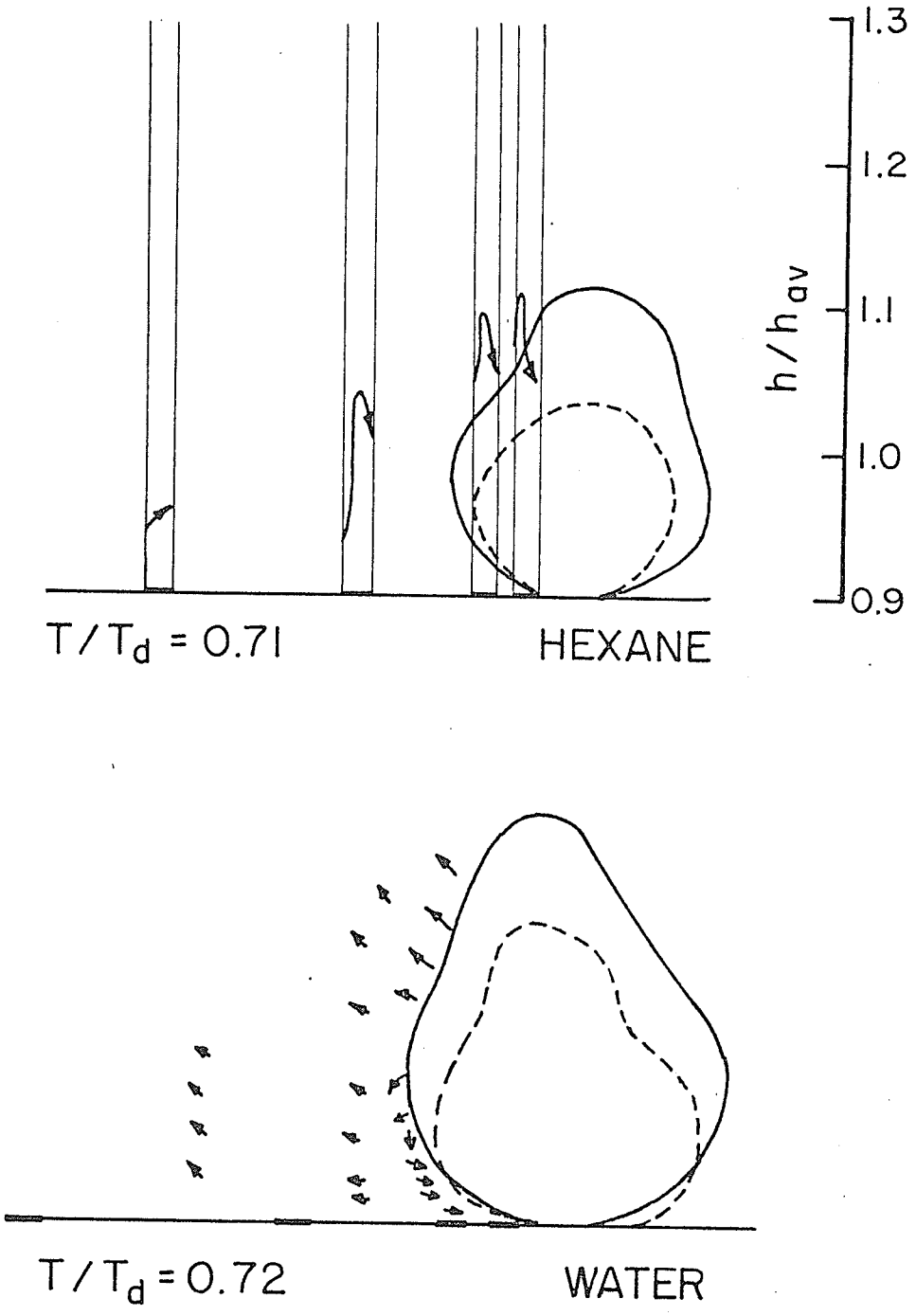

(d)

Fig. F.1

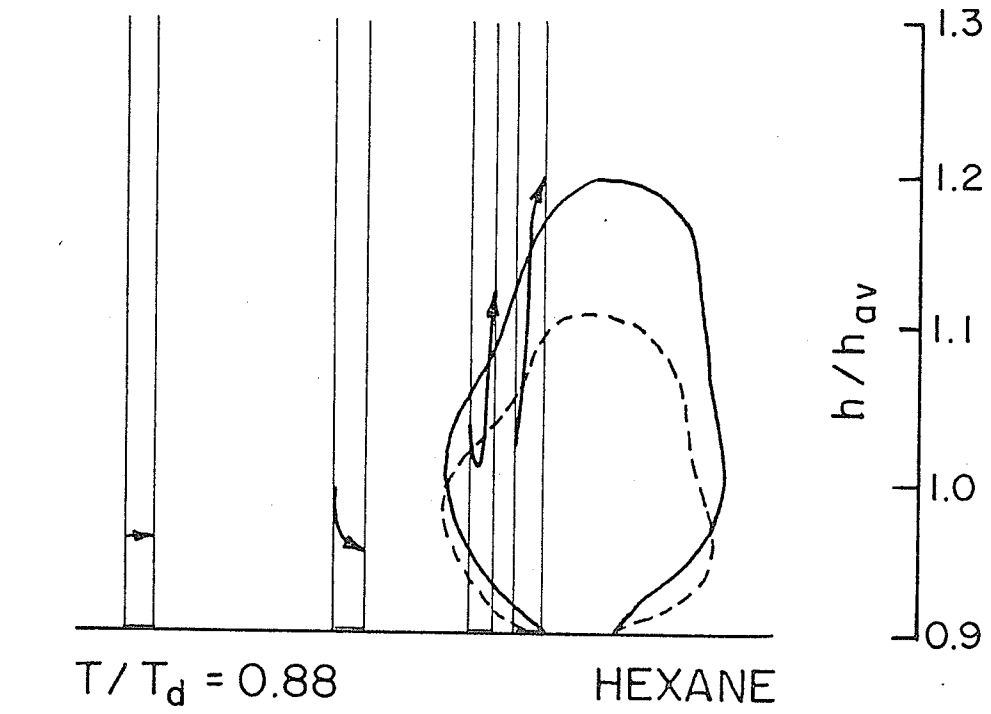

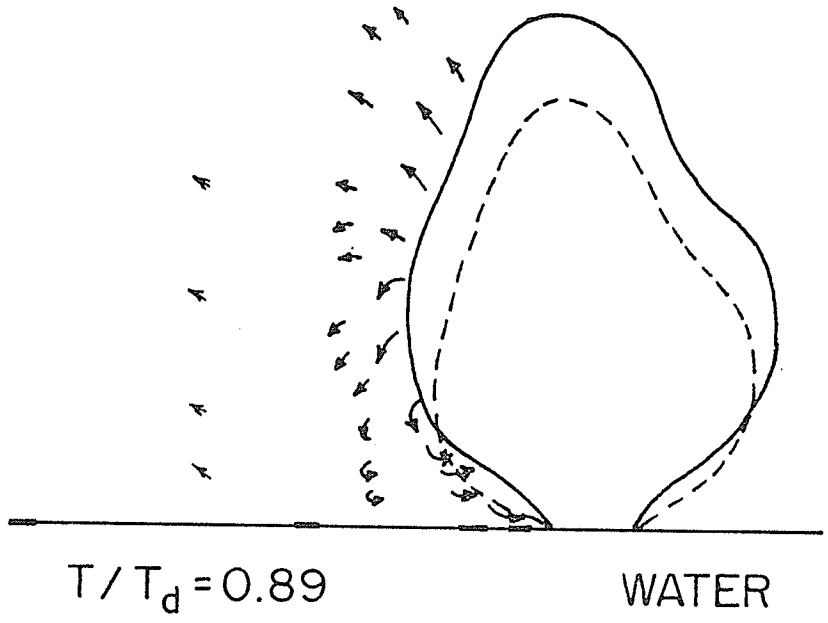

(e)

Fig. F.1

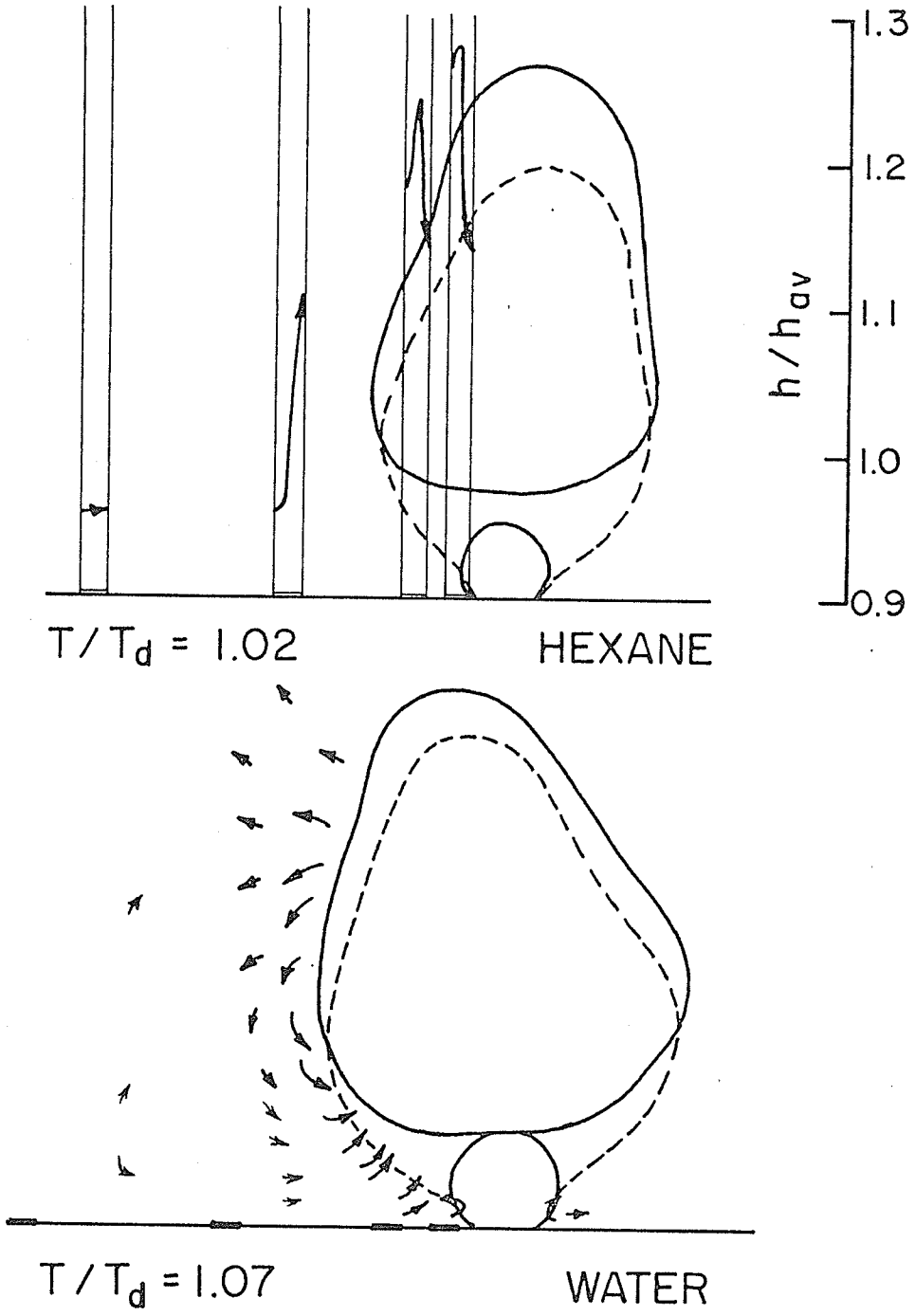

(f)

Fig. F.1

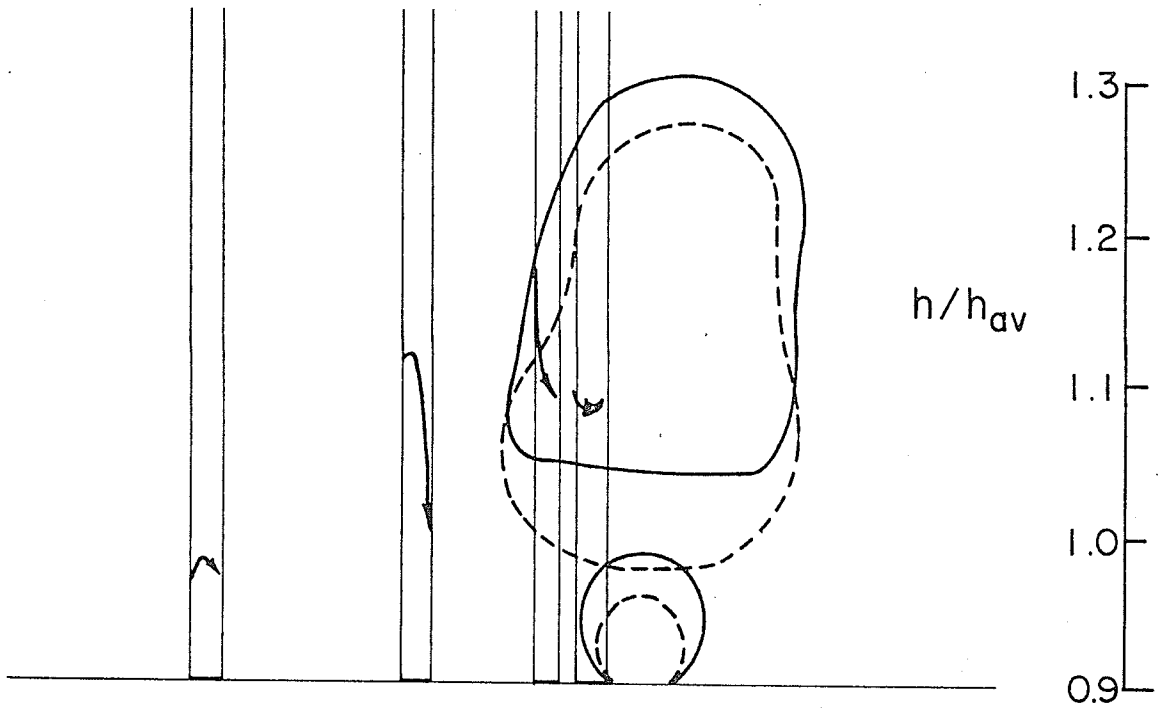

$T/T_d = 1.24$

HEXANE

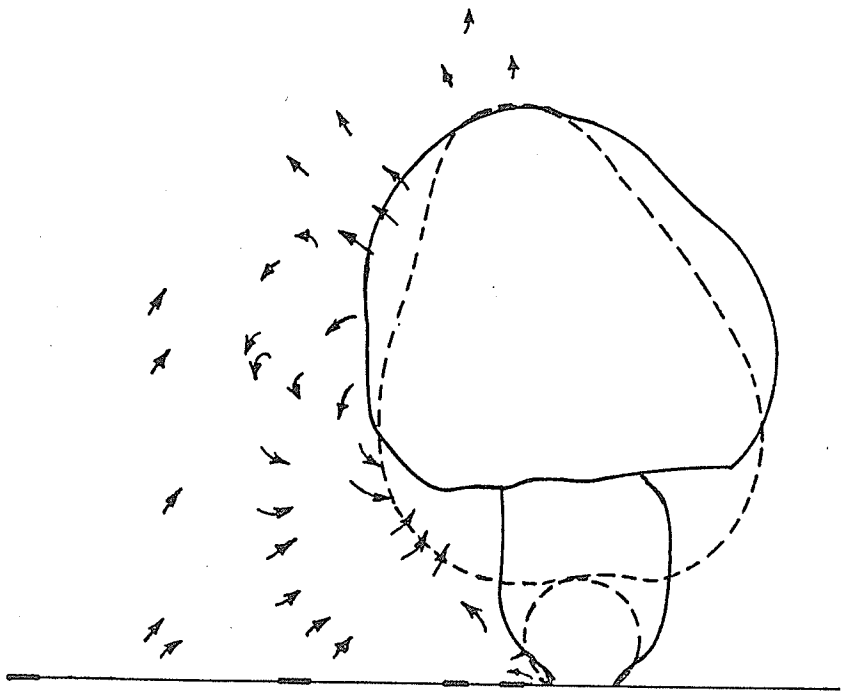

$T/T_d = 1.25$

(g)

WATER

Fig. F.1

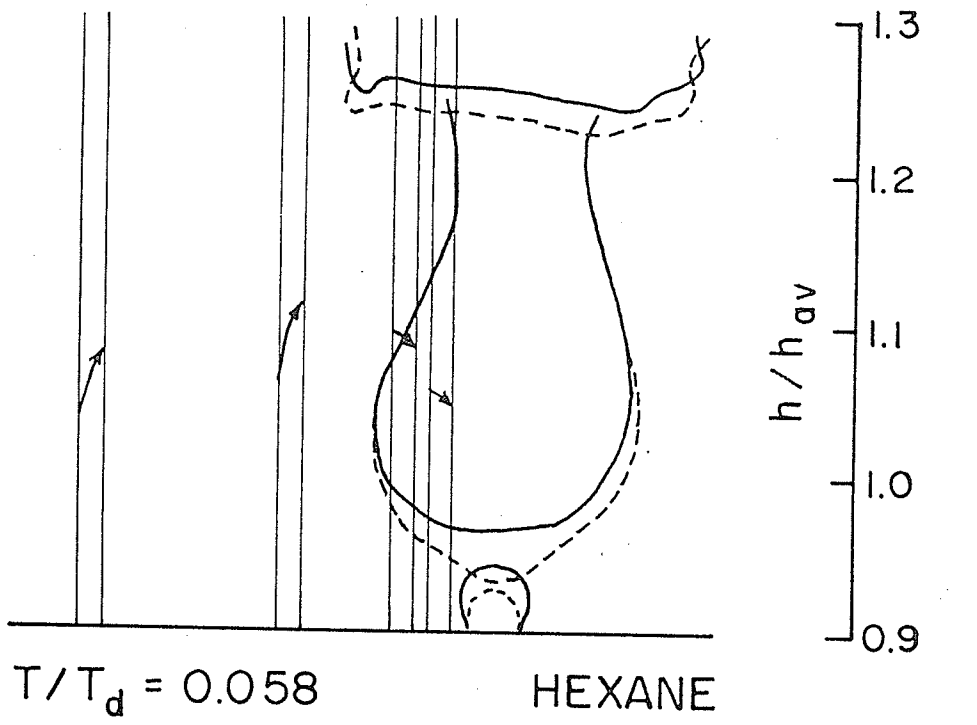

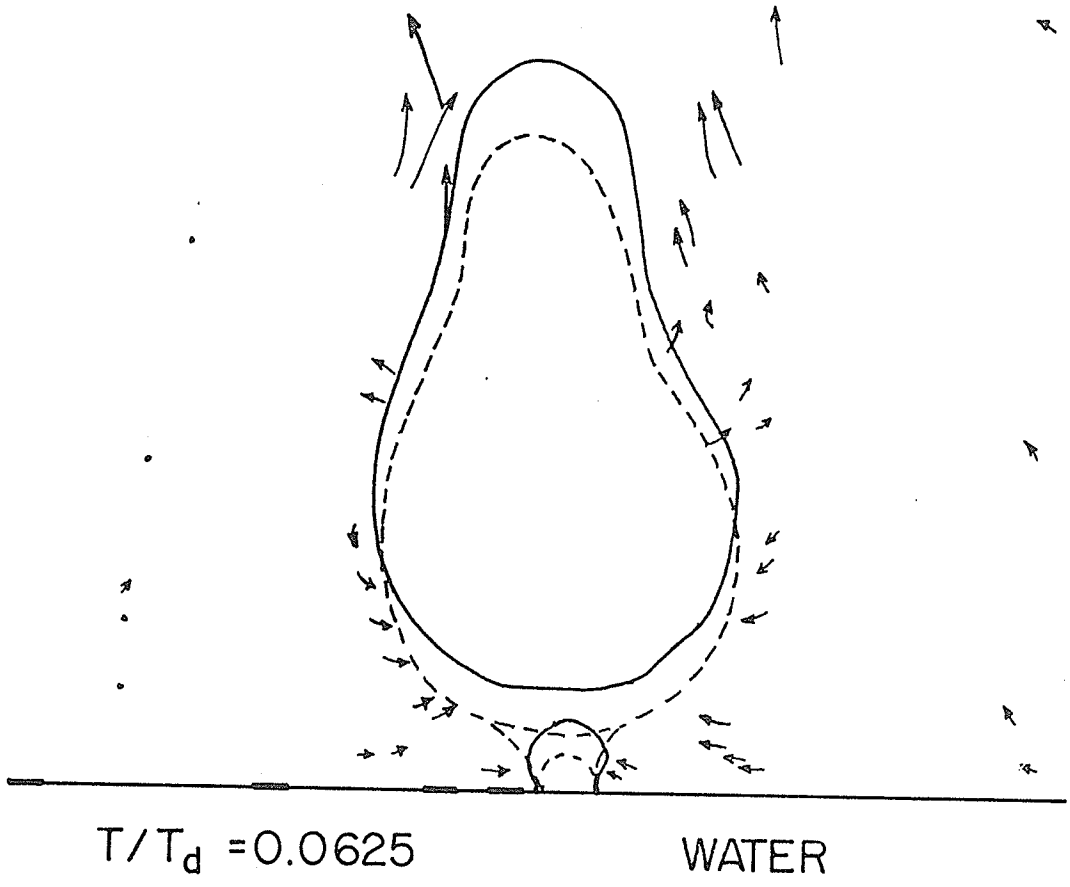

(a)

Fig. F.2 Combined Heat Transfer and Flow Visualization Results for the Last Bubble of a Series (Bubble 25-3-5 in Hexane and Bubble 18-1-5 in Water)

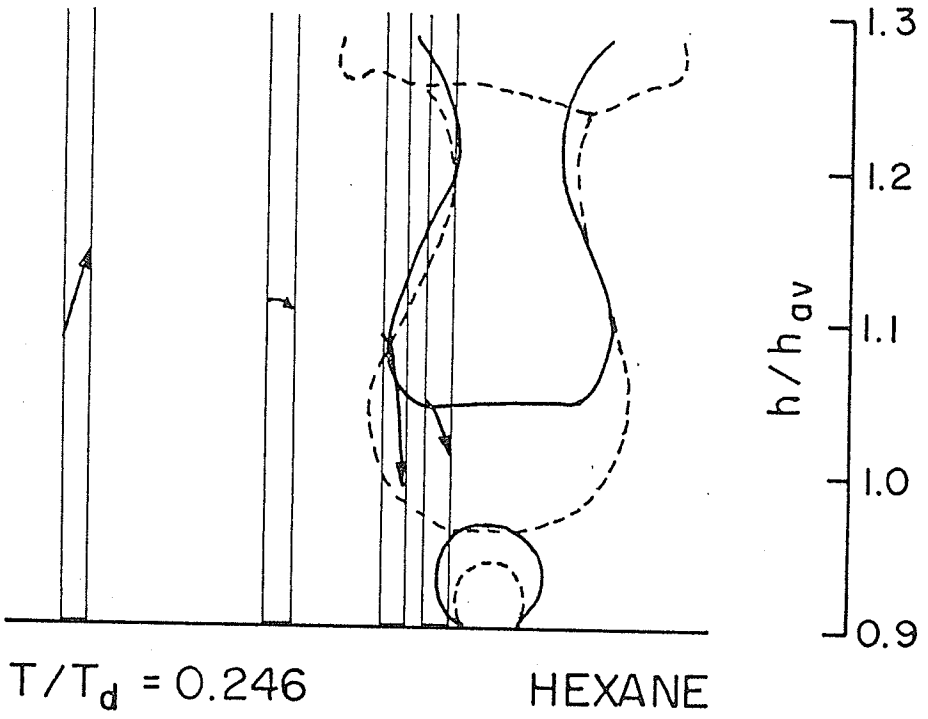

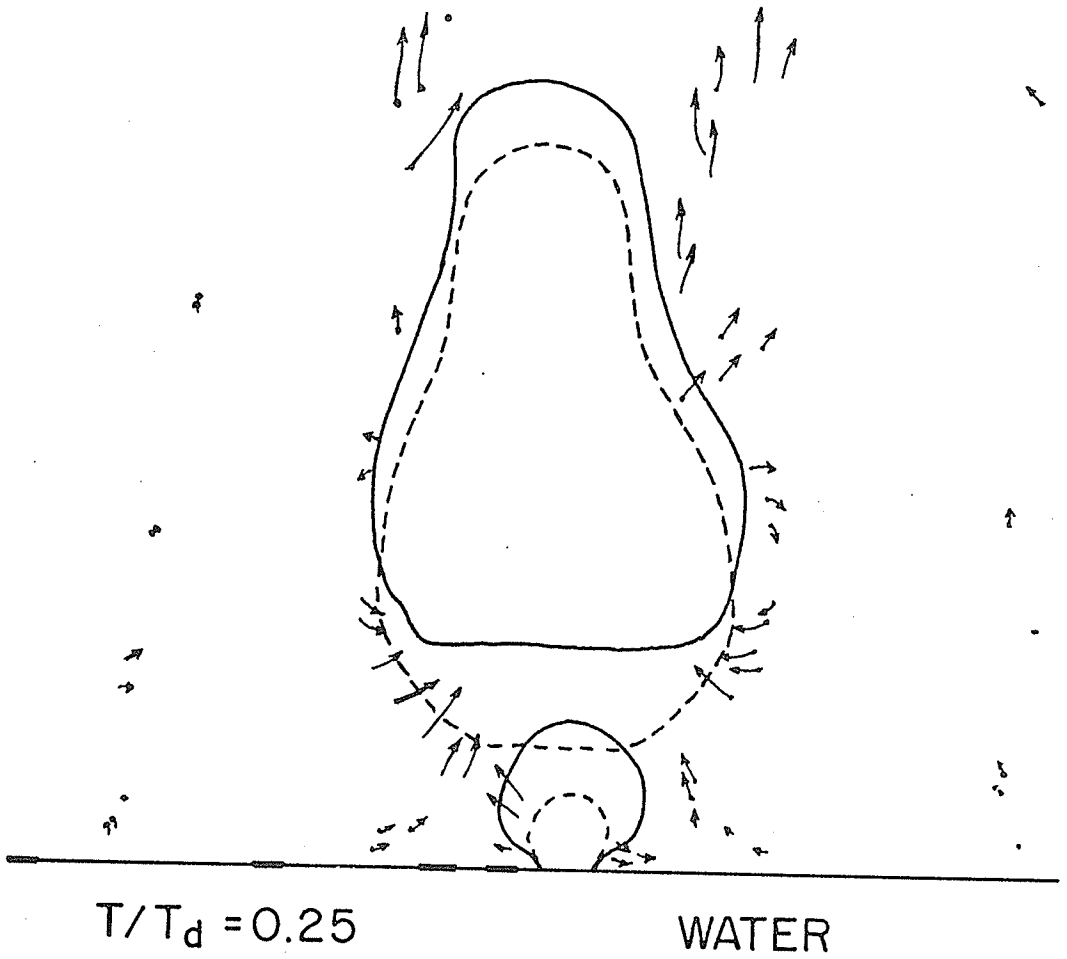

(b)

Fig. F.2

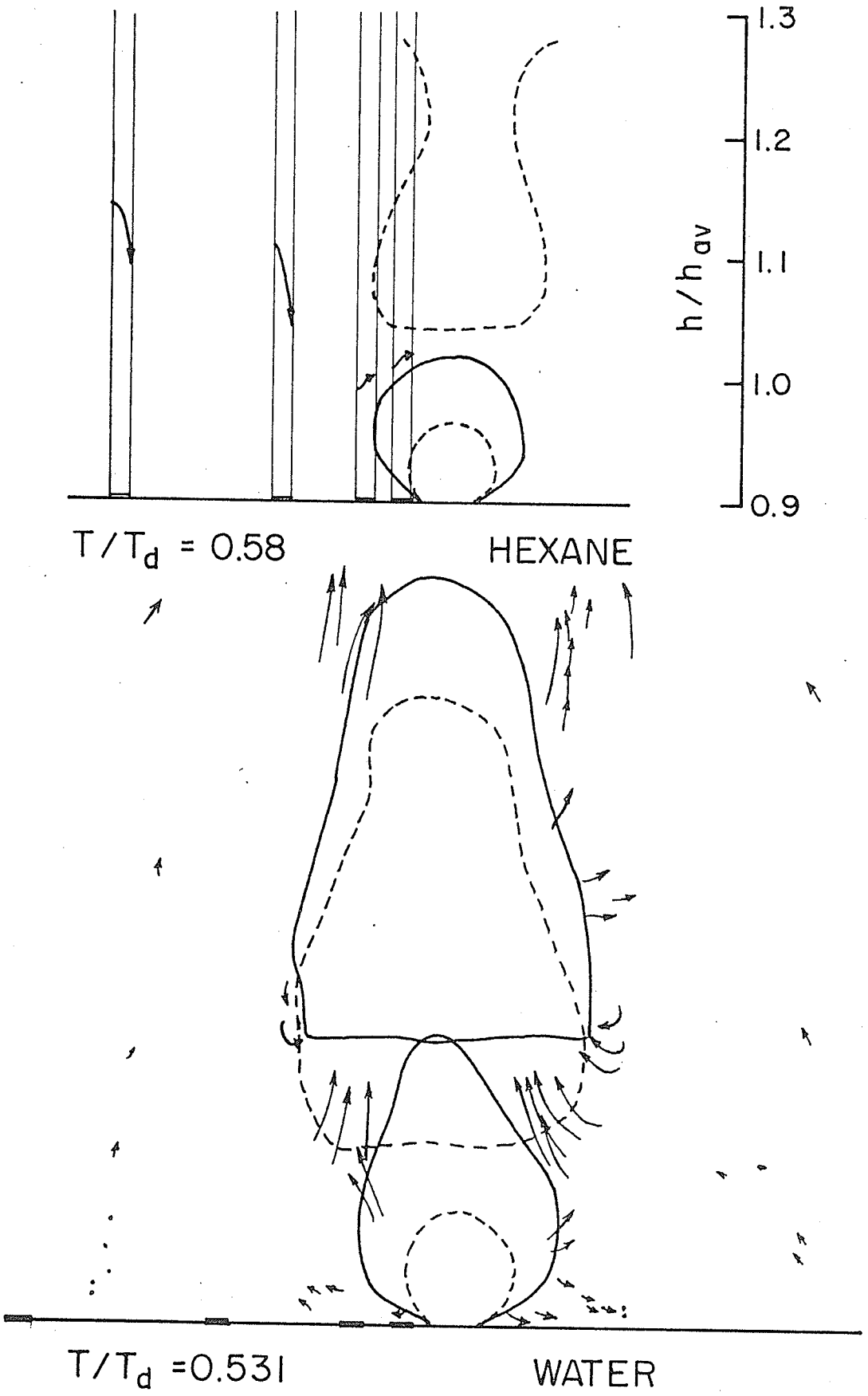

(c)

Fig.F.2

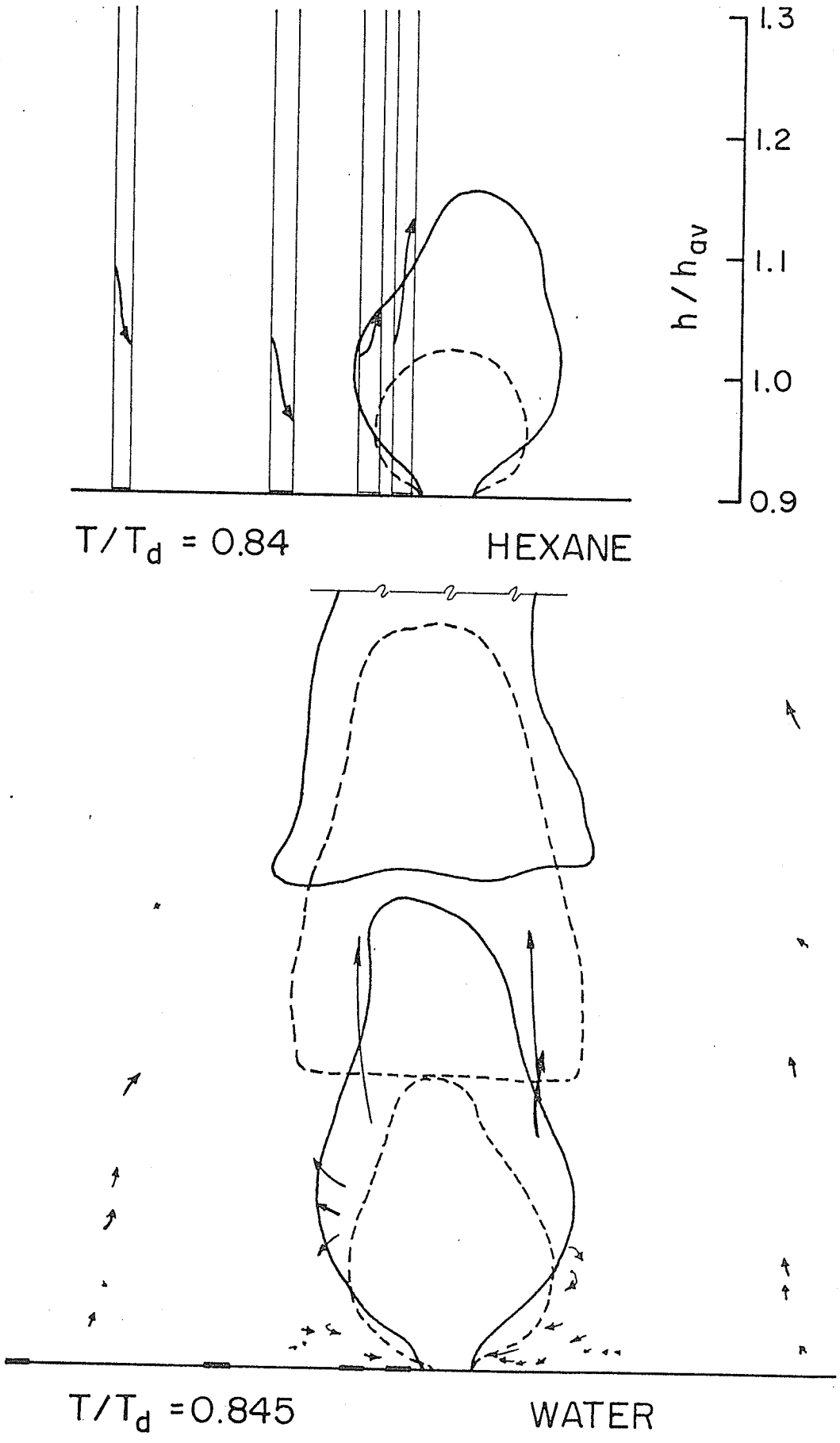

(d)

Fig. F.2

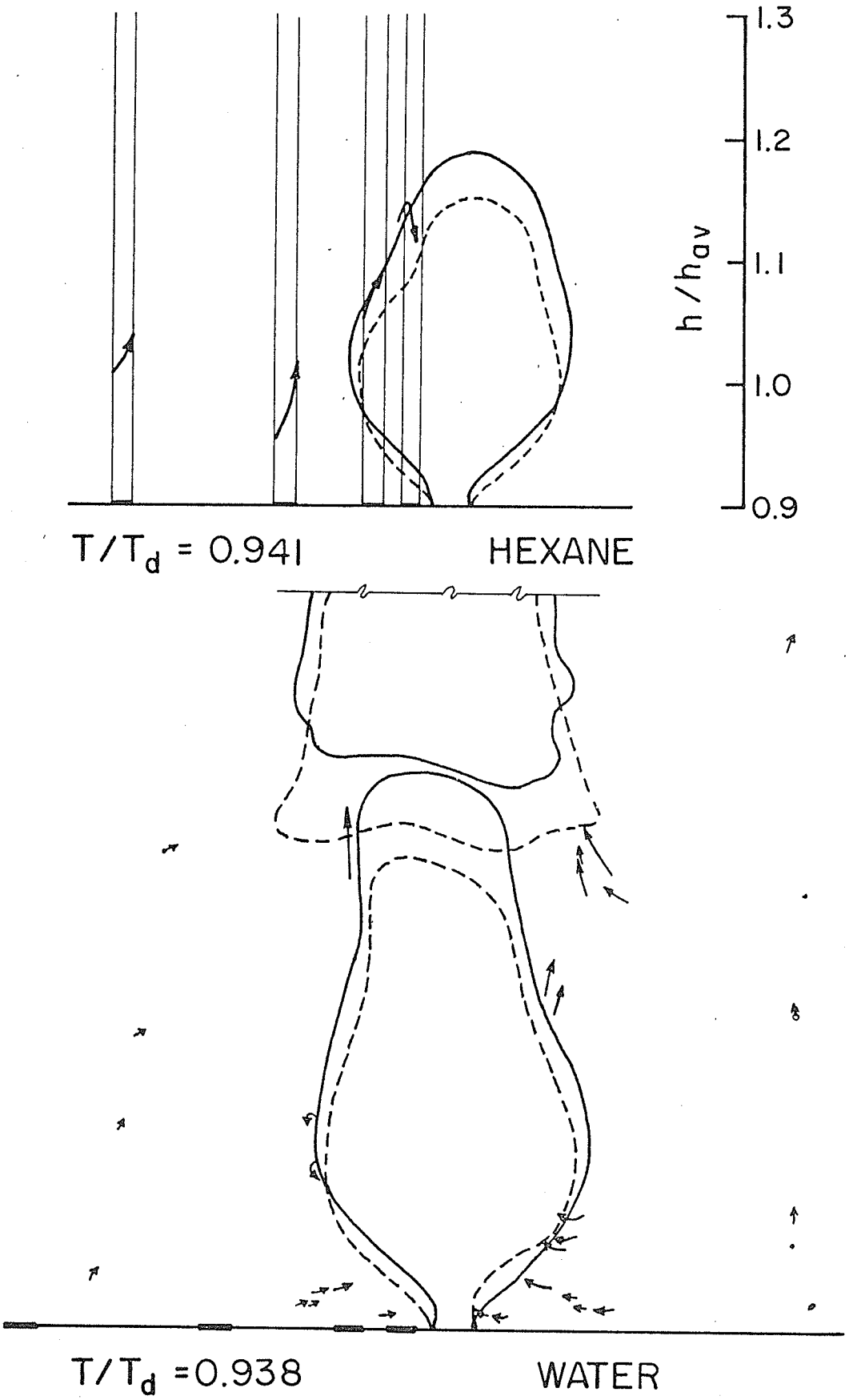

(e)

Fig. F.2

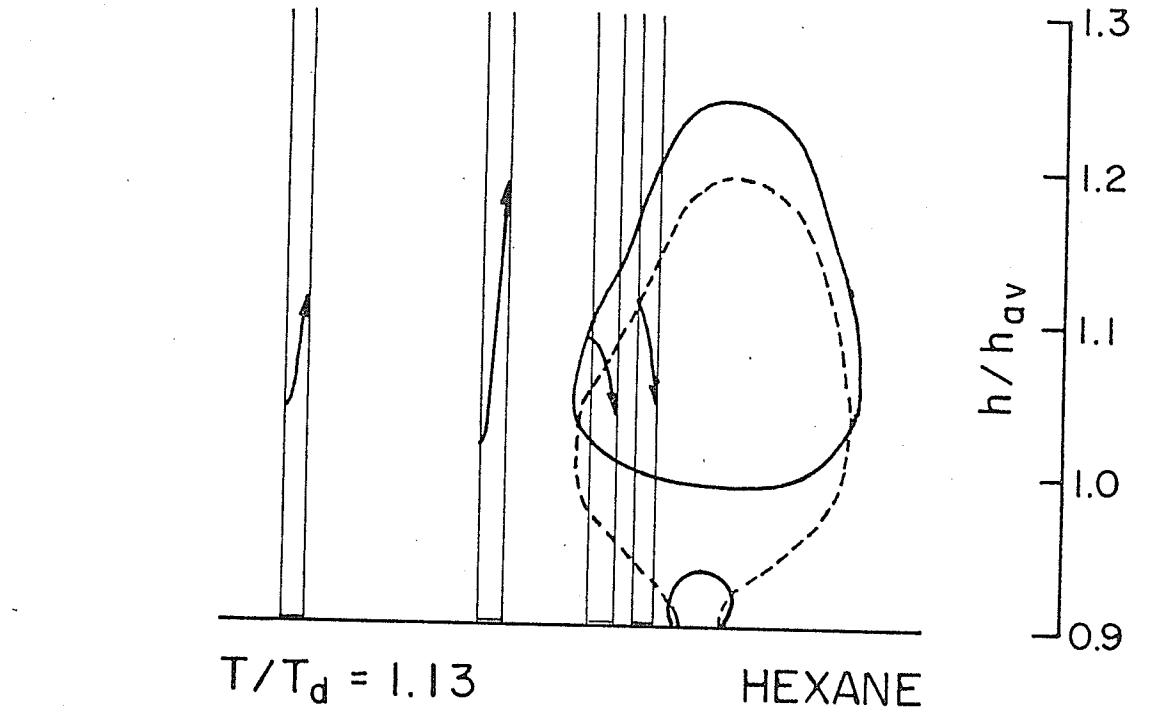

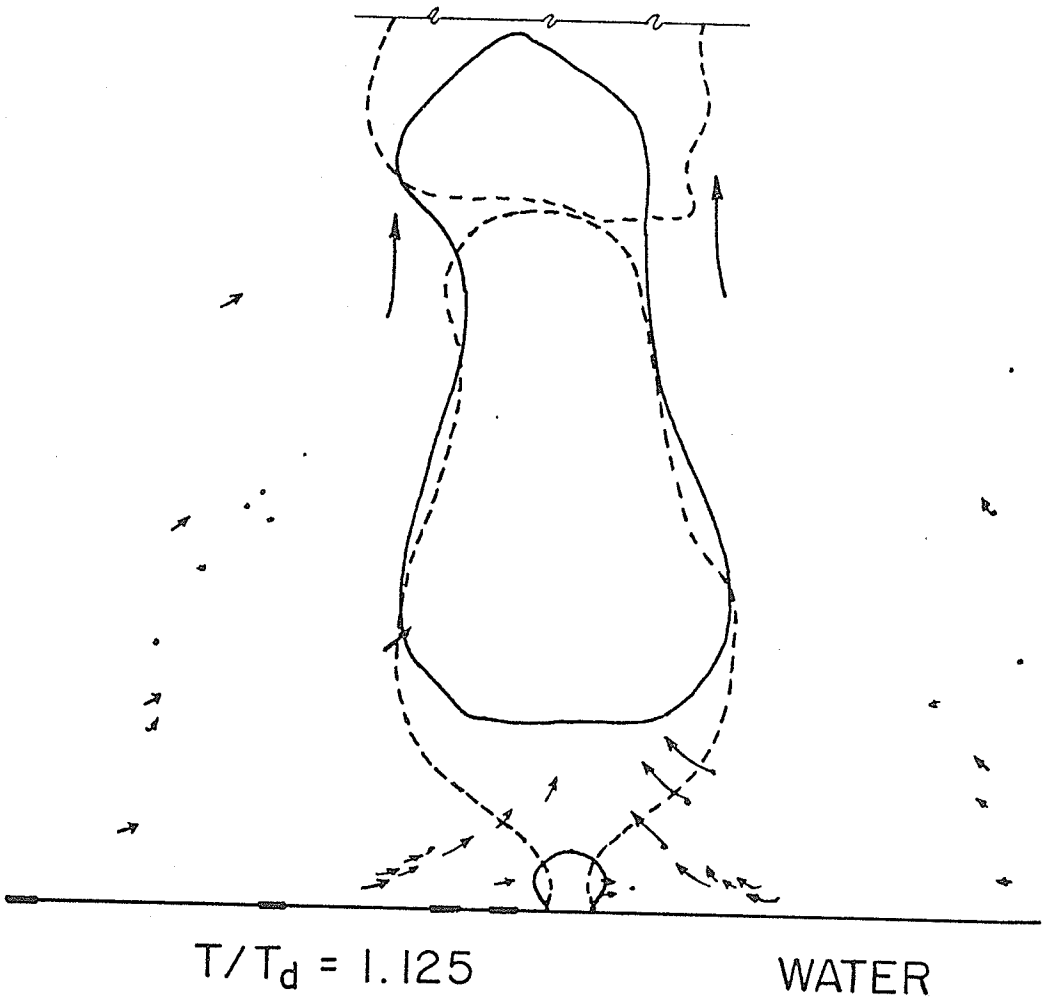

(f)

Fig. F.2

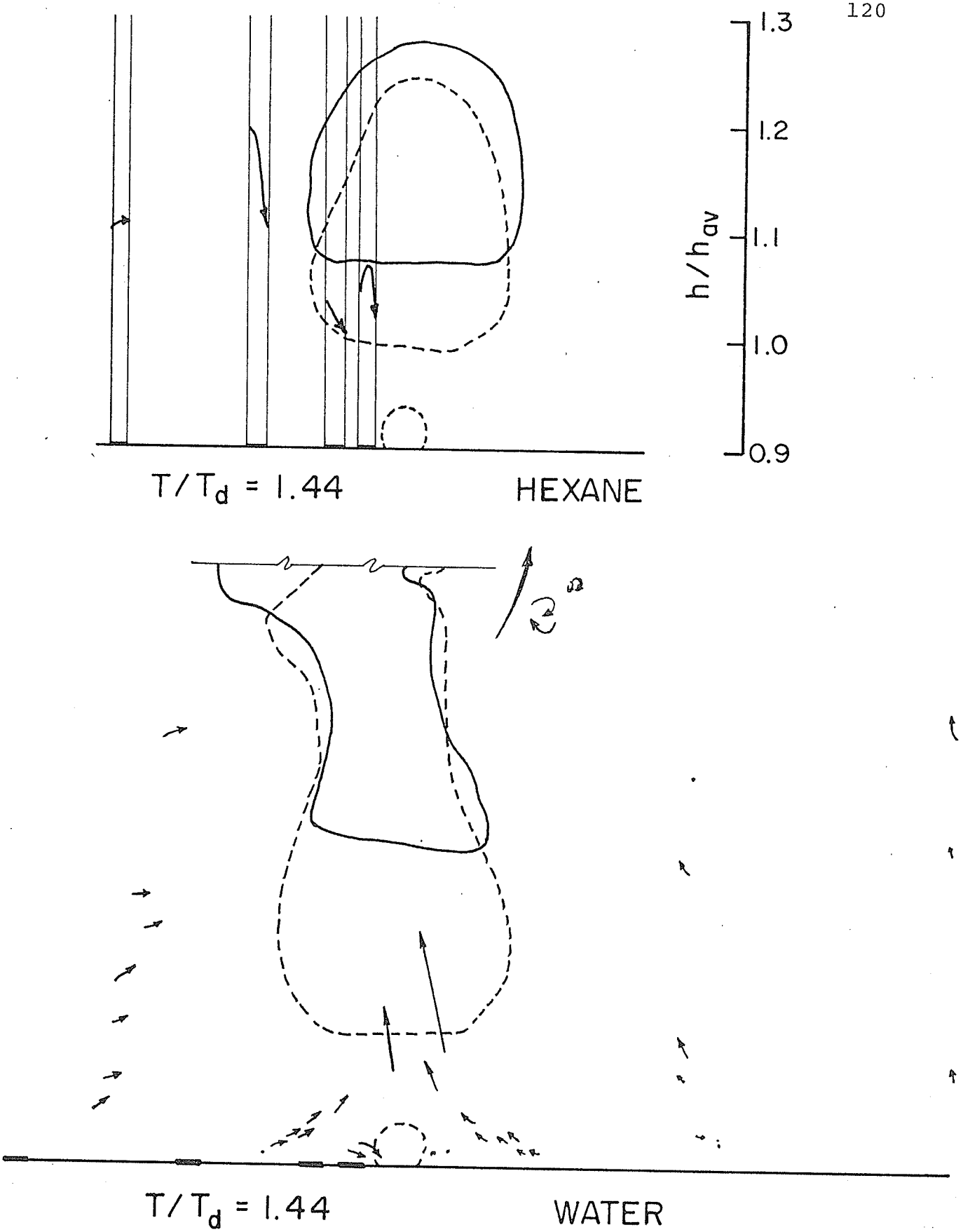

(g)

Fig. F.2

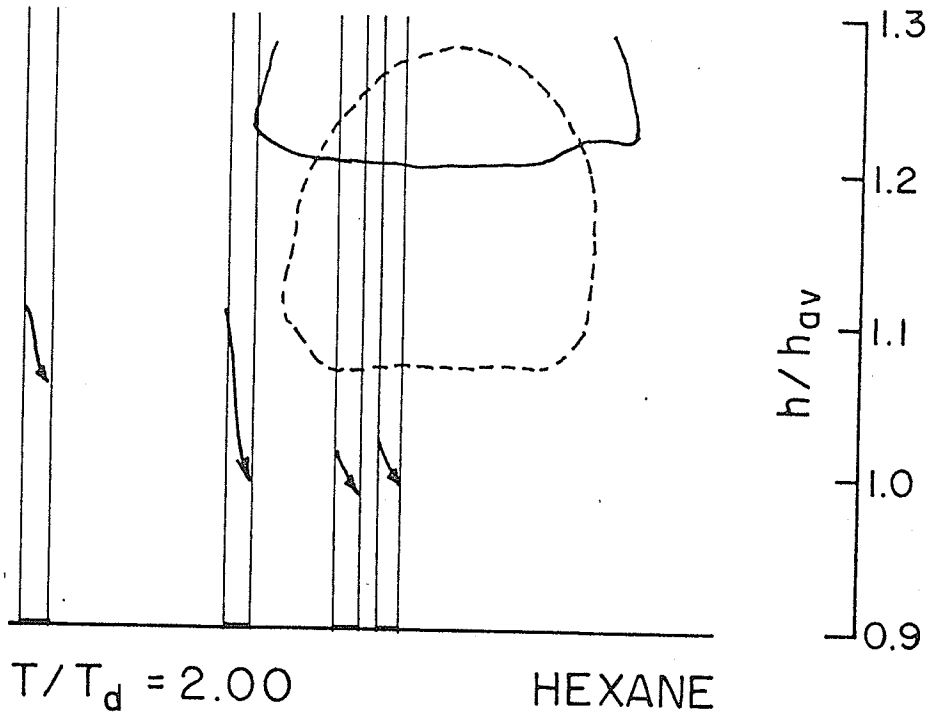

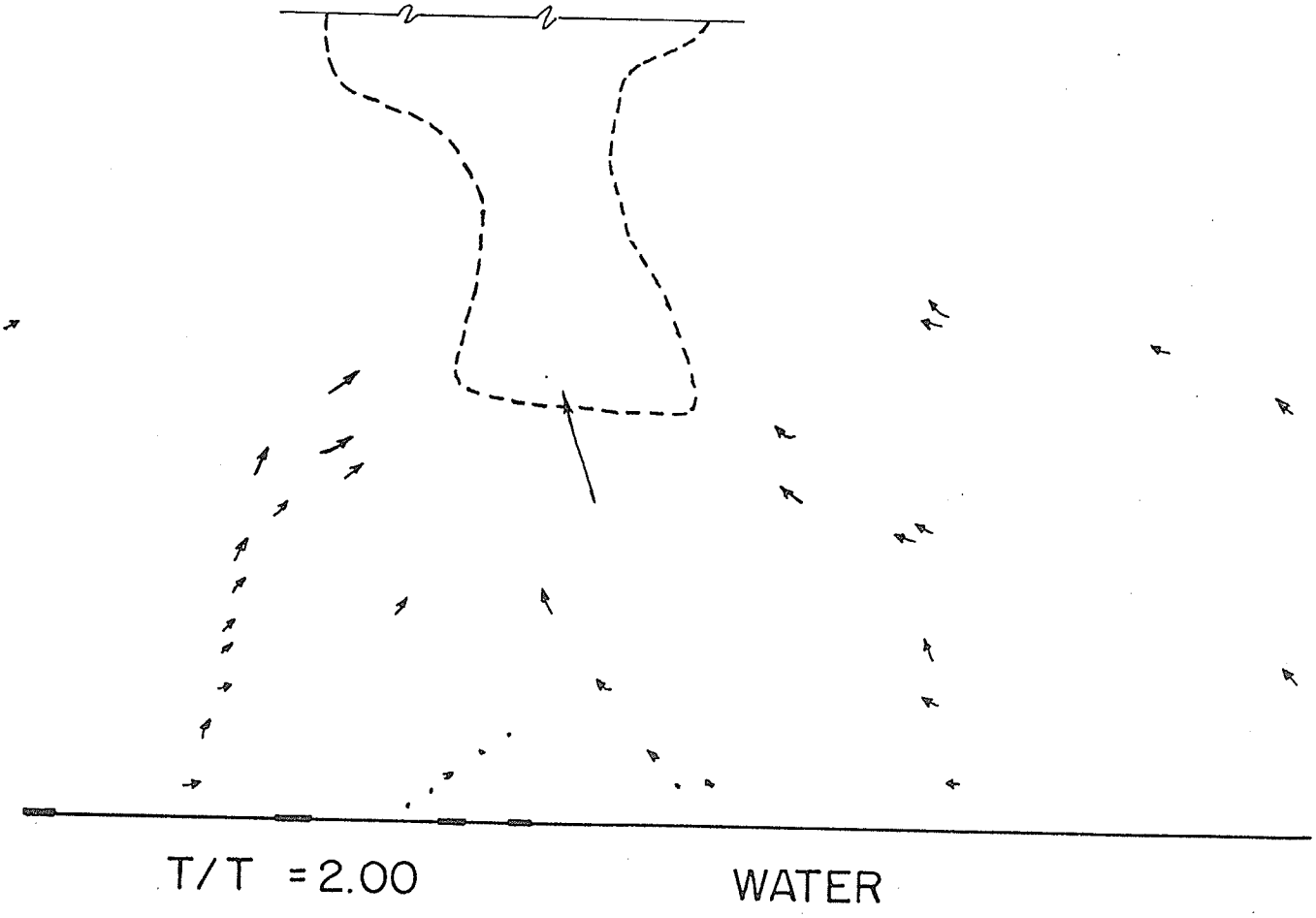

(h)

Fig. F.2